2

Department of Mechanical and
Industrial Engineering
University of Illinois at
Urbana-Champaign
Urbana, IL 61801

ORNL/SUB/82-22239/01
UILU ENG-88-4019

DEFORMATION AND FRACTURE OF LOW ALLOY STEELS AT HIGH TEMPERATURE

**D. L. Marriott, J. F. Stubbins,
Frederick A. Leckie, and Barrie Muddle**

Final Technical Report Prepared for

OAK RIDGE NATIONAL LABORATORY
Oak Ridge, TN 37831

Operated by

MARTIN MARIETTA ENERGY SYSTEMS, INC.
for the
U.S. DEPARTMENT OF ENERGY

Under

Contract 19X-22239 WBS Element UI-3.3
of the
DOE AR&TD Fossil Energy Materials and
Surface Gasification Materials Program

Printed in the United States of America. Available from
National Technical Information Service
U.S. Department of Commerce
5285 Port Royal Road, Springfield, Virginia 22161
NTIS price codes—Printed Copy: A06 Microfiche A01

ORNL/Sub--82-22239-01

DE90 001274

DEFORMATION AND FRACTURE OF LOW ALLOY STEELS AT HIGH TEMPERATURE

Final Technical Report for Period May 1 1982 to April 30 1985

by

Douglas L. Marriott

James F. Stubbins

Frederick A. Leckie

Barrie Muddle

December1988

Work Performed under Subcontract 19X-22239 WBS Element UI-3.3 of the DOE AR & TD Fossil Energy Materials and Surface Gasification Materials Program.

College of Engineering
University of Illinois at Urbana-Champaign
Urbana, IL 61801

List of Contents

1. INTRODUCTION

The work described in this report was carried out as part of the Department of Energy AR&TD Materials Program under Subcontract 19X-22239C. WBS Element UI-3.3 during the period May 1 1982 to April 30 1985.

1.1 BACKGROUND SUMMARY

This project formed part of the initiative in the AR&TD program to characterize high temperature, time-dependent damage processes in low alloy steels, for use in the construction of coal-gasification plant.

Economic, fabrication and reliability considerations dictated the need for a well established material for this purpose, and 2.25Cr 1Mo steel was originally considered as the basic material. The common form of this material is normalized to produce a ferritic-pearlitic microstructure which was deemed to have insufficient strength for the large sizes involved in coal-gasification plant construction. Considerable improvement in initial, short-term strength can be obtained in this material by quenching and tempering to produce a predominantly bainitic structure. However, the knowledge of the time-dependent properties of this class of material is relatively sparse compared with the more common ferritic-pearlitic form.

This project was broadly aimed at adding to the knowledge base for this bainitic form of 2.25Cr 1Mo steel, as it related to time-dependent performance at elevated temperature. Its original intention was to obtain information on specific grades of 2.25Cr 1Mo steel, in particular those containing reduced residual elements and microalloyed modifications, which were being considered as candidate materials at the time. This objective was subsequently modified, in the course of the contract period, to a more generic study of bainitic steel, using the 2.25Cr 1Mo material as a representative of the class. For this reason, the project at first involved two materials, a Lukens heat with reduced residuals, and a Japan Steel Works heat of Ti-V-B modified material (see Section 2 of this report for details). Later in the project, testing concentrated on the JSW material.

The main thrust of the project was directed initially at the detrimental effect of cyclic loading on creep resistance, as observed by Swindeman and others at ORNL, and manifesting itself in an apparently severe creep-fatigue interaction. This led to an extended study of the microstructural changes accompanying both creep and cyclic loading, with the objective of characterizing the interactive damage processes. This work evolved into a study of strain softening behavior under a number of different circumstances, but most noticeably under cyclic loading which, in bainitic, low alloy steels, can cause significant deterioration of strength of 30 percent or more.

Three distinct, but interrelated subtasks were eventually identified. These are:

(2) A study of the evolution of microstructural changes in bainitic materials during steady load creep and under constant amplitude cyclic deformation.

(1) Investigation of the effects of cyclic softening on the fatigue and creep strength of complex geometries, focussing on circumferentially notched bars.

(3) Investigation of the influence of environment as a possible cause of observed fatigue/elevated temperature interaction through its effects on crack initiation and propagation, using EDM notched specimens tested in air and vacuum.

The above tasks form the basis of the following three sections 2,.3 and 4 of this report. Details of theoretical and experimental work relating specifically to each task are given separately in each section. Further information on more general aspects of testing, such as development of electro-mechanical test frames for complex, long-term loading, are summarized in Appendix A. Section 5 is a summary of the main results of the project, integrating the conclusions from these tasks as far as possible. Section 6 is a discussion of promising research directions which have evolved from the work described here. In Section 6 the point is made that the effects of strain softening cannot be evaluated by an examination of the material properties alone, and that the combined material/component geometry interaction is important. Some work on this interaction effect has been initiated, and is presented in Appendix B.

1.2 SUMMARY OF PROJECT EVOLUTION

With the exception of a small number of fatigue tests at 20°C and 482°C, all other testing in this project was performed at 565°C. This is significantly higher than anticipated service temperatures, which are closer to 450°C, but was chosen so as to accelerate the time-dependent aspects of material deterioration to reduce test times. Guidance in selecting this temperature was taken from Klueh's work on the Lukens material, in which 565°C was the maximum temperature considered.

The first tests carried out were constant strain fatigue tests. These showed a modest, but consistent, reduction in fatigue life with decreasing cyclic frequency. A significant form of behavior observed in both materials included in the study, was a large amount of cyclic softening, up to 30 % of the initial stress range which furthermore, did not reach a stable plateau, but persisted throughout the life of the specimen.

Transmission Electron Microscopy (TEM) on interrupted fatigue and creep tests found major changes in the microstructural morphology of the former, indicative of strain induced recovery and precipitate aging, but only moderate changes under steady creep conditions. No indications of void-type creep damage were found at all, posing the question of where the apparent creep-fatigue interaction comes from. Since the uniaxial specimen is not a severe test of creep cavitation damage, a few notched bars and plastically prestrained specimens were tested to see whether cavitation damage could be induced. Only under the most extreme conditions of prestrain (about 6 %) was any indication of creep damage detected. While this does not exclude the possibility of creep damage occurring in this material under lower stresses and longer times, it was considered that it did not appear to be a contributory factor in the time scales and stress levels examined in this project. Even without creep cavitation a time-dependent influence on cyclic endurance still exists, which needs to be explained.

Following these early fatigue and creep tests, the project divided to pursue two distinct problems, representing extremes of a spectrum of creep/cyclic-load interaction.

a) Implications of cyclic softening as a mechanism in its own right as a means of reducing structural load capacity.

b) Experiments aimed at determining the cause, or causes, of the time-dependence of fatigue life.

The first of these problem areas approached the problem direction taken by Swindeman, who showed that creep life in cyclic softening low alloy steels is severely reduced, by an order-of-magnitude or more, by periodic load reversals. This project set out to determine why this was so and whether the softening effect, being confined to local zones of reversed stressing, necessarily causes degradation of overall component strength under the conditions of constraint existing in a complex geometry. Test performed on notched bars, described in Section 2, show that local cyclic softening is not necessarily indicative of general structural component deterioration. Some simple rules have been developed, which could be suitable for early design, such as material selection, based on the observation that cyclic softening appears to be a strong function of cycles, a weak function of cycle frequency, and largely insensitive to either load wave form or cyclic strain range. It was also observed that strain rate sensitivity, and strain softening, both individually complex phenomena, are linked in some, as yet undefined, way, so that their combined effect can be formulated in relatively simple terms. Further examination of this problem requires development of a constitutive model, which was not part of this project, but is one of the research directions which evolve from it.

The second problem area is to resolve the frequency effect for which two possible causes are apparent. The first is an environmental effect, as proposed by Challenger, et al., and the second is a creep/deformation effect, both of which can influence initiation and propagation phases of fatigue damage. In an attempt to isolate these possibilities, a test program was developed in which fatigue life in air and vacuum were compared, using specimens encapsulated in stainless steel belows. Initiation and propagation were differentiated by EDM notching some specimens, effectively eliminating the initiation phase, which turned out to be small in the low cycle range considered in this project anyway. The results of this program are described in detail in Section 4 of this report. They show that creep deformation and environment each has a significant effect on both initiation and propagation. Since Challenger has suggested a plausible model of the influence of environment on initiation, and since the initiation phase was small in any case, efforts to explain these frequency effects have

concentrated up to now on crack propagation. Some tentative hypotheses have been formulated, and are discussed briefly in Section 6 as new research directions.

1.3 PERSONNEL INVOLVED

Original co-principal investigators were Professors Marriott and Muddle of the Mechanical and Industrial Engineering Department. Professor Leckie, initially member of the same Department, since then Head of the Theoretical and Applied Mechanics Department, has acted in an advisory and consultancy role throughout the program. Approximately halfway through the program, Professor Muddle left the University of Illinois to return to Australia, and his responsibilities were taken over by Professor Stubbins, of the Nuclear Engineering Program.

Graduate students contributing to the program are as follows.

Paul Pejsa - Fatigue testing and TEM studies

Marvin Mehler - TEM studies of creep and fatigue tests

David Austin, Clinton Haynes, Paul Yousif - Development of elevated temperature creep test equipment

James Handrock - Commissioning of ATS test machines, slow cycle testing of plain and notched bars

Bruce Kschinka - Fatigue testing of plain and EDM notched specimens in air and vacuum

2. MICROSTRUCTURAL EVOLUTIONS IN BAINITIC 2.25 CR 1 MO STEEL DURING ELEVATED TEMPERATURE CREEP AND LOW CYCLE FATIGUE

The microstructure of bainitic 2.25 Cr 1 Mo steel consists of a fine lath structure and a finely dispersed distribution of carbides, primarily M_2C type with a needle-like morphology. The material used in the present study was taken from a 150 mm (6 in.) thick plate which had been heat treated to produce a 100 % upper bainite structure. This treatment yielded a pronounced strength advantage over typical "annealed" (ferritic) 2.25 Cr 1 Mo steel. The strength advantage arises, as in all bainitic structures, from the fine lath sizes, the fine carbide distribution, and transformation induced strains.

Controlled strain range fatigue testing of this material has shown that the strength advantage degrades rapidly during cycling, dropping by 10 to 20 % in the first 10 % of life and continuing to drop thereafter. Creep testing revealed no unexpected behavior; the failure life was controlled by typical plastic instability in a highly ductile mode. Both creep and fatigue testing were carried out in fairly short term tests with comparable elevated temperature exposure lives.

The microstructural response to both cyclic and steady state loading were analyzed by light optical microscopy (LOM) and transmission electron microscopy (TEM). In both cases, initial loading produced a rapid precipitation of additional intragranular M_2C carbides. In the case of reversed loading, a noticeable increase in bainitic lath size accompanied cycling, but no similar effect was found in the creep case. Material which was thermally aged without a load for longer periods than the elevated temperature mechanical test exposure times showed neither precipitation nor lath coarsening effects.

2.1 INTRODUCTION

Low alloy steels of 2.25% Cr 1% Mo 0.1% C nominal weight composition have been used successfully for containment purposes in the petrochemical and power generating industries for a number of years. Such vessels operate at elevated temperatures for extended periods of time and are exposed to a variety of conditions which may lead to the accumulation of different forms of damage. Creep deformation occurs when metals are exposed to constant loads at temperatures

above 1/3 of their homologous melting point, or about 600°K for this material. Mechanical fatigue damage may be incurred during start-up and shutdown procedures, and thermal fatigue may arise due to fluctuations in operating temperatures. The environment of operation may induce damage because there are usually corrosive charges or reactive atmospheres. In addition, simultaneously active damage mechanisms may present a more deleterious potential than the sum of independently operating mechanisms. Hence, interactions among creep, low cycle fatigue, and environmental effects must be well defined.

Since the ferritic (annealed) condition has been widely utilized over the years, an extensive data base has been developed for its behavior. However, that information cannot be reliably applied to the bainitic condition because of differences in initial strength levels and deviations in the behavior of microstructural constituents.

The ferritic condition is generally produced either by cooling from the austenite region at rates less than about 70°K per minute [2.1], or by isothermally transforming the austenite to proeutectoid ferrite at a temperature just above the A_1 temperature. The ferritic transformation occurs as a nucleation and growth process, with nucleation occurring preferentially at austenite grain boundaries. The ferrite grains then grow until they impinge on one another, resulting in an equiaxial microstructure.

The carbide population of the transformed ferrite depends upon the temperature of transformation. If the transformation occurs above the A_1 temperature, there will be few carbides and most of the alloying elements will remain in solid solution. As the temperature of transformation drops below the A1, however, Fe_3C becomes stable and will appear as pearlite or second phase particles.

The bainitic condition is produced by cooling from the austenite region at rates between about 50 and 500°K per minute [2.1]. The transformation begins with the nucleation of ferrite crystals at austenite grain boundaries. As the ferrite grows, carbides are nucleated but the reduced diffusion rate at the low temperature keeps them small. Continued growth of the ferrite results in the formation of additional small, discontinuous carbides.

Upper bainite, the predominant constituent in both materials, is generally formed above 623°K and is a result of the carbon enrichment of austenite due to rejection of carbon by the growing ferrite laths. Because of the crystallographic relationship of the ferrite with the matrix, and the high driving potential for the transformation, many laths nucleate and grow parallel to one another at low angles of misorientation. The enriched austenite then becomes trapped between laths, and causes nucleation of Fe_3C carbides. The carbides are generally elongated and lie parallel with the direction of lath growth.

2.2 EXPERIMENTAL PROCEDURES

The present work involved (a) an analysis of the microstructural evolution of a commercial steel during steady state creep, and (b) an evaluation and comparison of the elevated temperature, low-cycle fatigue properties of two commercial steels. In the former, samples were subjected to a stress of 246.5 MPa (35.7 ksi) at 838°K for increasing amounts of time, Fig. 2.1. For the latter, specimens of each steel were subjected to low cycle completely reversed, strain controlled fatigue tests at isothermal temperatures of 293°K, 755°K, or 838°K. The majority of the work was performed at 838°K with total strain ranges ($\Delta\varepsilon_t$) of one-half or 1 % for several cyclic waveforms.

Steel produced by Lukens Steel Company, from heat #A6660, slab 1, heat treated to meet SA-387 grade 22 class 2 specifications was used for the creep evaluation as well as the low-cycle fatigue evaluation. The second steel came from a 400 mm thick plate produced by Kawasaki. The compositions and heat treatments of each steel are presented in Table 2.I.

Samples for TEM analyses were either carbide extraction replicas or thin foils. The carbide extraction replicas provided information about the chemical composition of individual carbides from X-ray energy dispersive spectroscopy and electron diffraction. They also provided uncluttered images of the distribution of carbides within the material. Thin foils were used to study the evolution of dislocations, boundaries, and carbides. For tests which ran until failure, TEM samples were taken immediately adjacent to the fracture surface.

Carbide extraction replicas were produced from polished surfaces freshly etched with 2 % nital and ultrasonically cleaned. The film of arc-evaporated carbon was applied immediately, in order to minimize the oxide layer that forms upon exposure to the atmosphere. The surfaces were scribed into small squares, immersed in 5 % nital until the films were loose, and then immersed in distilled water. The individual films were then collected on either copper or beryllium microscope grids.

Thin foils were produced from 0.019 inch (0.48 mm) thick diamond sawed wafers by chemically thinning to about 0.010 inch (0.25 mm) thickness in a solution of 160 ml H_2O_2 (30-35 %), 30 ml H_2O, and 10 ml HF (48 %), punching the wafer into 3 mm disks, carefully wet grinding on 600 grit sandpaper to 0.003 inch (0.008 mm) thickness, and electrolytically polishing in 5 % perchloric acid in ethanol at -40°C and 125 volts potential in a twin jet polisher. The foils were stored in small vials filled with ethanol in order to reduce the rate of surface oxidation.

The foils were examined with either a Philips EM400T or EM420T TEM operating at 120 kV. In the interest of standardization, an attempt was made to examine the samples in the area of a lath packet oriented with the electron beam near an <001> zone axis.

2.2.1 Creep Results

In describing the microstructural changes which occurred during creep testing of the Lukens steel, three major areas will be discussed: carbide evolutions, dislocation changes, and boundary developments.

The as-received prior austenite grain size was on the order of 100 μm in diameter. The ferrite laths were typically 0.2 to 0.5 μm in width, and were clustered together in packets. The initial carbide structure consisted mainly of elongated Fe_3C particles lying parallel with the ferrite laths. Also present were M_7C_3 carbides uniformly distributed throughout the material and along grain boundaries. Acicular M_2C carbides were occasionally present, Fig. 2.2. X-ray peak height ratios and compositional ranges among particles of each variety are presented in Fig. 2.3.

Thirteen hours of uniaxial creep caused the precipitation of acicular M_2C carbides throughout the material, except for precipitate free zones approximately 0.3 μm in width near some boundaries.

The carbide needles were typically 0.19 μm in length and were spaced roughly 0.10 μm apart. Lattice strain was evidently a strong catalyst for the precipitation of M_2C carbides, because control samples aged several hundred hours at the same temperature but without strain exhibited little tendency for the carbides to precipitate, Fig. 2.4.

After the precipitation of the M_2C carbides, the carbide structure remained fairly stable throughout the remainder of the test samples. There were, however, areas of carbide instability associated with boundaries. Migrating boundaries caused the dissolution and subsequent re-precipitation of M_2C carbides. Grain boundary sliding and the associated intragranular shear caused deformation and breakup of the M_2C carbides, Fig. 2.5. An increase in fine scale grain boundary precipitates was noticed toward the end of life and are thought to be a plate-like morphology of M_2C. Finally, polygonal subgrains which formed near the end of life were usually free of the M2C precipitates, Fig. 2.7.

The second major area of microstructural change was the dislocation structure. The initial microstructure contained dislocations which had reacted with one another to form lower energy configurations with sessile nodes. At the end of primary creep (13 hours), many dislocations had piled up in parallel arrays against barriers, Fig. 2.7. At this stage, the material had achieved its optimum resistance to deformation by the combined interactions of precipitate particles, boundaries, and dislocation pile-ups. Further deformation at the constant stress would require the passage of dislocations around the barriers.

Samples taken during the secondary stage of creep exhibited very few of the parallel dislocation pile-ups that were observed after 13 hours. The ones which were observed were probably a result of recent stress redistributions. Those present earlier had either bowed around obstacles, undergone cross slip or climb to by-pass the obstacles, or had combined to form low angle boundaries. Such processes occurred throughout secondary creep, leaving behind dislocation segments tied to particles and other segments and new boundaries, Fig. 2.8.

Dislocation structures in the tertiary creep regime were quite variable, with some grains relatively dislocation free, some with pile-ups which had started to form nodes, and some with segments tied to particles, as in steady state creep, Fig. 2.9.

The third major area of microstructural change concerns boundaries. Lath boundaries of low angle crystallographic misorientation were the most unstable and began to disappear fairly early in the steady state creep regime. After 180 hours of creep (63 % time to rupture), the average lath width had increased from the as-received width of 0.2 to 0.5 μm to about 0.8 to 1.2 μm, Fig. 2.10. The loss of lath boundaries resulted in a decrease in dislocation obstacles and an increase in mean free paths. As additional lath boundaries disappeared with time, more and more dislocations were able to reach prior austenite grain boundaries and the interior of the prior austenite grains became less resistant to deformation. As a result, the prior austenite grain boundaries began to exhibit changes. The effects of grain boundary sliding became more pronounced and boundaries were seen to bow out between large grain boundary carbides. Eventually, boundaries were able to free themselves of their constraints and grow into adjacent grains. In order to do so, however, existing M_2C carbides had to be dissolved in front of the boundary and re-precipitated at the new orientation after the boundary had passed by, Fig. 2.11.

A limited amount of recrystallization also occurred near the end of the material's life. Polygonal grains relatively free of dislocations and precipitates had apparently nucleated at established boundaries and grown into the surrounding material, Fig. 2.12.

2.2.3 Low Cycle Fatigue Results

Uniaxial, isothermal, strain-controlled, low-cycle fatigue tests for various cyclic waveforms were performed for both Lukens and Kawasaki materials at 838°K. A summary of the waveforms and test conditions is presented in Fig. 2.13.

A summary of the duration of fatigue tests performed at 838°K is presented in Fig. 2.14, where the number of cycles to failure, N_f, is plotted for the two strain ranges employed for both Lukens and Kawasaki alloys. Plots of the variation in maximum tensile stress amplitude as a function of number of

cycles (N) for all waveforms at 838°K and total strain ranges of 1/2% and 1% are presented in Fig. 2.15 for Lukens material. The effect of introducing a 0.1 hr tensile hold time, a symmetric slow strain rate (1.4×10^{-5} sec^{-1}) cycle or an asymmetric slow/fast strain rate cyclic waveform was to reduce life by a factor of approximately two and the maximum tensile stress amplitude at half-life ($N_f/2$) by 6% to 15% compared to the fast strain rate (4×10^{-3} sec^{-1}) cyclic waveform. Lowering the strain range from 1% to 1/2% increased N_f approximately fourfold, except in the case of the fast strain rate test, where an approximately six fold increase was observed. The reduction in strain range resulted in a reduction in maximum tensile stress amplitude at $N_f/2$ of 7%, 10%, and 15% for the slow-fast strain rate, fast strain rate, and hold-time tests, respectively, values for the slow strain rate test remained approximately the same. Results representative of the effect of varying the test temperature are presented in Fig. 2.16. Tests were performed using a strain range of 1% and fast strain rate at 293°K, 755°K, and 838°K. Maximum tensile stress amplitudes of 64, 53, and 49 ksi at $N_f/2$, and lifetimes of approximately 3500, 1200, and 800 cycles were observed, respectively. The Lukens Steel was observed to undergo significant cyclic softening under all test conditions, with the major part of the reduction in strength occurring within 70 cycles at $\Delta\varepsilon_t$ = 1% and approximately 300 cycles at $\Delta\varepsilon_t$ = 1/2%. Fracture occurred within approximately 100 cycles of crack initiation at $\Delta\varepsilon_t$ = 1% and 250 cycles at $\Delta\varepsilon_t$ = 1/2%. The point of crack initiation was determined from observation of a significant loss of symmetry in the stress-strain hysteresis loop.

Plots of maximum tensile stress amplitude versus number of cycles for all cyclic waveforms at 838°K and total strain ranges of 1/2% and 1% are presented in Fig. 2.17 for Kawasaki steel. This alloy behaved in a similar manner to the Lukens material in terms of cyclic softening behavior and fracture. Cyclic strength in the Kawasaki material, however, was found to be significantly lower in all mechanical tests, the reduction in maximum tensile stress amplitude being between 25% in the case of the fast strain rate test and 32% in the case of the slow strain rate test. These values are typical of strength differences sustained throughout fatigue life. Lifetimes were similar to those of the Lukens alloy, with the exception of specimens tested at 1/2% $\Delta\varepsilon_t$ and at fast strain rate, in which case the Lukens steel endured 1.7 times as many cycles.

The microstructural features of various fatigue samples are described in the photomicrographs of Figs. 2.18 through 2.24.

2.3 DISCUSSION

To summarize, the bainitic 2.25 Cr 1 Mo Lukens steel subjected to a rapid creep environment behaved in the following manner: Primary creep caused the development of acicular M_2C carbides and dislocation pile-ups. Secondary creep entailed the diffusion controlled processes of dislocation climb and grain boundary sliding. The disappearance of low angle lath boundaries reduced the deformation resistance of the prior austenite grains. As total strain increased, geometrical changes of the sample caused the effective applied stress to increase. The increased stress allowed greater dislocation activity and the growth of cavities, and resulted in an increase in creep rate. This tertiary stage of creep continued until fracture.

The rapid precipitation of M_2C carbides during high temperature, uniaxial stress may have the following implications: it is known that the precipitates form at specific orientations within the matrix and have specific degrees of misfit with crystallographic directions [2.2]. If precipitation is enhanced by the relief of misfit by uniaxial strain, it would seem logical that different strain configurations could results in different precipitation behavior. Therefore, accelerated precipitation may not occur during hydrostatic strain. On the other hand, optimum carbide distribution could be produced by a specific strain aging pretreatment. Such behavior would warrant further investigation.

For the fatigue tests, the Lukens alloy was found to possess a significant strength advantage (25% to 30%) over the Kawasaki steel when initially stressed. This advantage was sustained throughout the cyclic lifetime. Both of the steels were observed to undergo rapid cyclic softening in the early stages of fatigue deformation to an approximate steady-state stress value that then decreased only slightly with further cycling. For each steel, this quasi-steady state value corresponded to approximately 70% of the initial flow stress of the material. The number of cycles required to achieve the steady state depended upon $\Delta\varepsilon_t$, but was typically approximately 70 cycles for

both alloys at $\Delta\varepsilon_t$ = 1%. Despite the strength difference of the alloys, the duration of fatigue (N_f) tests for similar test conditions was found to be remarkably similar.

Microstructural examination showed as-received Lukens alloy to have a smaller bainitic lath size and to be more densely populated with carbides than as-received Kawasaki steel. Similar differences were observed to be sustained in specimens subjected to similar degrees of cyclic deformation. In addition, the microstructures of both materials when cyclically deformed were found to have coarsened considerably compared to as-received alloys, and the cyclic strength was found to drop correspondingly.

Lukens alloy tested at a strain rate of 4×10^{-3} sec^{-1} (fast strain rate), $\Delta\varepsilon_t$ = 1% and 838°K failed after approximately 800 cycles. The interjection of a 0.1 hour hold period at the maximum tensile strain peak, use of a slow strain rate (1.4×10^{-5} sec^{-1}) or an asymmetric slow/fast strain rate waveform reduced lifetimes by a factor of approximately two. Although a difference of this order of magnitude is typically not significant in low-cycle fatigue testing and usually falls well within experimental scatter bands, the factor of two was observed to be reasonably consistent for the three cyclic waveforms involving either a slow strain rate under tensile loading or a tensile hold point for both Lukens and Kawasaki alloys tested at $\Delta\varepsilon_t$ = 1%, suggesting that it constitutes a true difference in N_f. Employing the slow strain rate or slow-fast cyclic waveforms reduced maximum tensile stress amplitudes roughly 30% and 10%, respectively, at $N_f/2$ for the Lukens alloy.

Strain range had a significant effect upon the low-cycle fatigue behavior of bainitic 2.25 Cr 1 Mo steel. The effect of lowering the total strain range from 1% to 1/2% increased N_f approximately four fold, with the exception of the fast strain rate test in which a six fold was observed.

Fast strain rate tests were also performed at 293°K and 755°K for $\Delta\varepsilon_t$ = 1% and the effects of temperature on mechanical behavior were observed. Increases in N_f of 1.5 times and 4 times, and maximum tensile stress amplitudes at $N_f/2$ of 7% and 28% were observed for tests at 755°K and 293°K, respectively, as compared to results obtained at 838°K.

The microstructures of as-received and cyclically deformed material were characterized extensively to aid in the explanation of observed mechanical behavior. The microstructure of as-

received Lukens steel comprised a matrix of ferrite lath packets. Fine scale carbide precipitates were found along lath boundaries, and M_3C carbides were associated with dislocations within individual laths. Rod-like M_2C carbides were distributed on a fine scale within laths and a uniform distribution of coarse M_3C and M_7C_3 carbides was observed throughout the structure. In comparison, the Kawasaki steel near the as-received plate surface comprised a coarser ferrite lath structure containing local regions that were more equiaxed in shape, with much less evidence of fine-scale precipitation at lath boundaries and dislocations, and of M_2C carbides within individual ferrite units. Both observed lath sizes and carbide distributions were compatible with a lower observed strength when compared to Lukens alloy.

Significant changes in microstructure were observed to accompany strain-cycling of the steels at elevated temperatures. In Lukens steel strain-cycled at 838°K, the fine lath structure was observed to break down and coarsen, forming a more equiaxed structure. New carbides precipitated, particularly those of the M_2C type, and existing carbides coarsened. Strain-cycling at 755°K produced similar changes in the microstructure, and tests run at ambient temperature produced a surprisingly large degree of recovery and coarsening of the lath structure, with some apparent changes in carbide distribution, though not to the degree observed at 755°K and 838°K. The effect of elevated temperature during strain-controlled cyclic loading is apparently to accelerate the coarsening of the microstructure of the bainitic material.

The microstructure of deformed Kawasaki steel was markedly different from that of Lukens alloy tested under similar conditions. Very large, equiaxed sub-grains of ferrite were observed in both fast strain-cycled and hold time specimens tested at $\Delta\varepsilon_t$ = 1% and 838°K. Dislocation networks and subgrain boundaries were relatively free of precipitation, and local areas within grains contained no acicular M_2C carbides.

The lath structure of the Lukens alloy aged isothermally 50 hours at 838°K showed signs of coarsening in only small, localized areas, and no major changes in carbide sized or densities were observed. Specimens examined after 100 hours and 150 hours remained similar in nature and scale to as-received material. Therefore, no significant reductions in strength due to elevated temperature

exposure alone would be expected. Although specimens were aged for times roughly equivalent to the durations of long-term mechanical tests, none of the pronounced coarsening observed in the latter deformed specimens was found, indicating that the importance of cyclic deformation of the material was in accelerating the development of a coarse ferrite subgrain structure and in enhancing the coarsening rate of existing carbide particles.

The most notable difference between the completely reversed low-cycle fatigue behavior of the annealed and the normalized and tempered 2.25 Cr 1 Mo steels lies in their cyclic strength. Brinkman et al. [2.3] recorded a maximum tensile stress amplitude (σ_a) at $N_f/2$ of 217 MPa for an annealed material containing carbon levels comparable to those of Lukens and Kawasaki alloys tested at $\Delta\varepsilon_t$ = 1/2%, 838°K and a strain rate of 4×10^{-3} sec^{-1}, which compares to values of 293 MPa and 227 MPa for Lukens and Kawasaki material, respectively, tested under similar conditions. In testing of annealed alloy at 838°K, $\Delta\varepsilon_t$ = 1% and a strain rate ($\dot{\varepsilon}$) of 1.67×10^{-4} sec^{-1}, Jaske and Mindlin [4] observed $\sigma_a \simeq$ 140 MPa at $N_f/2$. By comparison, specimens tested in this work under similar conditions, but with $\dot{\varepsilon}$ = 1.4×10^{-5} sec^{-1}, one order of magnitude lower, resulted in σ_a = 227 MPa and 184 MPa for Lukens and Kawasaki alloys, respectively. The latter material, although of lower strength than Lukens steel, still possesses greater strength than annealed 2.25 Cr 1 Mo.

Another notable difference between the annealed steels and normalized and tempered alloys was in their respective hardening/softening responses to strain-controlled fatigue cycling. The initial cyclic hardening - cyclic softening - secondary cyclic hardening response of annealed 2.25 Cr 1 Mo was been observed independently by several workers [2.3,2.4,2.5]. Brinkman, et al. [2.3] found initial hardening of annealed material to result from the formation of Mo-C atom clusters. Once these clusters began to precipitate as Mo_2C carbides, the material softened and, when a sufficiently high density of these carbides had accumulated, secondary hardening occurred. Other examination of annealed material deformed under conditions of strain-controlled cycling at elevated temperatures [6] showed evidence of breakdown of pearlitic regions and coarsening of existing carbides. The formation of M2C carbides extending from the edges of pearlitic regions into the proeutectoid ferrite was noted, although little change in the ferrite structure was observed. Dislocation density was

higher, but cellular dislocation structures were not observed to develop. By comparison, both bainitic materials examined in this work and those examined by Swindeman and Strizak [2.7] were observed to initially cyclically soften to a steady-state stress level.

Examination of specimens aged isothermally at 838°K together with those strain-cycled to failure at both ambient and elevated temperatures aided in the qualitative determination of the relative roles of mechanical work and temperature in the establishment of the deformed microstructures of bainitic 2.25 Cr 1 Mo steels. These microstructures in turn establish mechanical properties. The recovery and coarsening of the ferrite lath structure were largely the result of cyclic deformation of the material as evidenced by the microstructural changes in Lukens specimens tested at ambient temperature.

These effects are accentuated at elevated temperatures where higher diffusion rates will lead to more rapid precipitation of carbides and coarsening of the existing precipitate structure. It is important to note, however, that this coarsening does not occur to any significant degree in the absence of cyclic deformation. Isothermally aging the alloy up to 150 hours, greater than the duration of any elevated-temperature fatigue test, caused only very localized coarsening of the lath structure and little change in either carbide sizes of densities. Strain cycling at elevated temperature produced an increased volume fraction of coarse carbides and a coarser ferrite substructure than was observed at ambient temperature. Another important effect of elevated temperature was the lowering of maximum tensile stress amplitude of $N_f/2$ from 434 MPa at 293°K to 338 MPa at 838°K and $\Delta\varepsilon_t = 1\%$.

Correlations between microstructural changes and observed mechanical behavior can be made by examining the microstructure in three conditions: as-received, after initial softening, and at failure. The most dramatic changes occurred during the first 10% of fatigue life, in which the observed cyclic softening took place. The drop in stress amplitude appears to be caused by the rapid coarsening of the bainitic microstructure, and steady-state strengthening is thereafter thought to be provided by the M2C carbides that precipitated during the softening. Modest coarsening of both the lath structure and carbides, and the appearance of a small amount of additional precipitates within laths and at

boundaries were the only appreciable changes noted between the end of cyclic softening and fracture.

Although the mechanical behavior of Kawasaki material is similar to that of the Lukens alloy in terms of observed cyclic softening and N_f, there are marked differences in their cyclic strength levels, the former having 25% to 32% lower maximum tensile stress amplitudes. These differences can be rationalized in terms of Pickering's derivations [2.8]. Whereas the Lukens material was completely bainitic in the unstressed state, comprising a relatively fine ferrite lath structure and containing fine uniform distributions of both M_2C within the laths and carbides at boundaries, the Kawasaki alloy comprised a mixture of coarse bainitic lath structure and large subgrains of ferrite similar to those observed in annealed 2.25 Cr 1 Mo steel, with a much lower density of M2C and few boundary precipitates. Deformed Kawasaki material contained very coarse subgrains of ferrite and a low density of precipitates both within grains and at the subgrain boundaries. The Lukens material comprised significantly smaller equiaxed grains containing a heavy, uniform distribution of M_2C and subgrain and lath boundaries decorated with large amounts of precipitates. The observations of a combination of less precipitation and larger ferrite subgrains found in the weaker Kawasaki alloy were compatible with expectations expressed in Pickering's expression of the 0.02%-proof strength of a bainitic steel [2.8] in which the bulk of strengthening in bainitic steels was determined to arise from the dimensions of ferrite substructures and particle spacing.

2.4 REFERENCES

2.1 Atkins, M., Atlas of Continuous Cooling Transformation Diagrams for Engineering Steels, British Steel Corporation, Sheffield, England.

2.2 Dyson, D. J., S. R. Keown, D. Raynor and J. A. Whiteman, "The Orientation Relationship and Growth Direction of Mo_2C in Ferrite," Acta Metallurgica, Vol. 14, July 1966, pp. 867-875.

2.3 Brinkman, et al., "Time Dependent Strain Controlled Fatigue Behavior of Annealed 2 1/4 Cr 1 Mo Steel for use in Nuclear Steam Generator Design," J. Nuclear Materials, Vol. 62, 1976, p. 181.

2.4 Jaske, C. E., and H. Mindlin, "Elevated Temperature Low Cycle Fatigue Behavior of 2 1/4 Cr 1 Mo and 1 Cr 1 Mo 1/4 V-Steels," Symposion on 2 1/4 Cr 1 Mo Steel in Pressure Vessels and Piping, ASME, 1971, p. 137.

2.5 Jones, W. B., and J. A. Van Den Avyle, "Substructure and Strengthening Mechanisms in 2.25 Cr 1 Mo Steel at Elevated Temperatures," Metallurgical Trans. A., Vol. 11A, 1980,. p. 1275.

2.6 Baird, J. D., and A. Jamieson, "High Temperature Tensile Properties of Some Synthesized Iron Alloys Containing Chromium and Molybdenum," J. Iron and Steel Institute, Vol. 210, Nov. 1972, p. 841.

2.7 Swindeman, R. W., and J. P. Strizak, "Response of Bainitic 2 1/4 Cr 1 Mo Steel to Creep Fatigue Loadings at 482°C," Oak Ridge National Laboratory, 1982.

2.8 Pickering, F. B., Physical Metallurgy and the Design of Steels, Applied Science Publishers, 1978.

Table 2.1 Compositions and Heat Treatment of Alloys

	Lukens	Kawasaki
C	0.13	0.13
Mn	0.33	0.53
P	0.012	0.003
S	0.02	0.003
Cu	0.15	0.16
Si	0.05	0.25
Ni	0.12	0.15
Cr	2.34	2.33
Mo	0.99	0.96
Sn	0.008	0.001
Al	0.004	0.011
V	-	0.01
As	-	0.002
Sb		0.005

Heat Treatments: Lukens------900°C-12h-AC-690°C-17h-AC

Kawasaki--1070°C-18h-Q-650°C-17h-AC

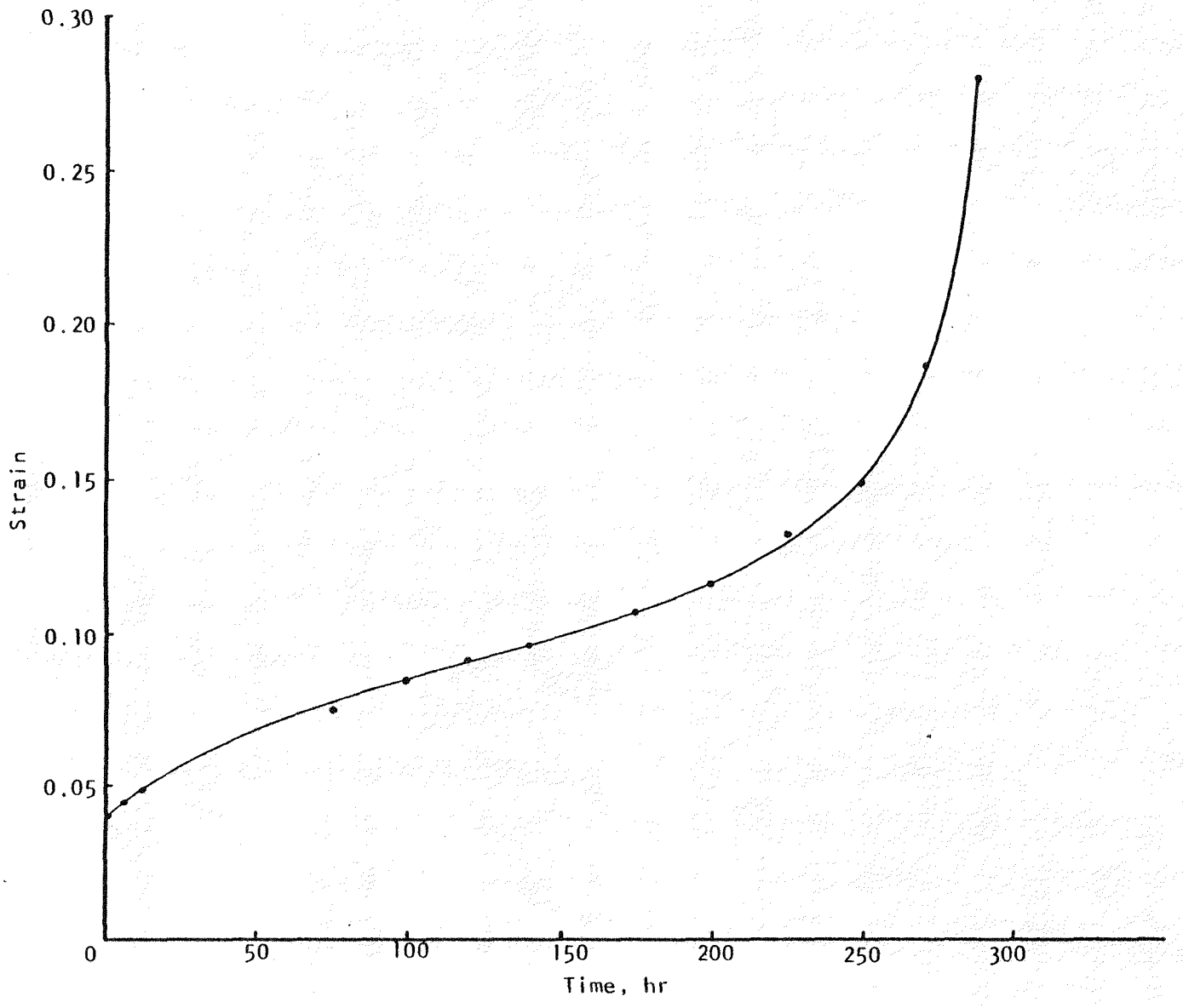

Figure 2.1 Strain versus time creep curve for 2.25 Cr 1 Mo steel at 35.75 ksi and 565°C. Total time to failure was 289.25 hours.

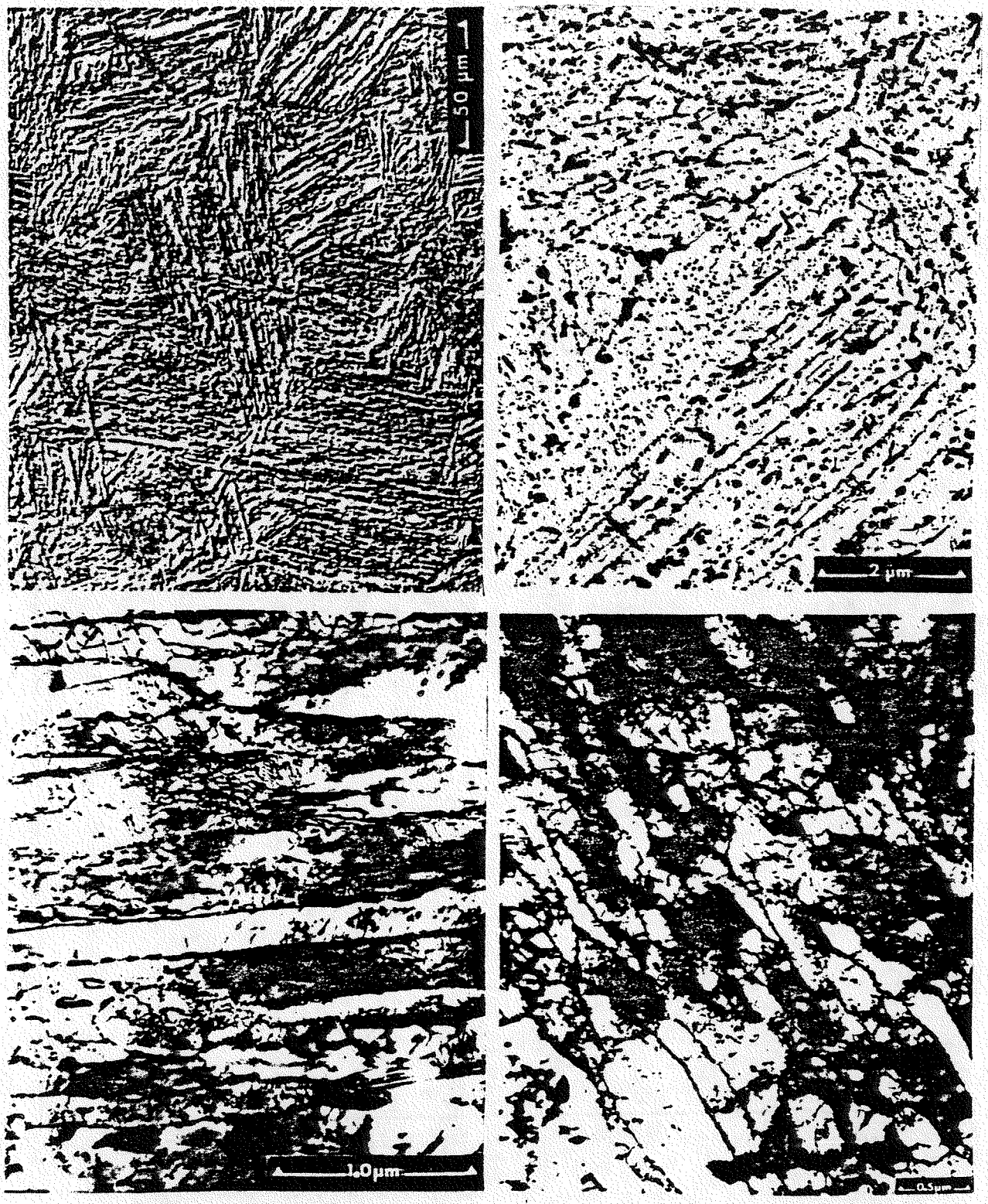

Figure 2.2 The microstructure of as-received Lukens steel was composed of ferrite lath packets, three predominant types of carbides, and occasional dislocation networks. Imaging techniques were: Nomarski Differential Interference Contrast (DIC0, carbide extraction replica, and thin foils.

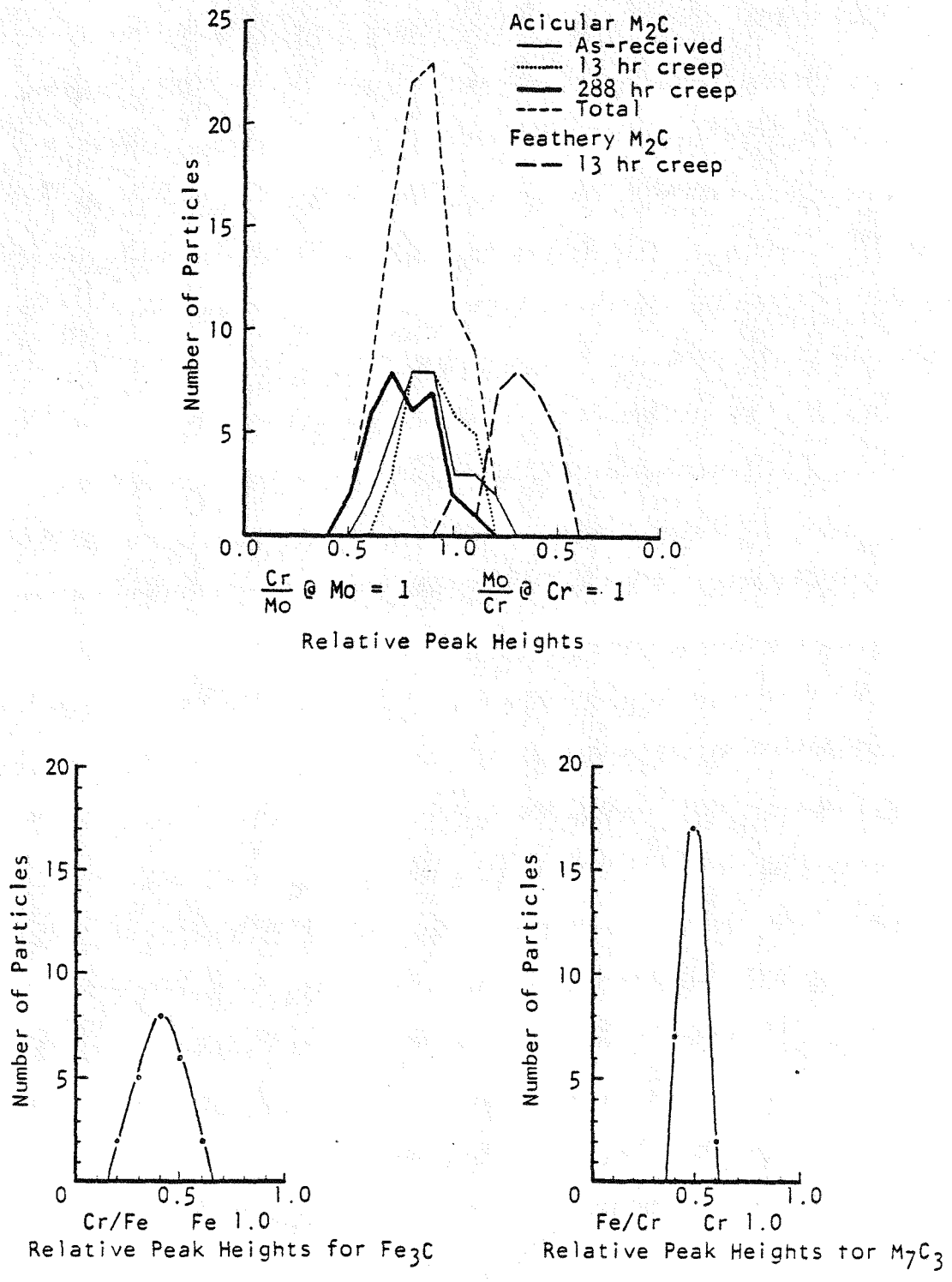

Figure 2.3 Distributions of relative peak height ratios from energy dispersive x-ray spectroscopy of extracted carbides.

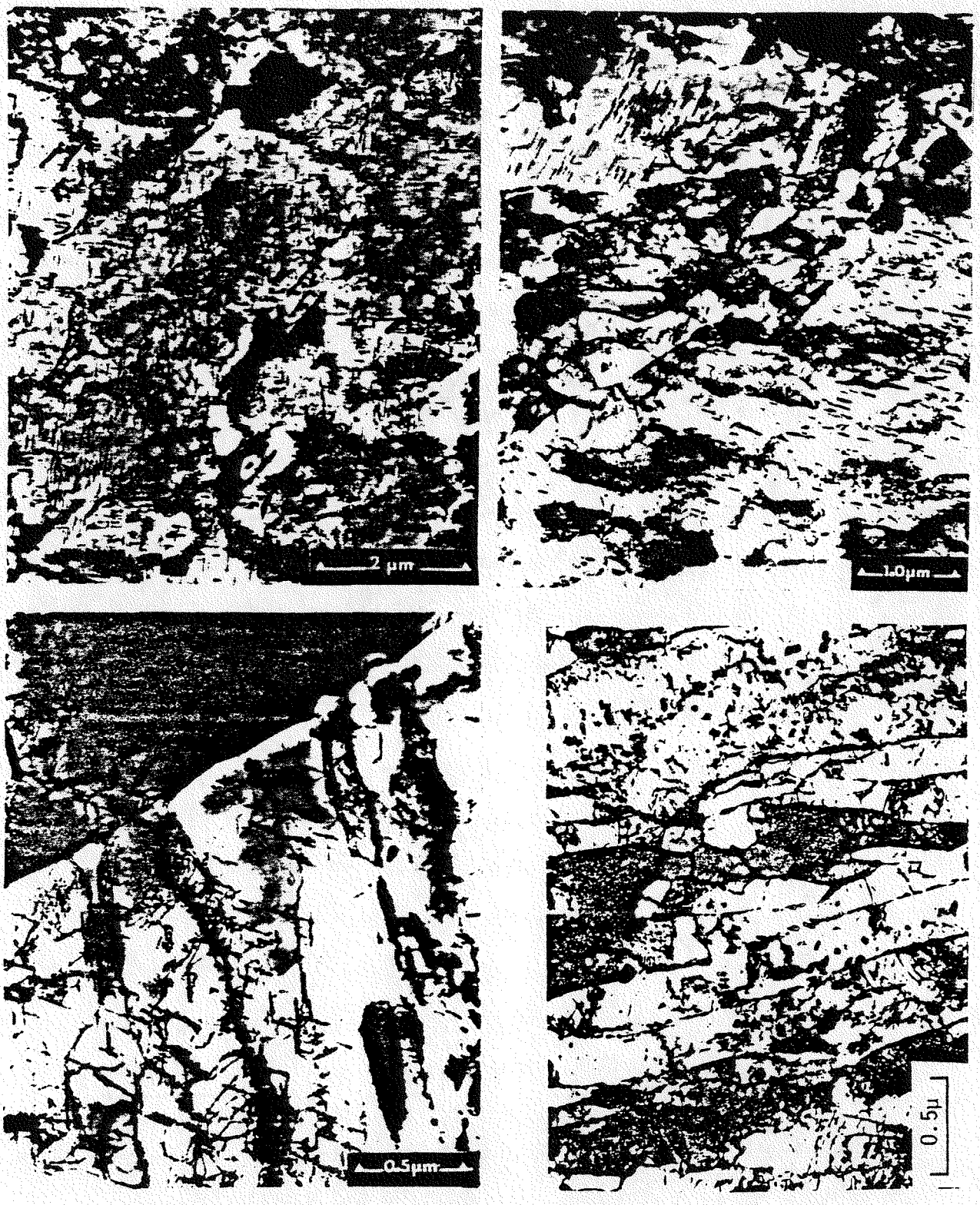

Figure 2.4 Thirteen hours of creep resulted in extensive precipitation of acicular M_2C carbides, except near boundaries. Unstrained aging for 100 hours did not result in similar precipitation (frame 4).

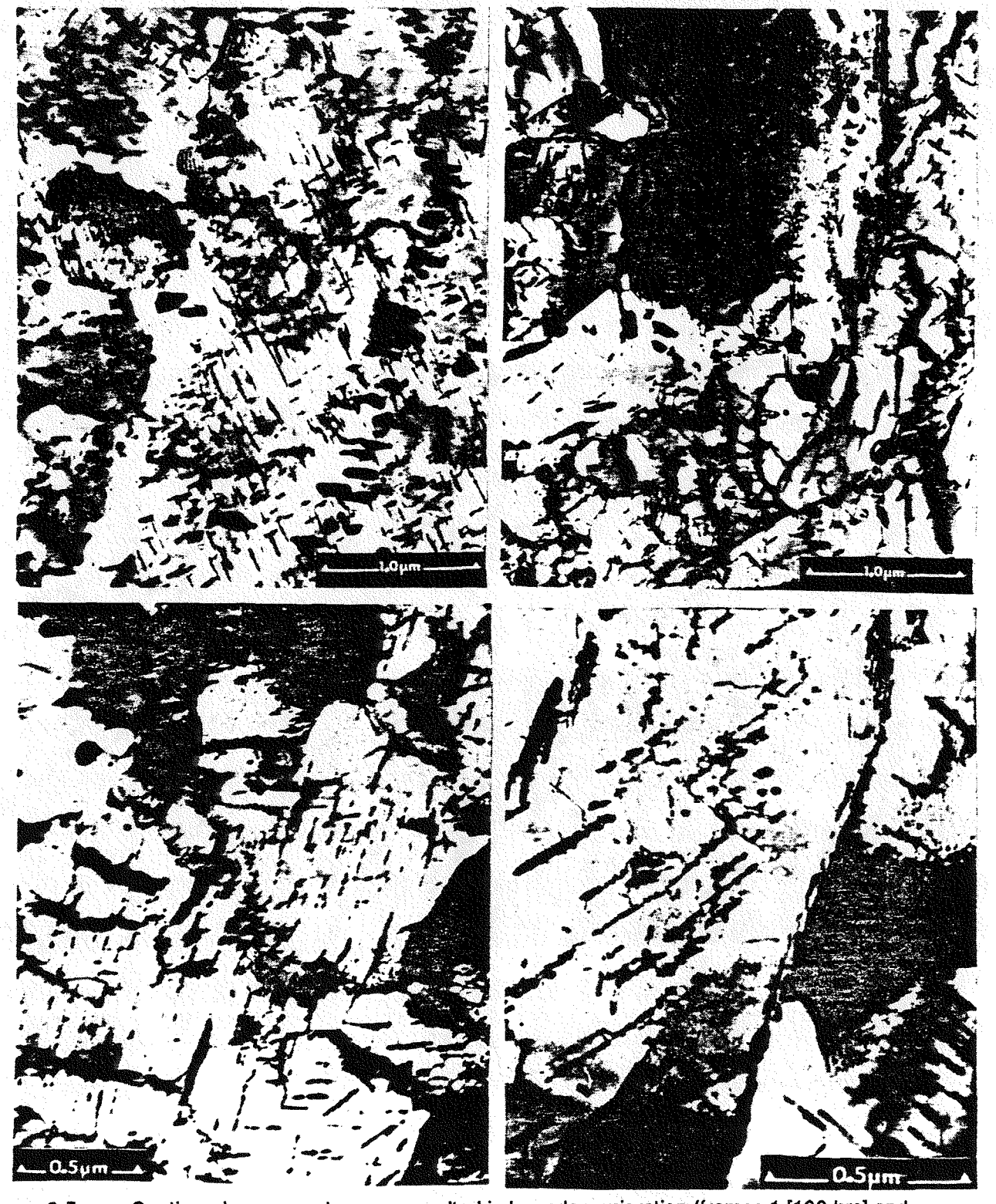

Figure 2.5 Continued exposure to creep resulted in boundary migration (frames 1 [100 hrs] and 2[250 hrs]) and eventually to the deformation of acicular carbides as a result of grain boundary sliding (frames 3 and 4 [288 hrs])/

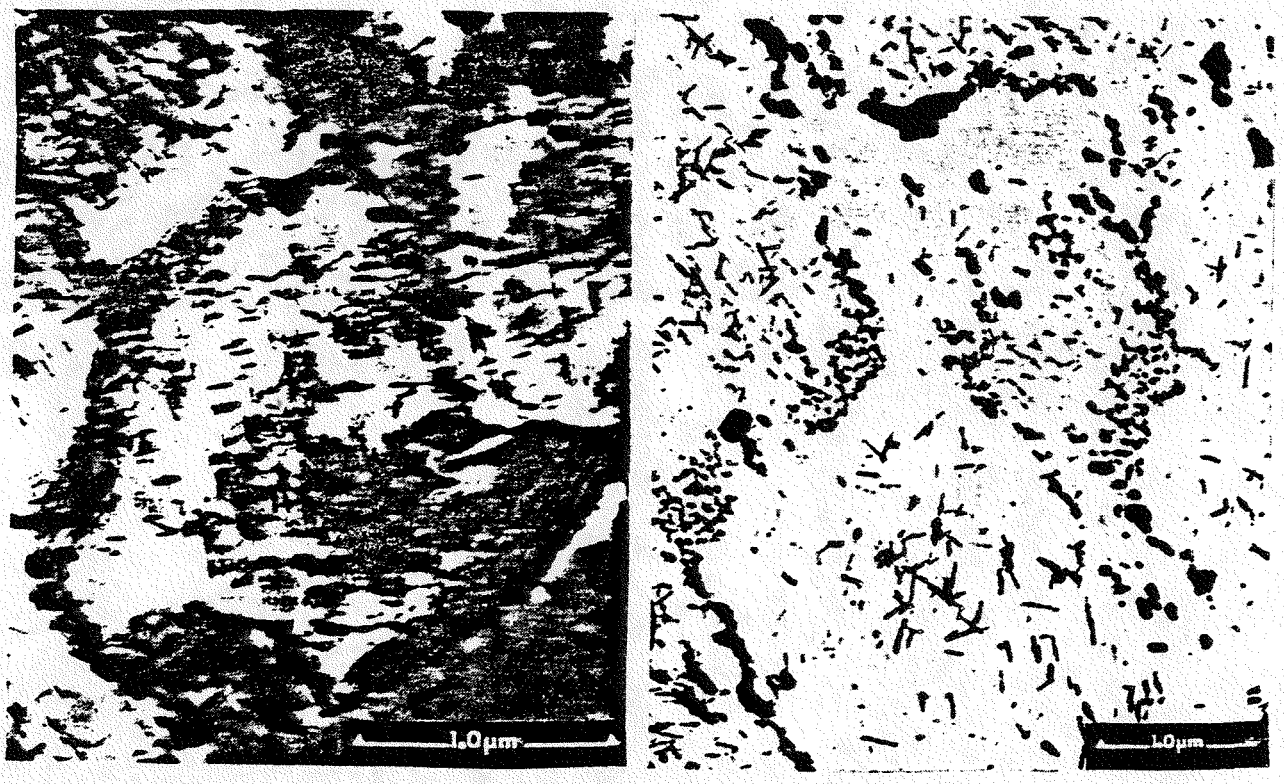

Figure 2.6 Occasionally, many precipitates were observed within boundaries, and are believed to be a plate-like form of M_2C. They may form in conjunction with boundary migration, which necessitates the dissolution of existing M_2C followed by reprecipitation within the reoriented matrix. Frame 1 is of 100 hour material; frame 2, of a carbide extraction of 288 hour material.

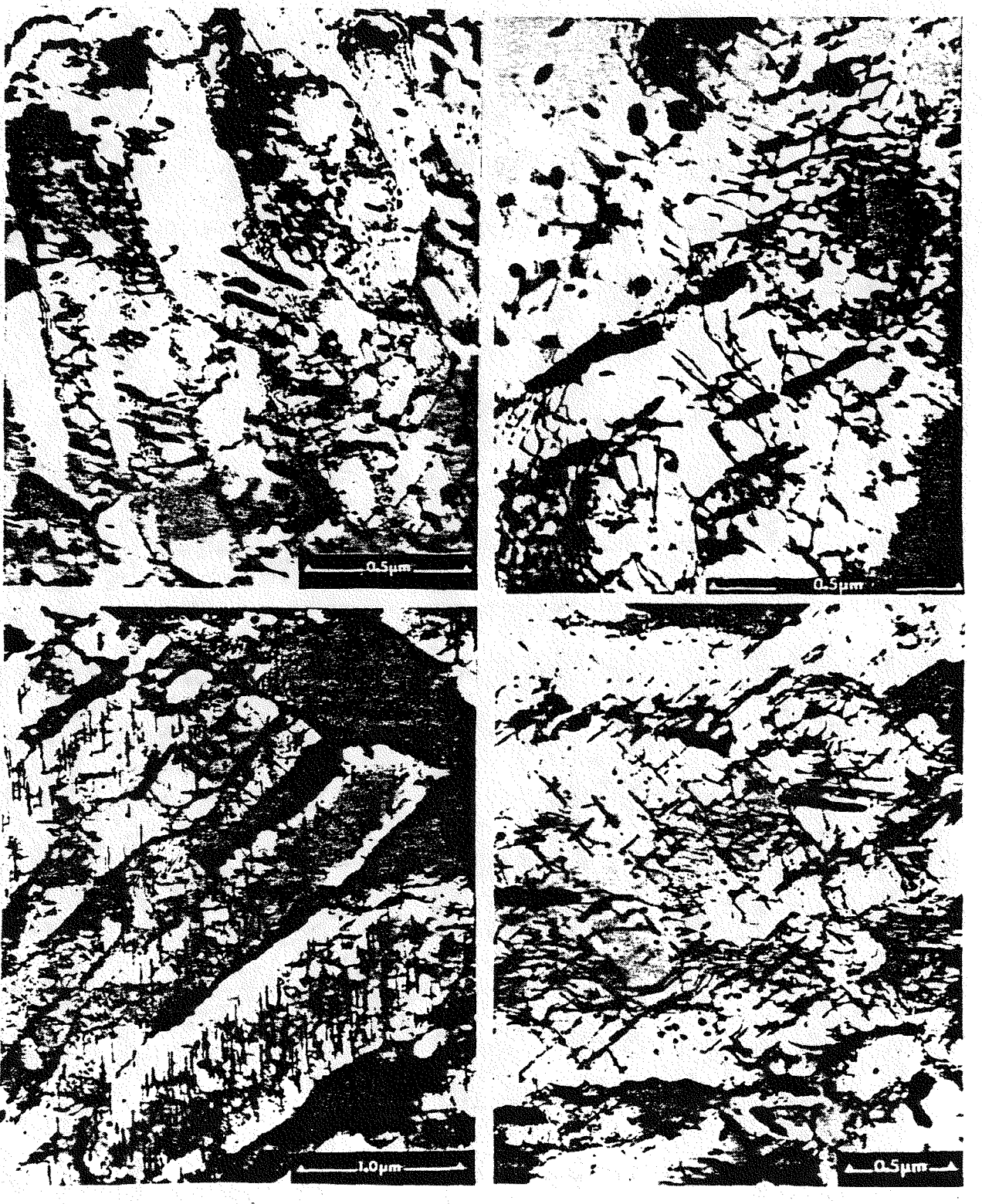

Figure 2.7 Dislocation networks were rarely observed in as-received material, and had usually formed nodes (frames 1 and 2). Dislocations in parallel arrays were common aftger 13 hours of creep, and were piled up against the acicular M_2C barriers (frames 3 and 4).

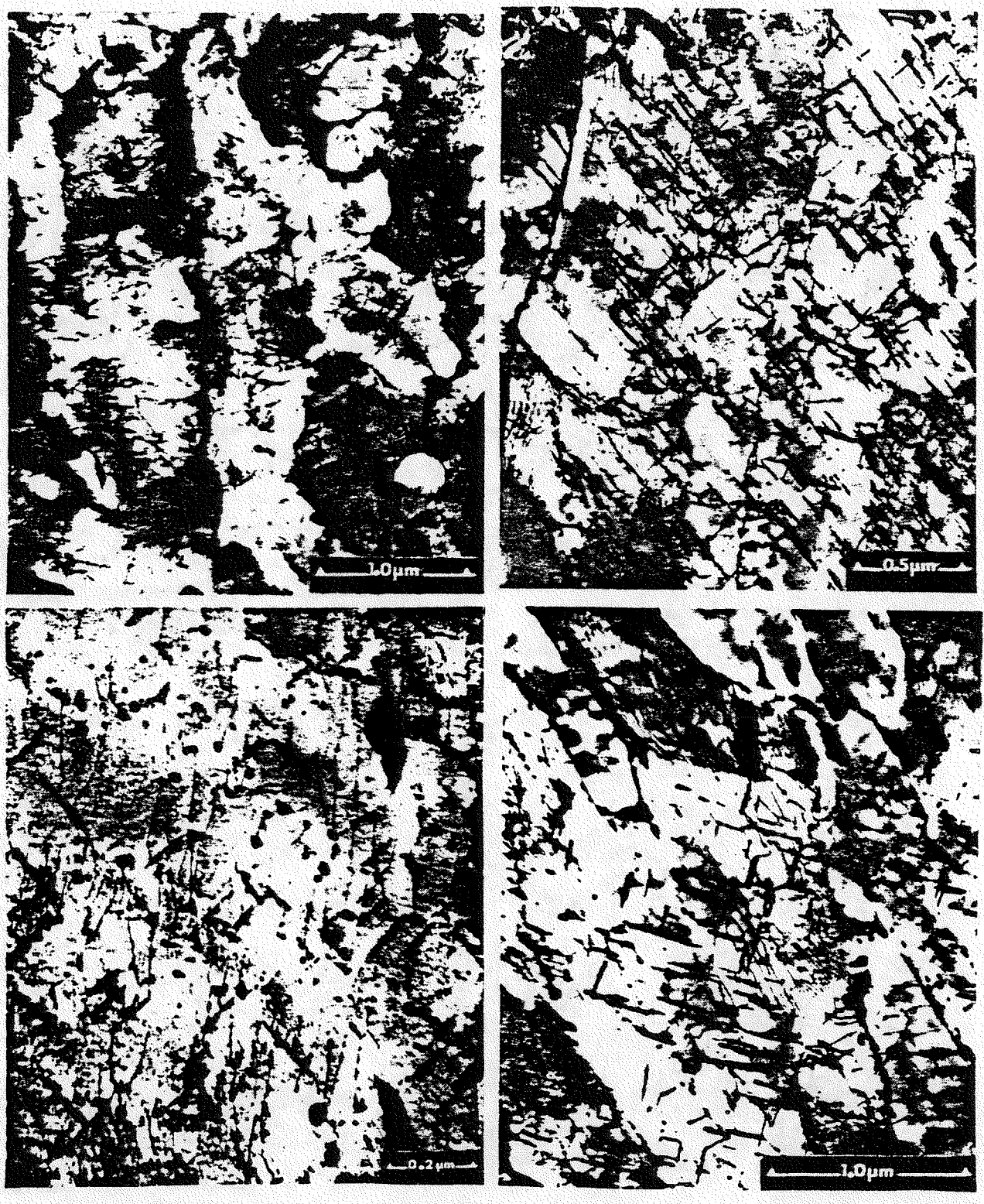

Figure 2.8 During steady state creep, parallel dislocation arrays undergo climb, cross lip, or other maneuvers in order to bypass obstacles of to form lower energy boundary networks. A T-shaped array is precent in frame 1 (48 hours), and dislocation segments trapped by particles are visible in the remaining frames (48 hour, 100 hour, and 180 hours, respectively).

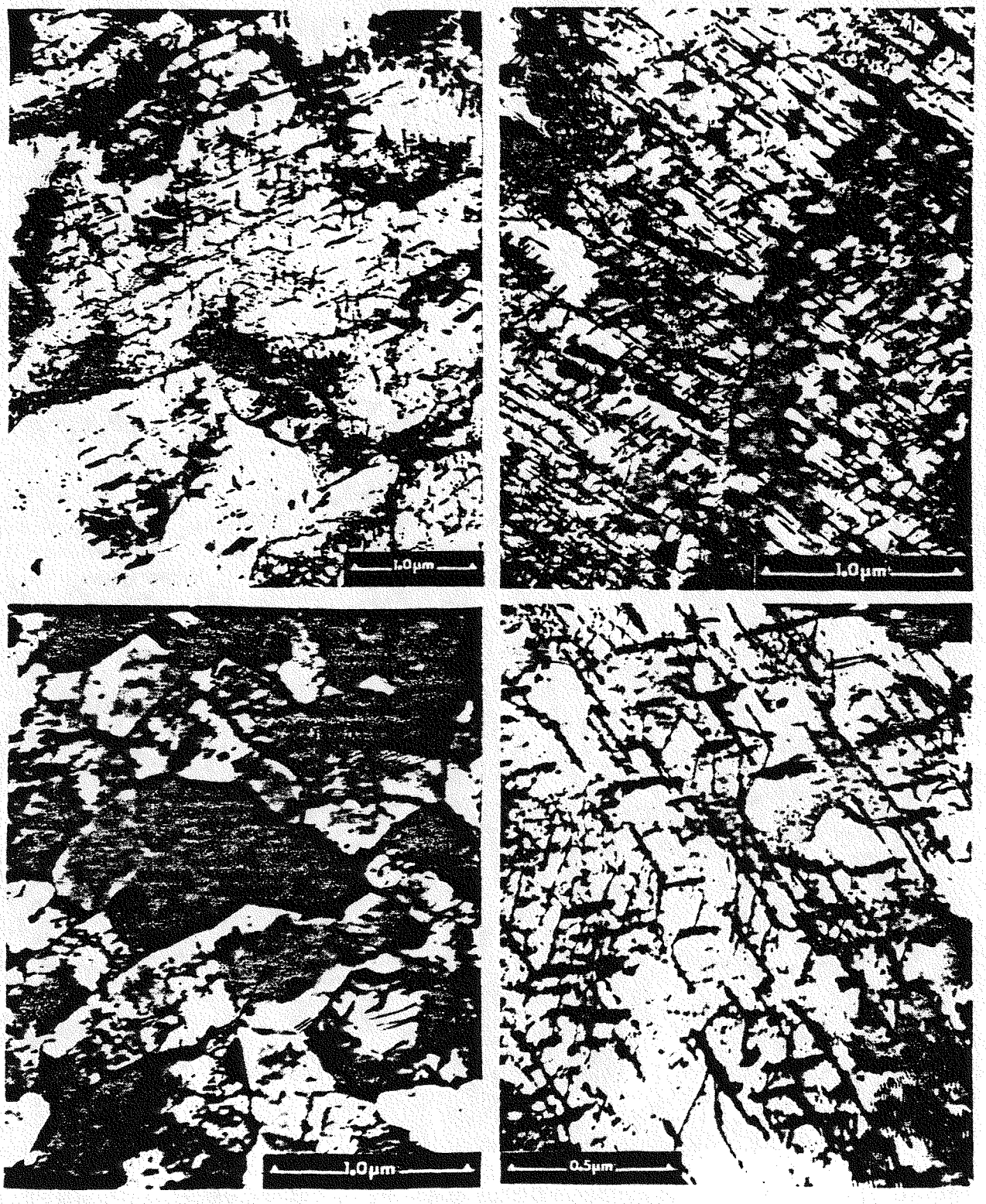

Figure 2.9 Material in the tertiary stage of creep exhibited the full spectrum of dislocation structures, from nearly disloction free new grains to parallel pile-ups, to trapped segments, to boundary arrangements (288 hours).

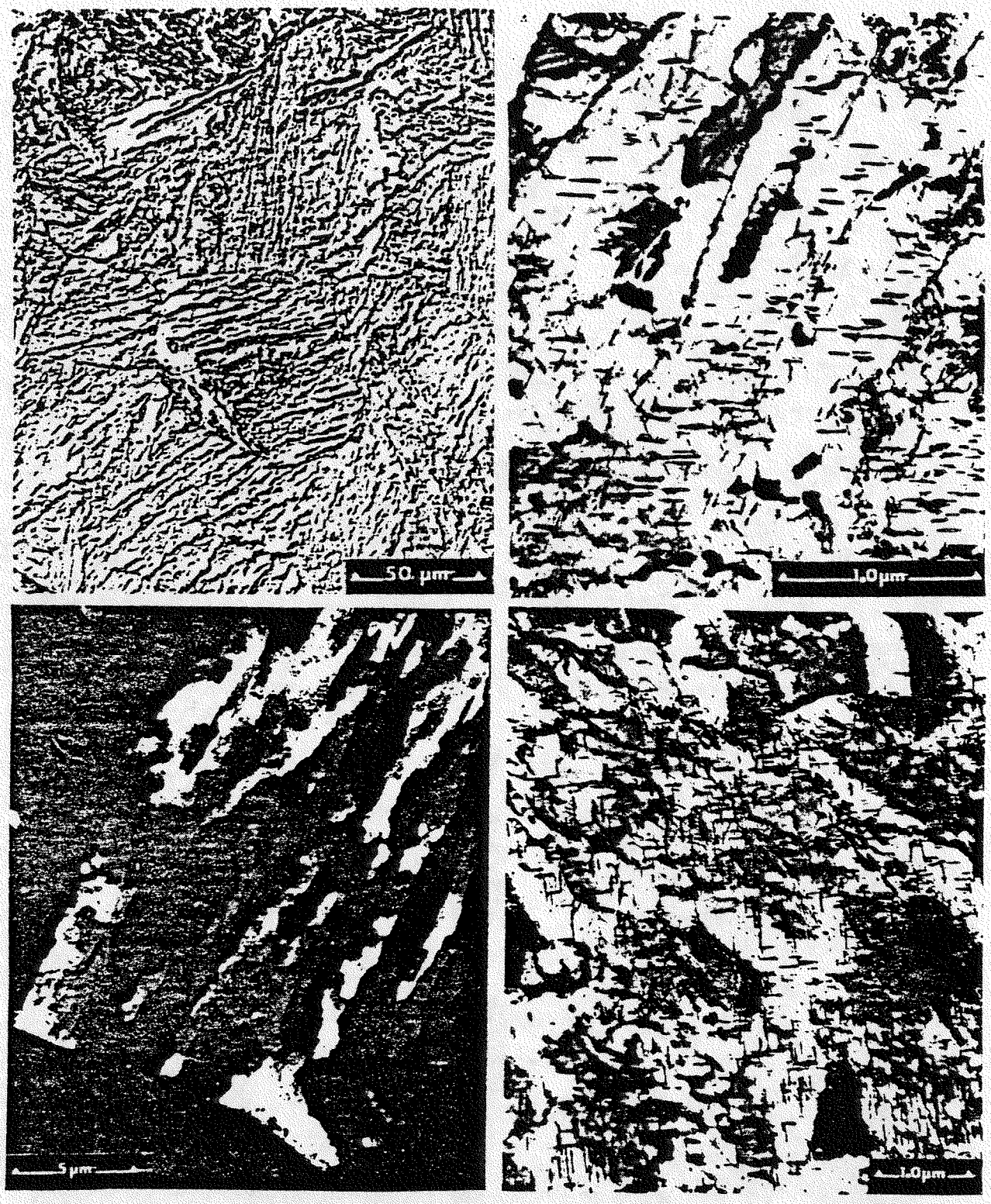

Figure 2.10 Lath boundaries disappeared during creep. Frame 1 exhibits blocky regions of a single orientation (DIC image), and Frame 2 is a thin foil image of coalesced laths, both at 100 hours. Frame 3 is a dark field image of a lath packet which exhibits coalescence and boundary migration (180 hours). In frame 4, carbides mark the prioer positions of lath boundaries (180 hours).

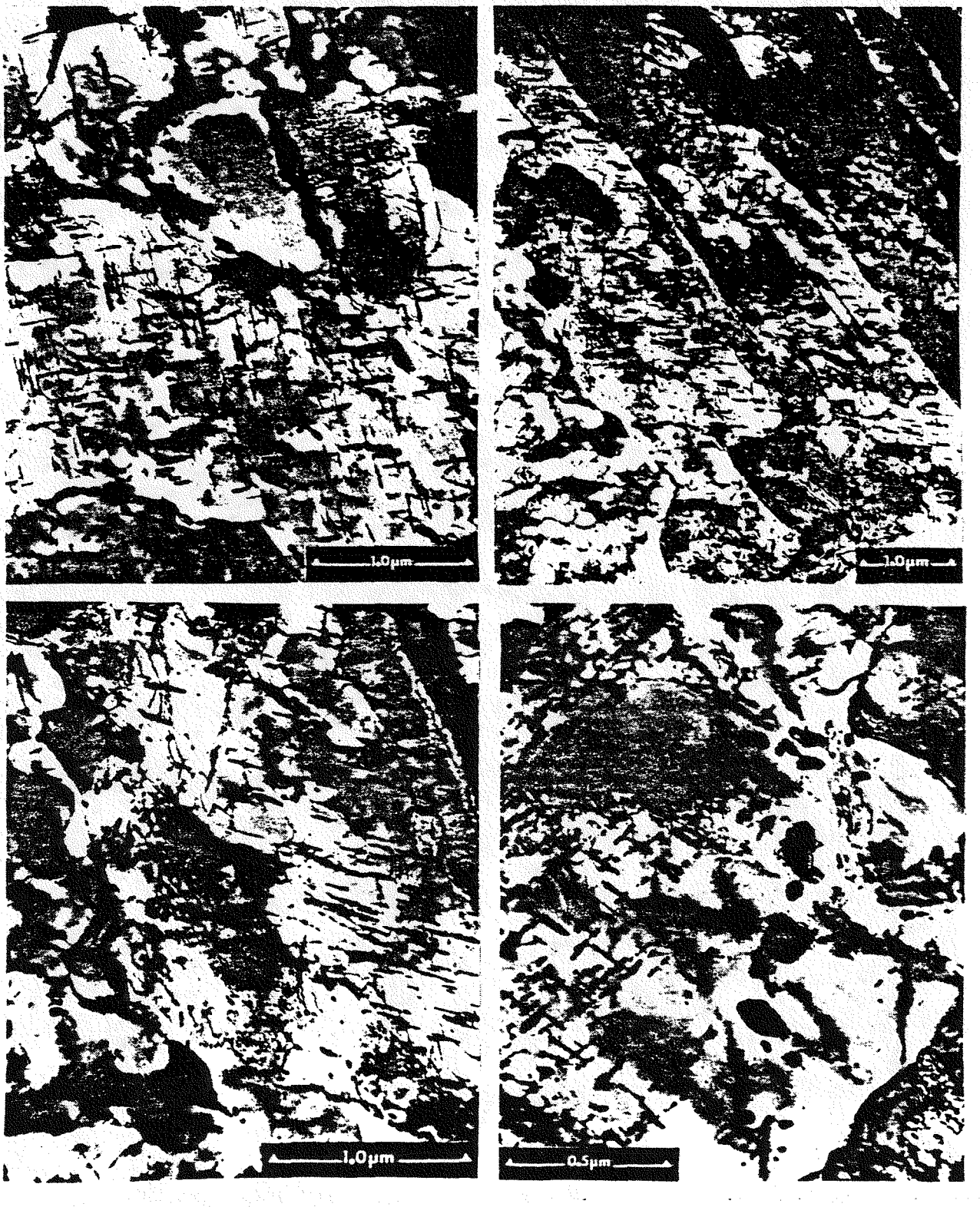

Figure 2.11 Boundary activity was not limited to lath boundaries (frame 1 at 180 hours), but also to the prior austenite grain boundaries. Frames 2 and 3 (180 hours) show a boundary bowing between large precipitates. Frame 4 (288 hours) exhibits a boundary which was able to break away from its constraining carbides.

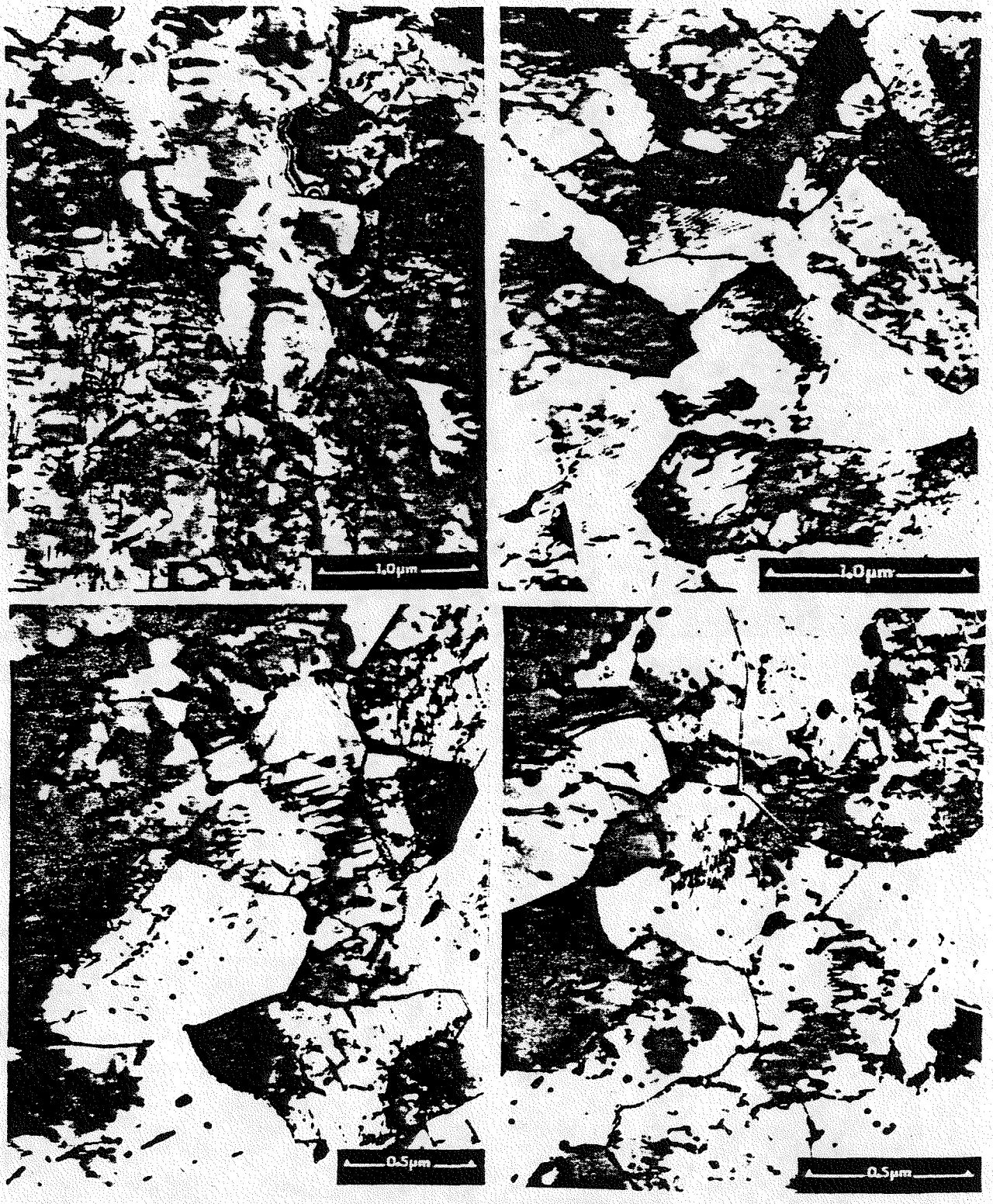

Figure 2.12 Polygonal grains appeared near the end of the material's creep life Frame 1, at 180 hours, indicates that prior austenite grain boundaries provide nucleation sties. The remaining frames, at 288 hours, illustrate polygonal grains with very few acicular carbides.

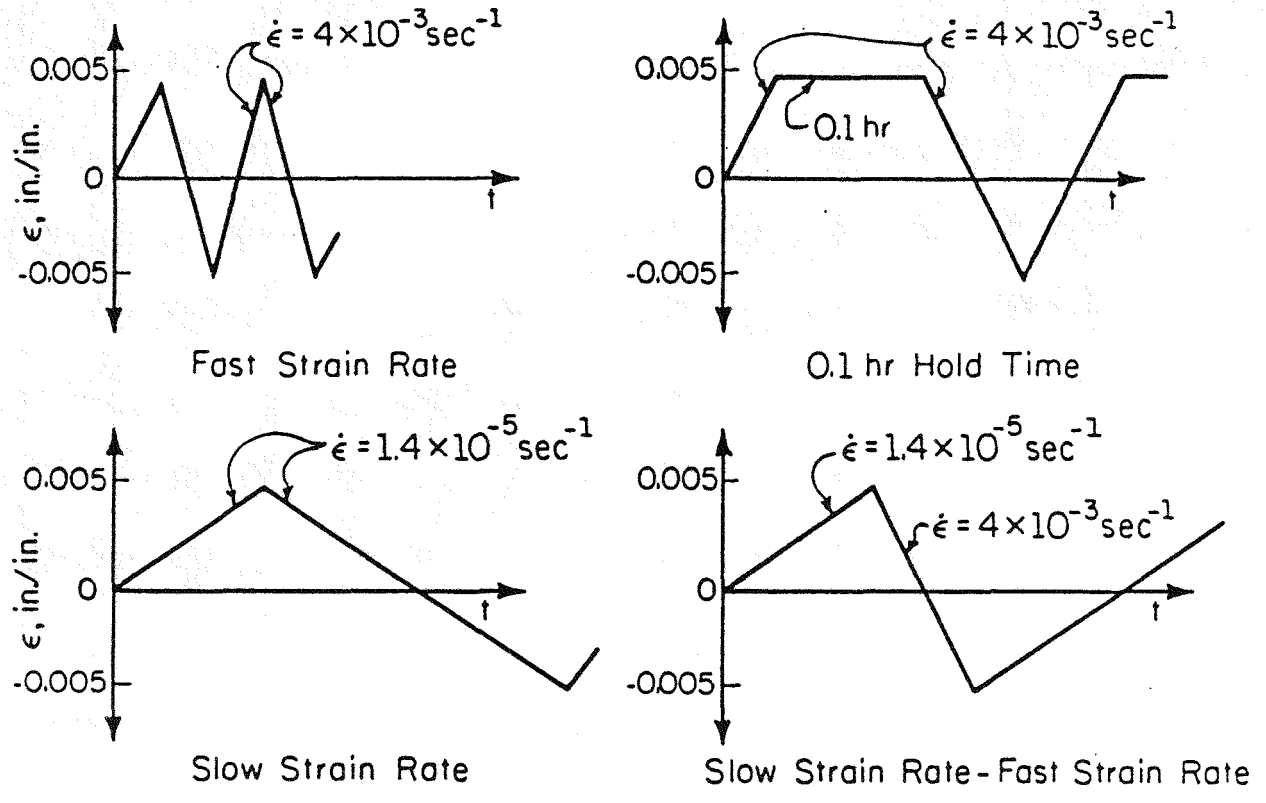

Figure 2.13 Schematic representations of cyclic waveforms used in mechanical testing

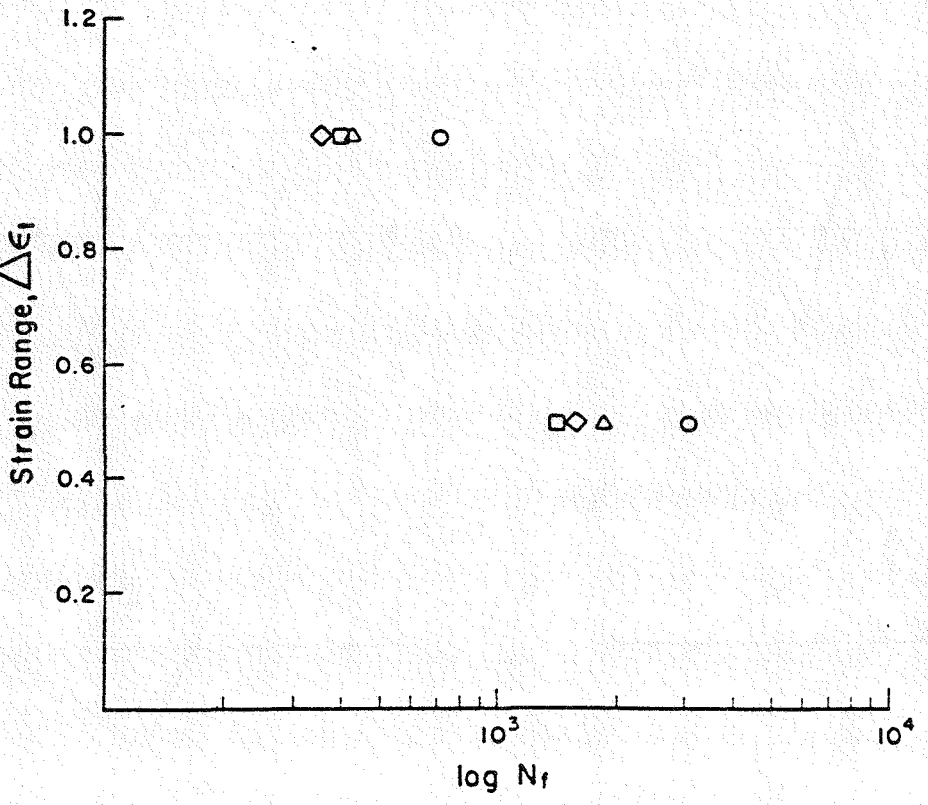

Figure 2.14 Plots of strain range as a function of log cycles to failure, Kawasaki alloy

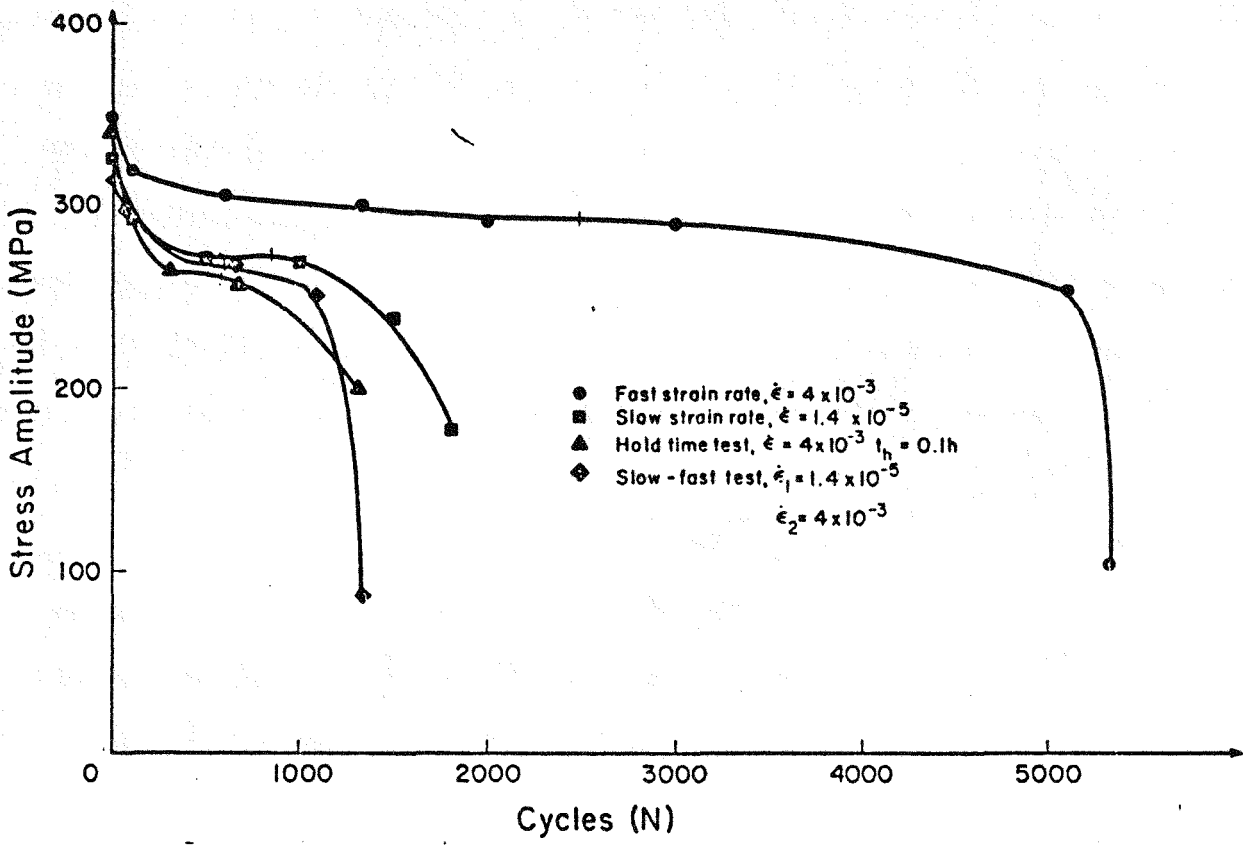

Figure 2.15 (a) Plots of maximum tensile stress amplitude as a function of cycles at $\Delta\varepsilon_t$ = 1% for four cyclic waveforms, Lukens alloy

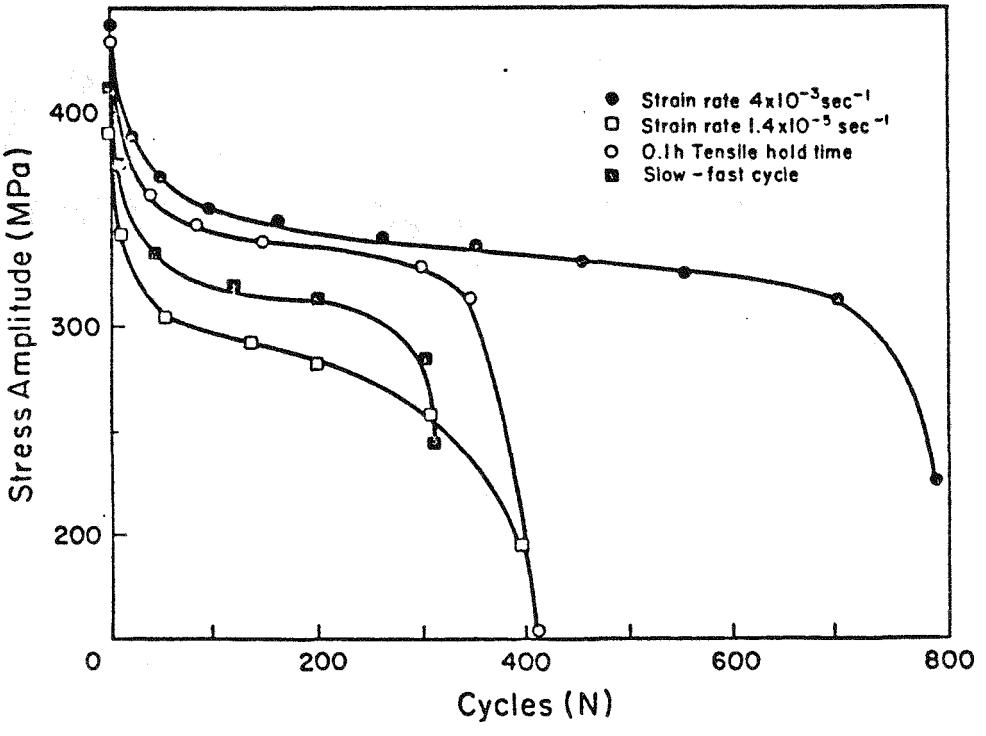

Figure 2.15 (b) Plots of maximum tensile stress amplitude as a function of cycles at $\Delta\varepsilon_t$ = 0.5% for four cyclic waveforms, Lukens alloy

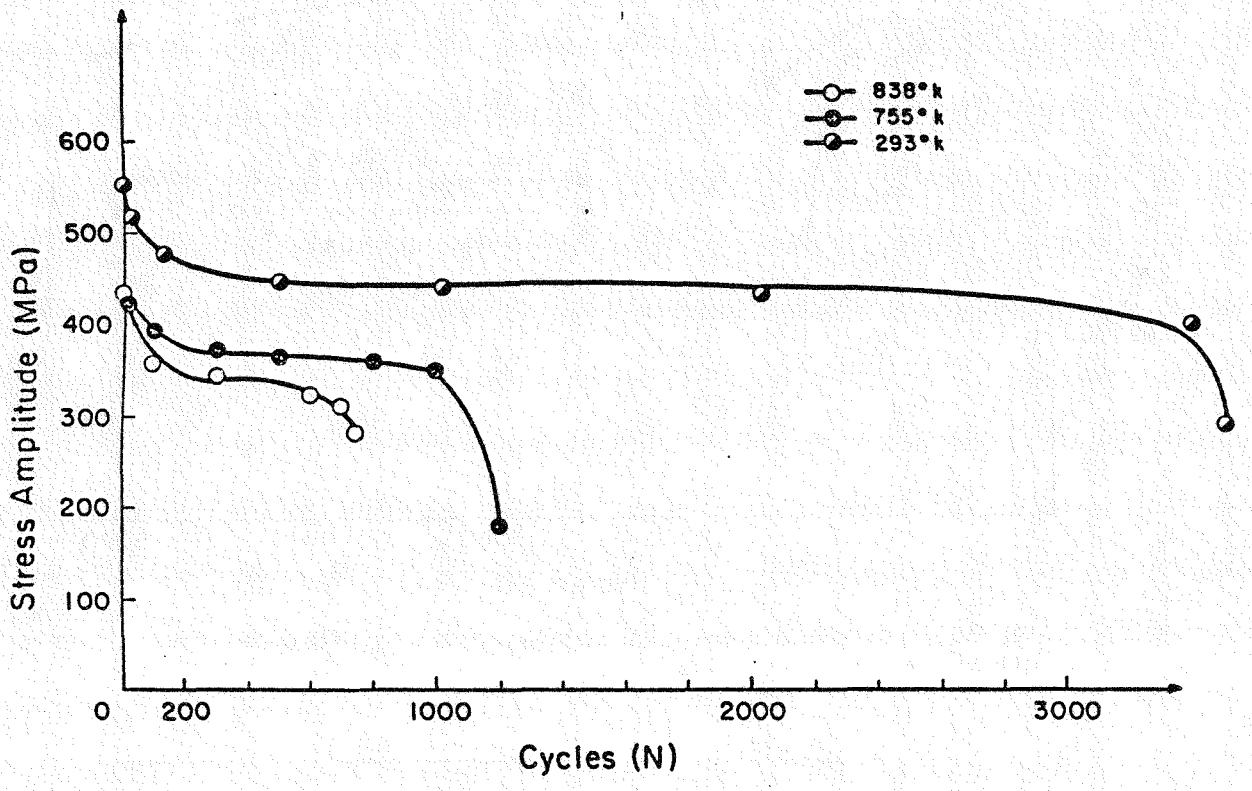

Figure 2.16 Plots of maximum tensile stress amplitude as a function of cycles at $\Delta\varepsilon_t = 1\%$ and $\dot{\varepsilon} = 4 \times 10^{-3}$ sec^{-1}, Lukens alloy at 293, 755 and 838°K

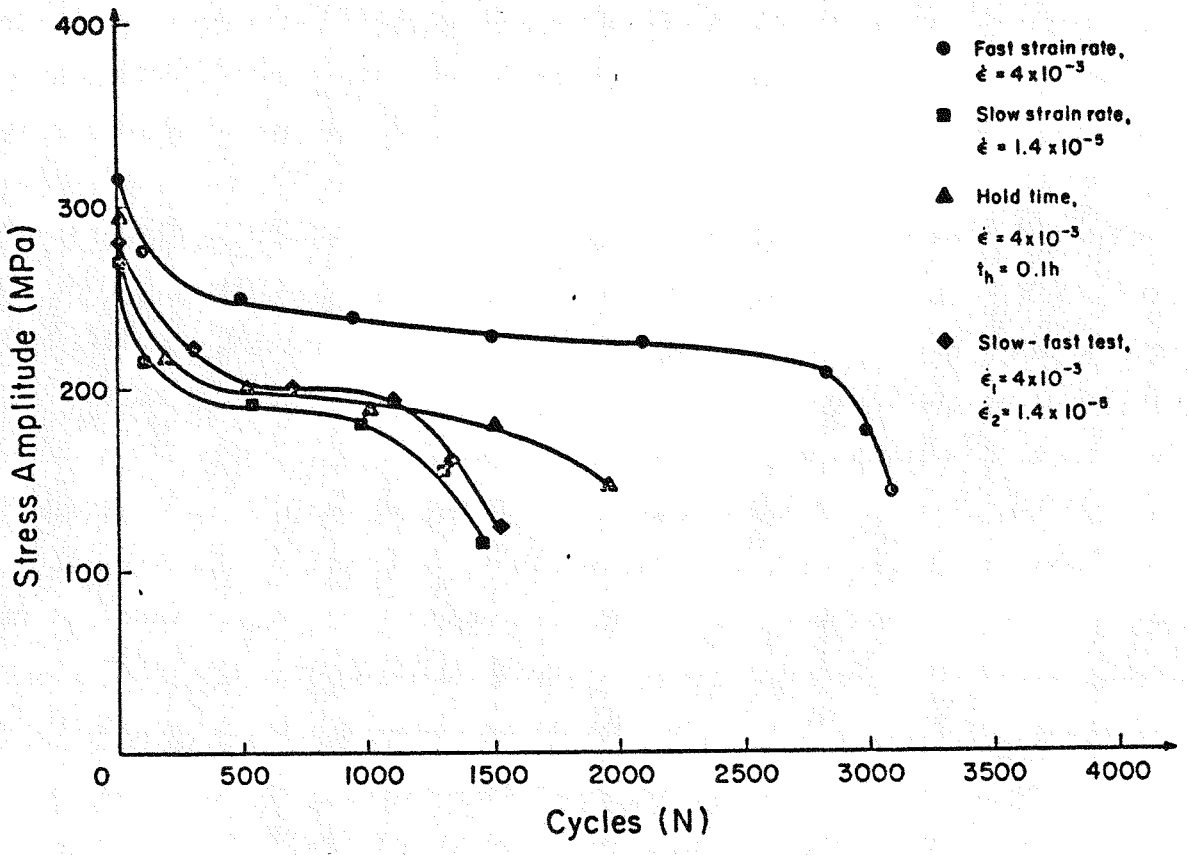

Figure 2.17 (a) Plots of maximum tensile stress amplitude as a function of cycles at $\Delta\varepsilon_t$ = 1% for four cyclic waveforms, Lukens alloy

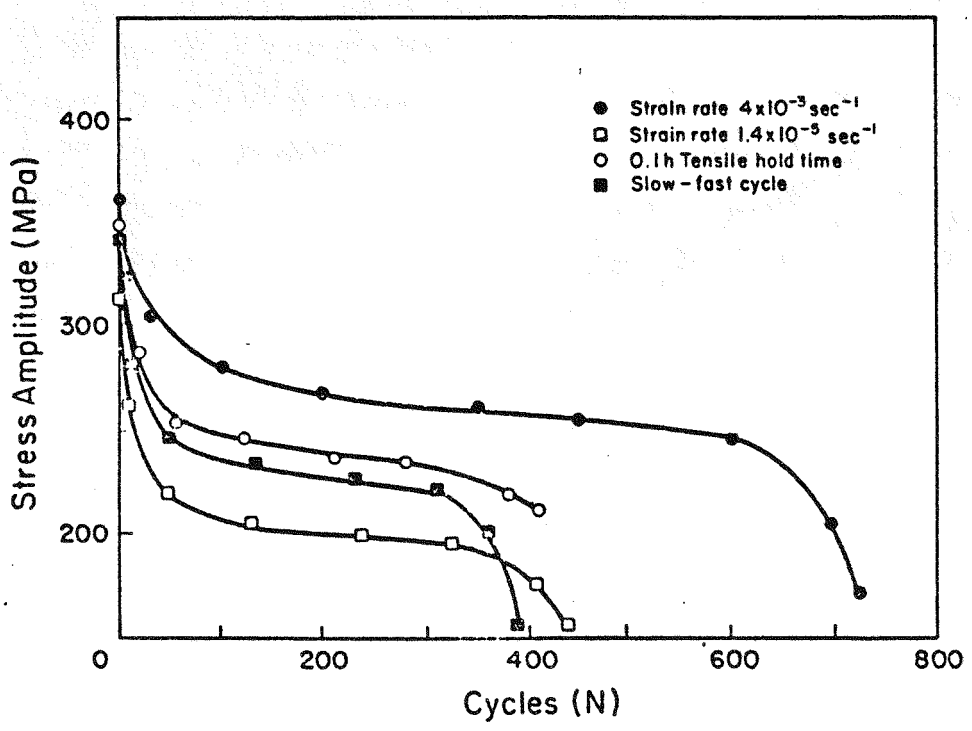

Figure 2.17 (b) Plots of maximum tensile stress amplitude as a function of cycles at $\Delta\varepsilon_t$ = 0.5% for four cyclic waveforms, Kawasaki alloy

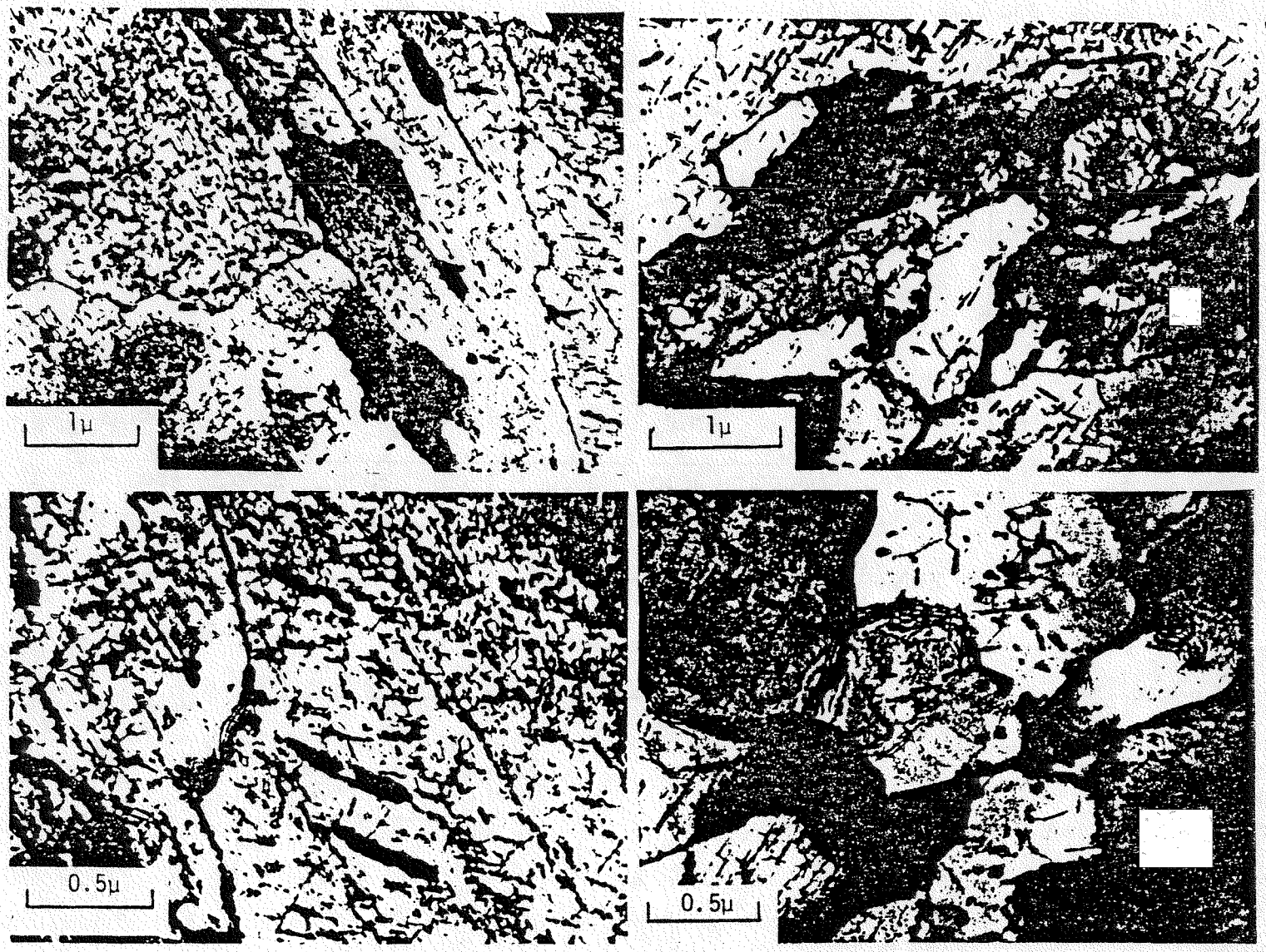

Figure 2.18 Lukens steel exposed to slow strain rate fatigue contained acicular M_2C carbides and extensively reorganized boundaries. The material of frames 1 and 2 was exposed to 1/2% strain cycles, frames 3 and 4 to 1% strain cycles.

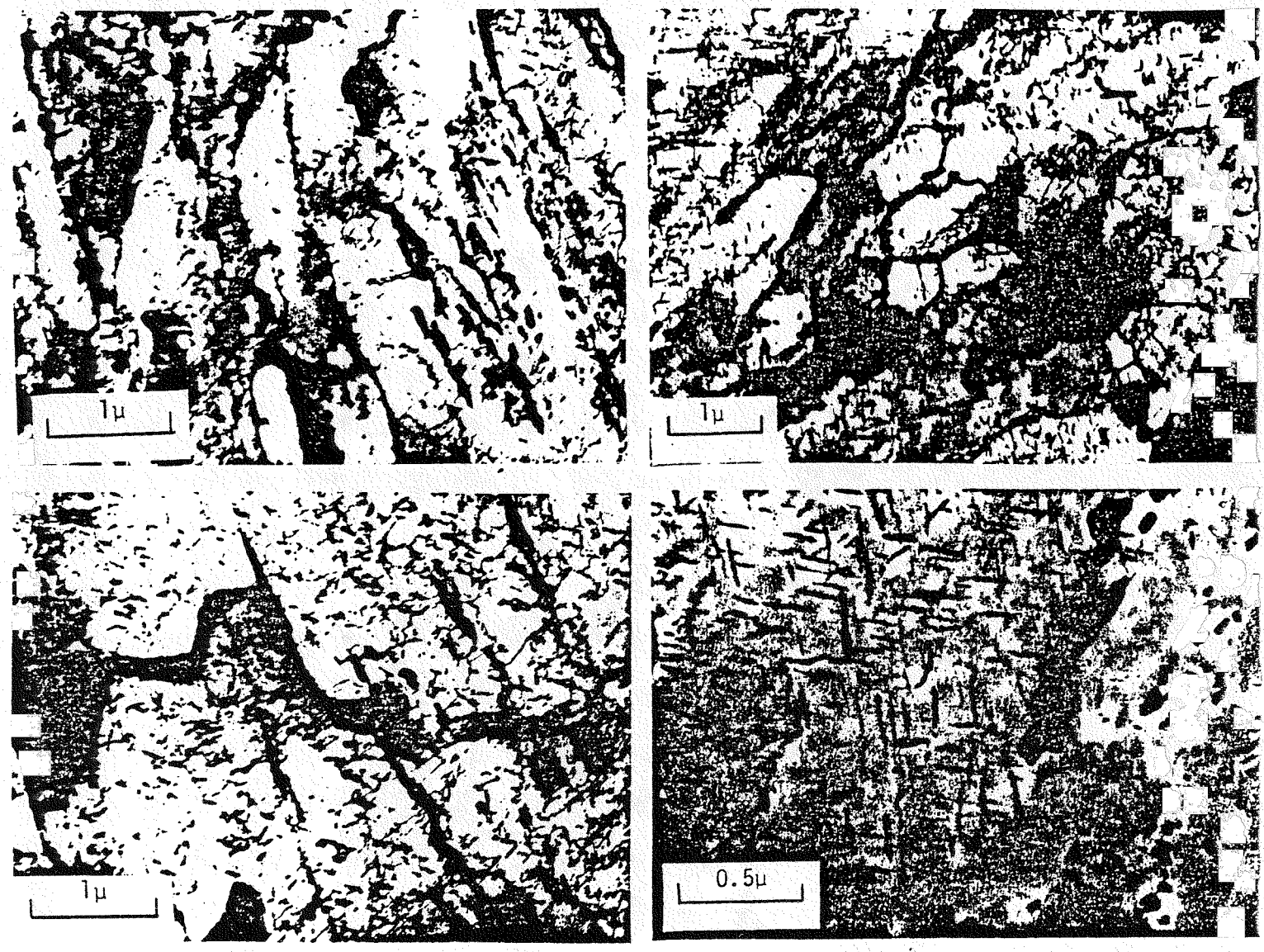

Figure 2.19 Lukens steel subjected to 1/2% strain at fast strain rates also had acicular carbides and extensively reorganized boundaries. The material of frames 1 and 2 was testedat room temperature, frames 3 and 4 at 838°K..

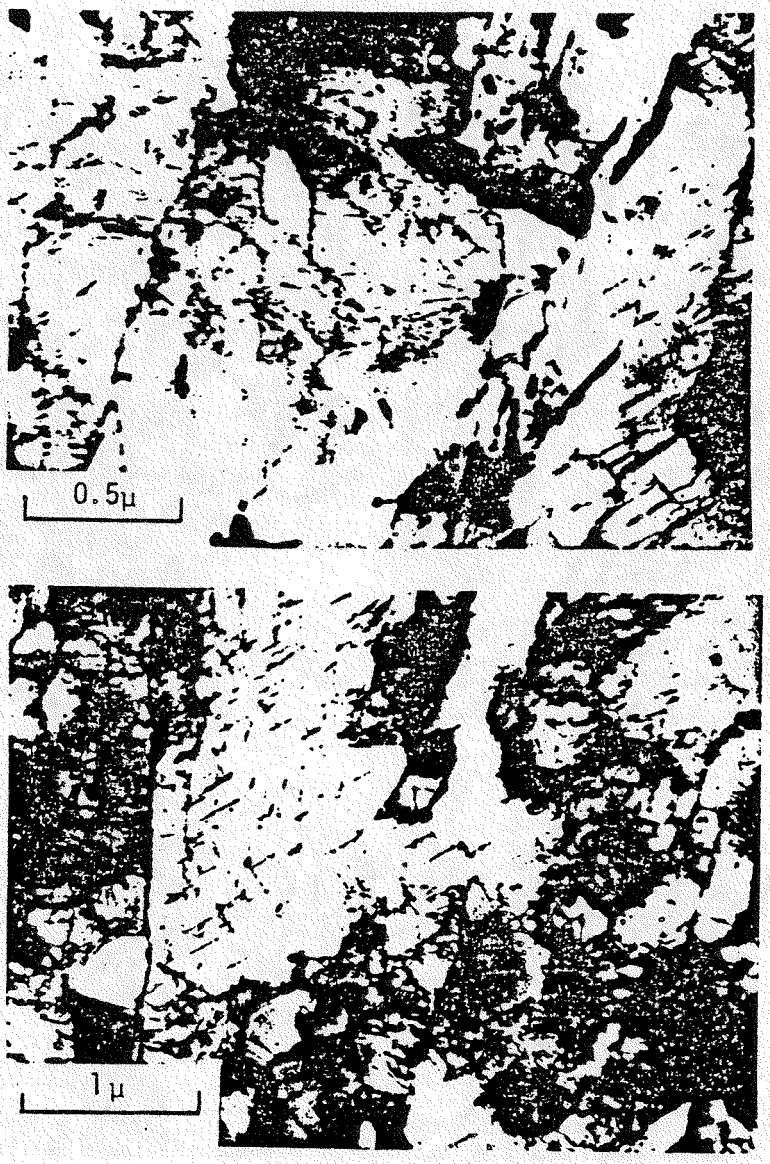

Figure 2.20 Lukens material after 70 cycles at 1% strain and fast strain rates had already undergone precipitation and boundary migration.

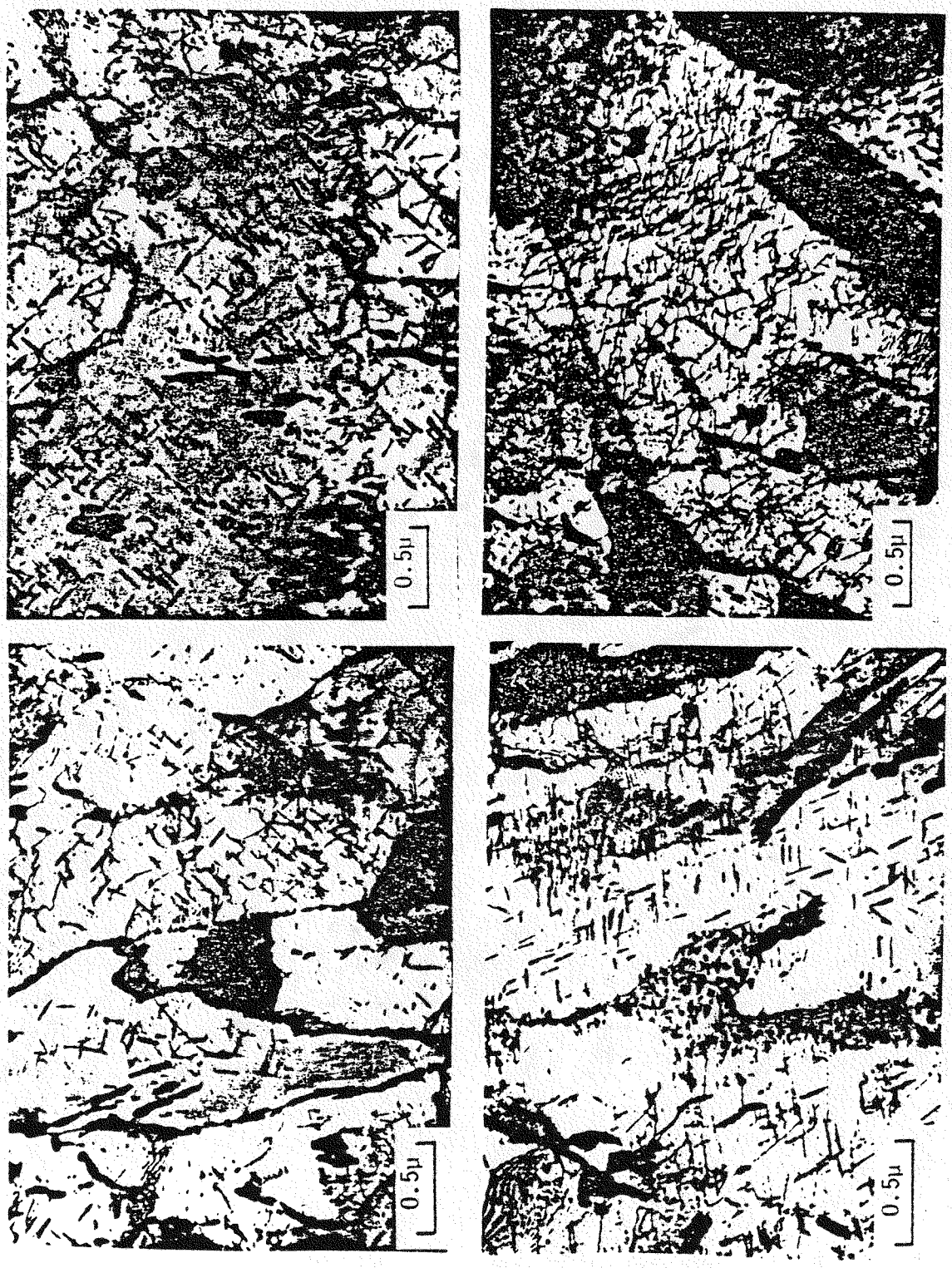

Figure 2.21 After full term exposure of Lukens steel to 1% strain and fast strain rates, the M2C population was similar to that achieved in steady state creep. Large subgrains had developed which provided avenues for extensive dislocation activity, and fine scale precipitates associated with migrating boundaries were observed.

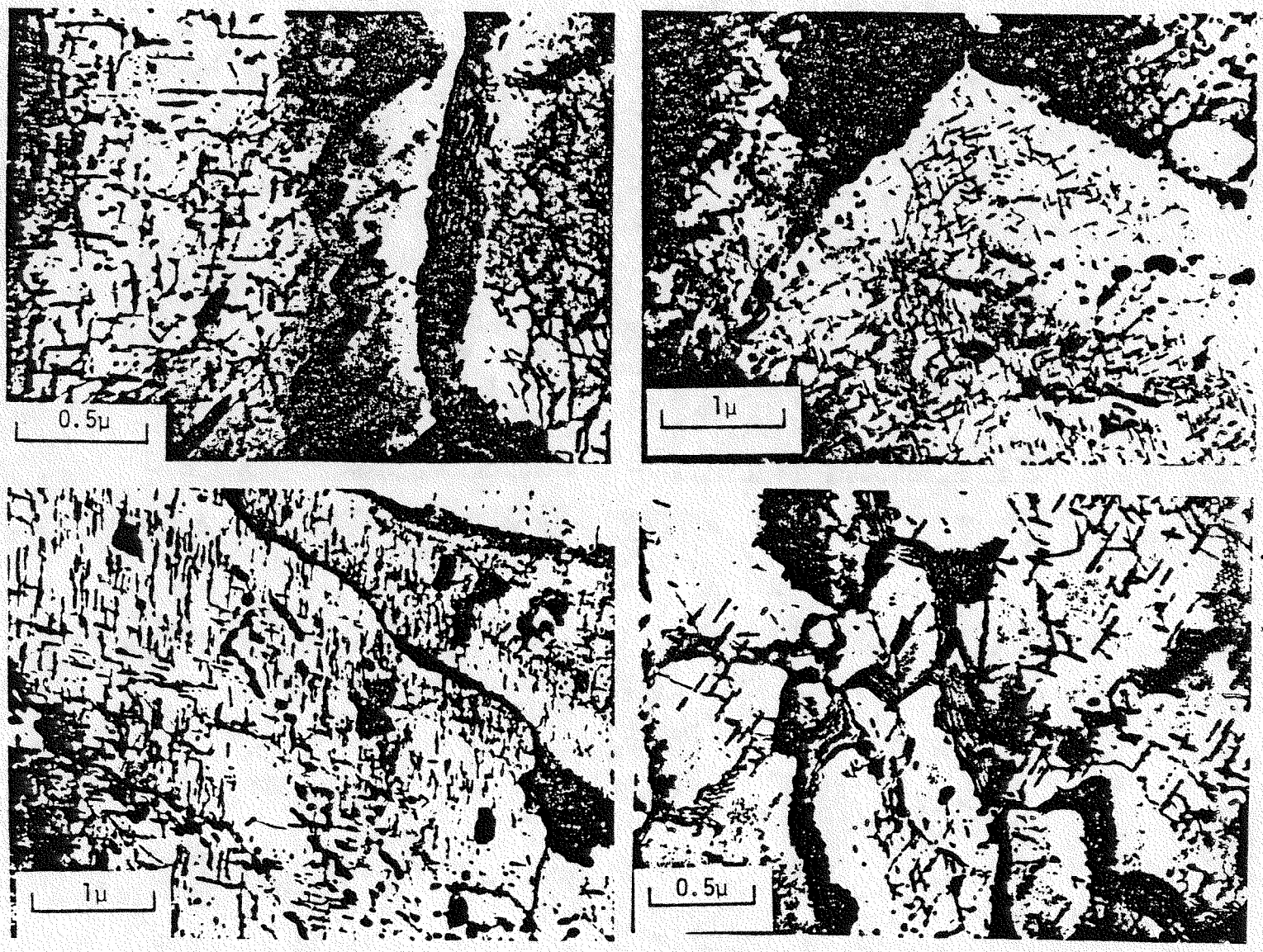

Figure 2.22 Introducing a 6-minute tensile hold time into the Lukens 1% strain, fast strain rate test resulted in well defined boundaries along with the previously determined precipitation and coarsening behavior.

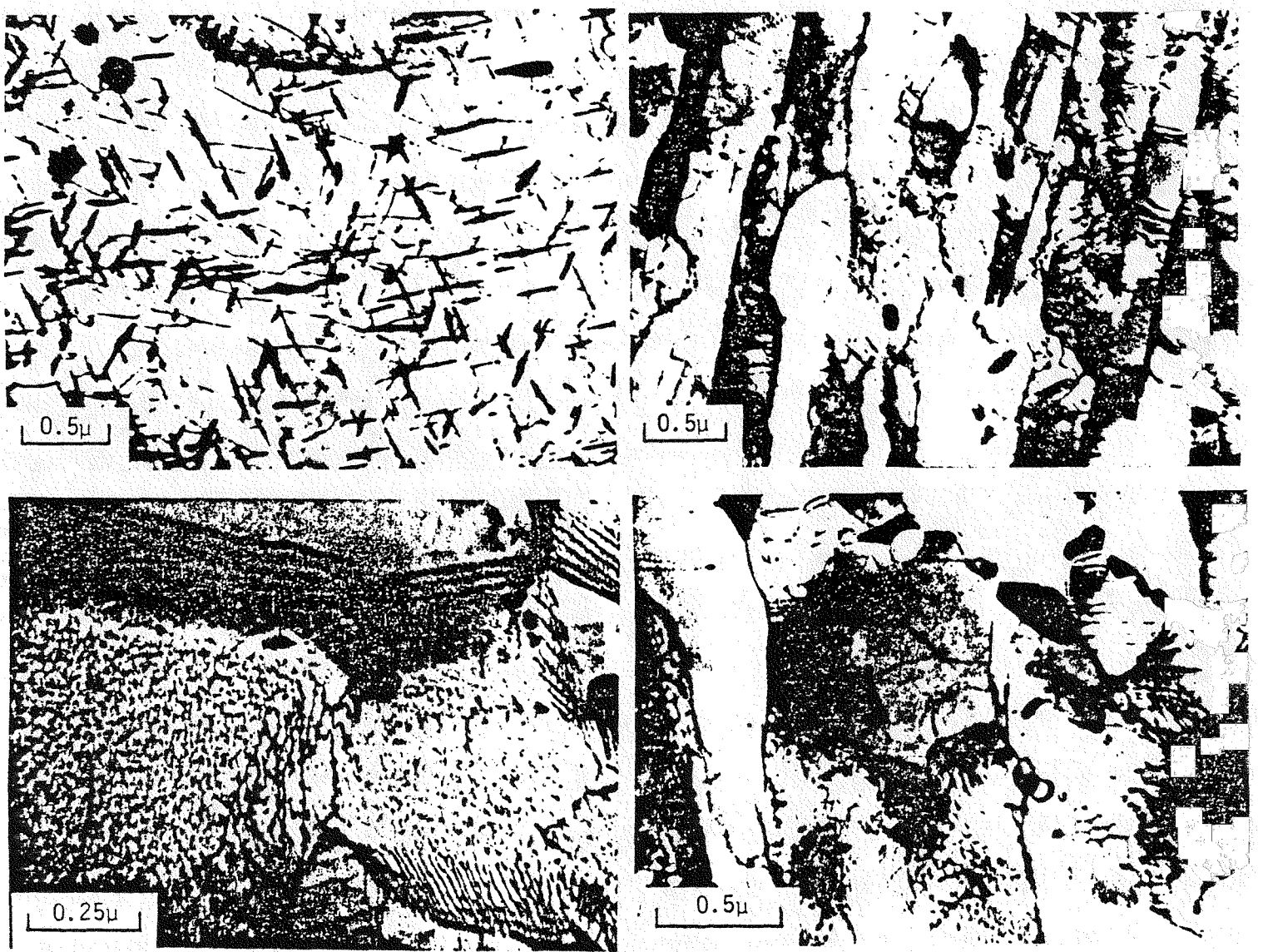

Figure 2.23 As-received Kawasaki steel was composed of bainitic lath structures of quite variable dimensions, some pro-eutectoid ferrite grains, occasional areas with acicular precipitates, and fewer grain boundary precipitates than Lukens steel.

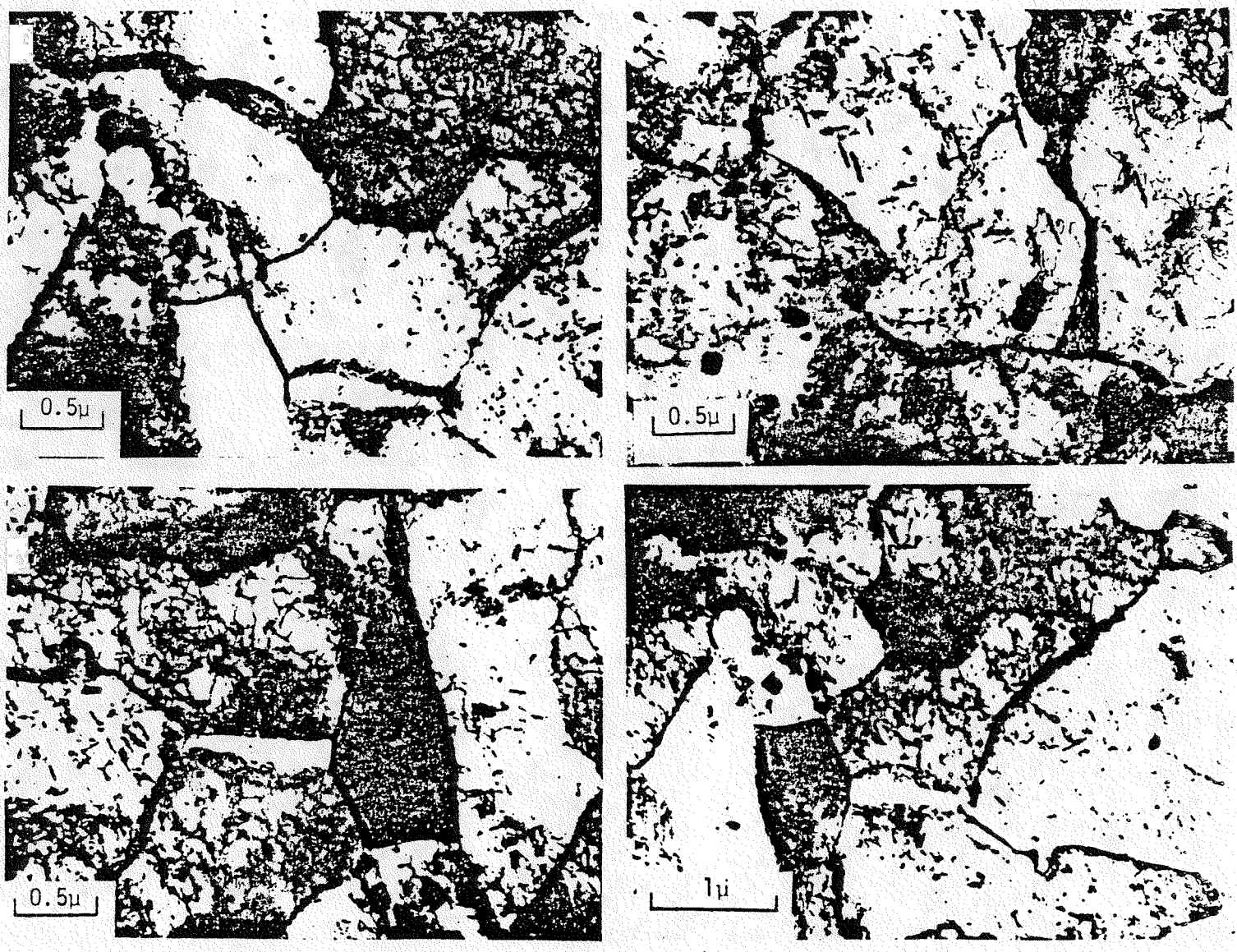

Figure 2.24 The introduction of a 6-minute tensile hold time into the 1% strain, fast strain rate test of Kawasaki steel also resulted in well defined bour.daries of an equiaxial nature, as were observed in the Lukens hold time test.

3. CYCLIC SOFTENING EFFECTS ON CREEP RESISTANCE OF BAINITIC LOW ALLOY STEEL PLAIN AND NOTCHED BARS

Tests in which periodic load reversals were superimposed on a steady load creep test have shown reductions of creep life of an order of magnitude or more. One major mitigating factor is that it appears that cyclic softening only occurs in material subjected to significant stress reversals. In a typical pressure vessel such conditions are only achieved in localized areas such as notch-like details and areas experiencing high cyclic thermal gradients. The investigation described here is aimed at determining the effect of local cyclic softening on creep resistance of components. This has been done by performing load controlled creep tests on two types of notched bars, a relatively blunt Bridgman notch with an elastic SCF of I.6, and a sharper Vee-notch with an SCF of 4.4, together with a small number of uniaxial specimens as controls. The material investigated is a low residual element 2.25 Cr 1 Mo steel manufactured by the basic oxygen process.

3.1. INTRODUCTION

Several Cr Mo low allow steels are currently being considered for pressure vessel construction in quench and tempered form. While this provides a considerable enhancement of the monotonic strength characteristics, materials tested in this way suffer a significant loss of strength due to cyclic softening. In simple axial loading, this effect has been found to significantly reduce the long term creep strength, even when the stress range is well below the initial yield strength of the material. On this evidence alone it might be concluded that, where cyclic loading is expected, there may be little or no advantage in using the bainitic structured material in preference to the more common ferritic-pearlitic form. On the other hand, most practical instances of significant stress reversal in components only occur in localized regions such as notch details or surface layers in pipes under cyclic thermal gradients. It is therefore feasible to suppose that conditions may arise where local softening has an insignificant effect on the overall load carrying capacity of the component, thus allowing the full strength attained by heat treatment to be utilized in determining primary stress limits for design.

In order to explore the influence of cyclic softening on component load carrying capacity, a series of tests has been performed on plain and notched, axially loaded specimens. The object was to determine the relative effects of periodic load cycles on creep strength of the material alone as opposed to its response to complex strain reversals in which local behavior is kinematically constrained to some extent by the remainder of the structure.

3.2. MATERIAL

The material used in this study consists of a 2.25 Cr 1 Mo steel containing reduced residual impurities. The chemical composition of this alloy is given in Table 3.1. This material was produced by Kawasaki Steel and was supplied to the University of Illinois by Oak Ridge National Laboratory (ORNL) in the form of sections from a 400 mm thick ring forging.

The heat treatment of this material involved holding the material isothermally at 1070°C for 18 hours followed by a water quench. The material then tempered at 650°C for 17 hours and then air cooled to ambient. This was followed by a simulated post weld heat treatment at 695°C for 19 hours. From this heat treatment the material near to the surface has a coarse ferrite lath structure with local regions that are more equiaxed in shape. The ferrite lath or sub-grain boundaries comprise regular, fine dislocation networks and there is much less evidence of fine scale precipitation at these boundaries. There is also a much lower density of M_2C carbides within individual ferrite units than is evident in other similar steels such as the Lukens material used in several ORNL studies [3.1]. For specimens cut from approximately the center of the 400 mm forging, the microstructure comprises a mixture of fine-structure similar to that observed in surface sections and coarse grains of polygonal ferrite. The coarse ferrite grains contain a uniform fine dispersion of M_2C carbides.

The material used in this study has significantly lower strength than the steel used by Klueh [3.1] and others. The reason is that it has a higher tempering parameter. The resulting coarseness of the ferrite substructure within the Kawasaki steel combined with the decrease in the density of carbide particles both at ferrite sub-grain boundaries and within the ferrite structure, is largely responsible for the lower strength observed in the Kawasaki steel at elevated temperatures.

3.3. TEST EQUIPMENT

Two 5-ton load capacity screw-driven electromechanical test machines manufactured to an ORNL mechanical design by Applied Test Systems, Inc. (ATS), provide the basis of the creep-fatigue testing performed in this study. The combined stepper-motor screw-jack driven features of this equipment produces an essentially low strain rate machine capable of producing strain rates from a maximum of 0.05%/s to as low as 6E-6%/hr. This capability allows the performance of creep-fatigue tests containing very slow ramp loadings and hold times of almost indefinite duration. This ability allows long term creep-fatigue tests to be completed which approach a more realistic representation of actual service conditions. For elevated temperature (up to 1000°C), these test frames are fitted with three zone resistance split furnaces, each zone containing an independent temperature controller.

Test control and data storage of the creep-fatigue test frames is provided by a microprocessor based combined digital controller and datalogger supplied by Engineering Technical Services (ETS) (now renamed SOMAT). This controller allows a block loading to be defined which consists of any combination of up to eight segments, each of which is then subjected to either load or strain control (through slight equipment modification, the capability exists for the application of computer controlled temperature histories). These segments can then be controlled in the form of a linear ramp, a hold period, or a sinewave. Once defined, the block loading may be repeated cyclically for any duration desired. The versatility of the above controller allows the specification of a wide variety of load histories, from simple steady load controlled creep tests to mixed mode strain/load controlled loading paths.

In addition to the screw-driven creep-fatigue test set-up, two other types of high temperature test systems were utilized in this investigation. The first, an electrohydraulic MTS System 810 test machine, has a 10-ton load capacity and is controlled through the use of a DEC PDP/1134 computer. This piece of equipment can achieve much greater strain rates than the screw-driven machines and was primarily used to run high frequency elevated temperature pure fatigue tests and high strain rate monotonic tests. The second type of equipment, Arcweld Creep Test Machines, are deadweight

creep machines upon which steady load creep and steady load creep with interspersed unloading period tests were performed.

3.4. TEST SPECIMENS

Three types of specimens were used in this test program, the dimensions of which are given in Fig. 3.1 for specimens to be used on the screw-driven and MTS test machines. Larger, though geometrically similar, specimens were used on the Arcweld Creep Test Machines. The first type of specimen is of a plain smooth dog-bone type. This specimen is used to obtain baseline material properties data.

The second two types of specimens consist of notched bars, the first of which contains a Bridgman notch with a moderate stress concentration factor (SCF) calculated by Hayhurst and Henderson [3.2] of 1.6. The second type of notch is a BS standard Vee-notch having a relatively high SCF of 4.4 [3.2]. These notched geometries were chosen firstly since they can be used to obtain a wide range of hydrostatic stress state conditions and secondly because they both experience widespread stress redistribution under creep conditions. Under conditions of general yielding, the $\sigma_{eff}/\sigma_{net}$ ratio in the neck is 0.746 and 0.714 for the Bridgman and Vee-notch specimens, respectively, (compared with 1.00 in uniaxial tension). Here, σ_{eff} is the Mises effective stress and σ_{net} is the nominal stress at the root of the notch. Development of hydrostatic stress is important since multiaxial effects can be examined. Furthermore, development of hydrostatic stresses should accelerate creep cavity void formation and growth, and thus creep damage, should this mechanism be present. Obtaining significant stress redistribution is crucial as this should be representative of the stress conditions present in the regions of stress concentration (such as those caused by nozzles) in pressure vessels.

The Bridgman notch, containing a moderate stress concentration, provides an almost uniform zone of hydrostatic stress, under steady-state conditions, which extends through the cross section of the specimen. This allows for testing under conditions of general yielding over a relatively large

volume of material. The Vee-notch on the other hand, containing a local area of high stress concentration, simulates conditions of small, highly localized, regions of plasticity.

3.5. PRESENTATION OF DATA

Information compiled for use in this study includes both basic material properties data and component geometry related results. Basic fatigue, creep, and monotonic properties were established in order to lay a foundation upon which the geometry-dependent results could be related to. The results of testing conducted in each of these areas will now be presented in turn.

3.5.1 Basic Fatigue Test Results

Strain controlled fully reversed fatigue tests performed by Pejsa [3.3] show this material to experience significant cyclic softening. Tests were conducted on material in the as-received condition at 565°C for a variety of waveforms at total strain ranges of 0.5% and 1.0%. Figure 2.13 shows the four types of waveforms used in this testing. Results for the 0.5% and 1.0% strain range tests were given in Figs. 2.15a) and b). In these figures, stress range has been plotted against number of cycles for each of the waveform shapes. Both sets of results share a number of common features. The softening behavior is a nearly continuous process from initial cycling right up to the point of failure. In all cases though, a significant portion of the softening occurs in the initial portion of the fatigue life. In the case of a 1.0% strain range, this region of accelerated softening occurs within the first 50 to 100 cycles of fatigue life. In the case of the lower strain range, this region of accelerated softening is somewhat longer in terms of number of cycles, covering the first 250 to 300 cycles of fatigue life. Both sets of results also show a significant increase in loss of strength towards the end of the fatigue life. This acceleration of strength loss marks the onset of cracking in the specimen. In all cases, failure soon followed the onset of crack initiation, occurring within about 50 to 100 cycles at 1.0% strain range and 200 to 400 cycles at 0.5% strain range.

At both strain ranges the effect of decreasing the strain rate by a factor of nearly 300 caused the fatigue life to be cut nearly in half. A similar halving of the fatigue life was experienced when a 0.1 hour

hold time was placed in the fatigue cycle at the point of maximum tensile stress or when an asymmetric slow-fast cycle was used.

From Pejsa's original data, it is possible to plot the maximum and minimum stress as a function of log cycles and strain range for each of the waveforms tested. Such a plot is shown in Fig. 3.4 for selected cyclic conditions. These results in effect represent the strength of the material under conditions of cyclic softening and will later be shown to correlate very well with load control tests performed on both plain and notched bars.

3.5.2 Basic Creep Test Results

Only a limited amount of creep tests to failure have been performed on this material to date. The form of the creep strain versus time curves is similar to other material which has been more extensively tested by Klueh. As can be seen in Fig. 3.3, the minimum creep rates show similar trends to the material tested formerly but with slightly lower stresses for a specified strain rate.

Creep behavior at stresses other than those for which direct tests are available was inferred indirectly from constant strain rate tests. As shown in Fig. 3.3, there is good correlation between minimum strain rates at constant stress in creep tests and maximum stress at specified strain rate in constant strain rate tests.

Time-to-rupture which can be deduced with reasonable accuracy using the Monkman-Grant relation [3.4] $C = t_R \cdot \dot{\varepsilon}_{min}$, where C = 4.14E-02 obtained from Klueh's data for tests of duration less than 450 hours applies equally well to the material considered here (see Fig. 3.3).

3.5.3 Constant Strain Rate Tests

Constant strain rate tensile tests were performed on smooth specimens to obtain elevated temperature strain rate effect data for this material under monotonic loading. For comparison room temperature tests (20°C) were completed at strain rates of 0.5%/min and 0.05%/min from 0 to 10% strain. Elevated temperature tests (565°C) were completed at strain rates of 0.5%/min, 0.05%/min, 0.005%/min, and 0.0005%/min. The first three of these tests were continued up to 10% strain

whereas the last test was stopped upon reaching maximum load. The stress versus strain data from these tests are plotted in Fig. 3.4. The room temperature tests showed essentially no strain rate effect. After reaching the 0.2% offset yield strength, the material continued to harden up to a strain of about 7.0%, approximately 16 times that at which the 0.2% yield strength occurred. The strength at this point was 1.23 times the yield strength, indicating a moderate amount of hardening.

When tested at elevated temperatures (565°C) this material shows a much different stress-strain response than that experienced at room temperature. After reaching the 0.2% yield strength, the material experienced a small amount of hardening after which softening was observed. Not only was the amount of hardening very slight (maximum strength equal to 1.02 to 1.08 times the yield strength), the region over which hardening occurred was much less than that experienced at room temperature. At elevated temperatures, maximum strength was reached within 2 to 3 times the 0.2% yield strain, much less than the factor of 16 found in the room temperature tests.

The elevated temperature tests also show significant strain rate effects. As strain rate increases, both the yield strength and the ultimate strength increase. Figure 3.5 shows that the rate of increase of the yield and ultimate strengths decreases slightly with increasing strain rate. After reaching the ultimate strength, the material softens at a rate which, to a first approximation, is insensitive to strain rate.

Closer examination of Fig. 3.5 and Table 3.2 shows two second-order deviations from the condition of strain rate insensitive softening. Firstly, as strain rate decreases, a slight knee in the softening region appears to occur. After reaching the ultimate strength, the material begins to soften in a uniform manner. Following initial softening, a point is reached where the rate of softening slightly decreases and then remains essentially a constant. This change in softening rate becomes more pronounced as the strain rate decreases. At a strain rate of 0.005%/min, this knee occurs at approximately 3% strain where the softening modulus changes from -1055 MPa to -483 MPa. The final second-order effect involves the slight change in softening rate with decrease in strain rate. From Table 3.1 one notices that there is actually a slight decrease in final softening rate with decreasing

strain rate. These tests showed an approximately 30% decrease in softening rate over a two decade decrease in strain rate.

From these constant strain rate tests, the minimum creep rate is plotted versus the maximum stress achieved at each given strain rate, on Fig. 3.3, along with results obtained by Klueh [3.1] from a similar material. The data show similar trends with Klueh's results.

3.5.4 Periodic Load Reversals On Plain And Notched Bars

The phenomenon on which this program is focused is the fact that low alloy steels in quenched and tempered form have been shown by Swindeman [3.5] to display considerable loss of creep endurance as a result of periodic load reversals even when the stress range is significantly lower than the initial yield stress range. For instance, in creep tests performed by Swindeman, the rupture life was reduced from 625 hours to 105 hours by load reversals at 6-minute intervals.

Tests performed in order to further investigate the effects of load reversals on the cyclic softening behavior and creep resistance of this material in plain and notched bars can be divided into three distinct, but related, groups. The first group of tests, the results of which are given in Table 3.2, were all completed on the screw-driven creep-fatigue test machines. These tests were performed over a wide variety of loading conditions and provide the basis of this investigation into the softening behavior of this alloy when subjected to other than uniform uniaxial stress distributions.

The second group of tests were performed by Kschinka [3.6], in part, to provide baseline property data on the fatigue behavior of this material under the stress distributions imposed by the chosen specimen geometries. The results of these tests are given in Table 3.3. As indicated these were all conducted at a frequency of 0.4 Hz over a variety of loading conditions.

The final group of tests were performed to provide creep data under conditions of both steady loading and steady loading with superimposed off-load on-load cycles. These tests were all conducted on the Arcweld deadweight creep machines. The results of these tests are given in Table 3.4.

3.6. POSSIBLE INFLUENCES OF SOFTENING ON DESIGN

Cyclic softening has two potential effects on design stresses. Firstly, it causes a reduction of the instantaneous and long term material strength over all or part of the component volume, reducing both the limit load and the resistance to creep deformation. This could mean that design stresses may have to be reduced from the values obtained from monotonic tests on uncycled material. Secondly, increased plastic deformation at notches can accelerate fatigue mechanisms. The latter effect will not be considered here. Discussion will be confined to the influence of cyclic stress on the general load carrying capacity of material and components.

Figure 3.6 shows a plot of effective net section stress versus time to failure for tests completed on both plain and notched bars. In all tests, loading consisted of a 5-minute hold time followed by a one-minute reversal cycle. The smooth specimen results available show only a moderate amount of life reduction due to the presence of the completely reversed load cycles. The Bridgman specimen, containing a moderate stress concentration factor, shows virtually no reduction in life when the load is reversed back to zero. A significant reduction in life of about an order of magnitude is experienced when the load cycle is completely reversed. The Vee-notch specimen, containing a relatively large stress concentration, similarly experiences about an order of magnitude reduction in life when completely reversed load cycles are superimposed upon the steady creep load. There is also, however, a noticeable loss of life due simply to a zero to maximum superimposed load cycle. The reduction in life is not nearly as great as in the case of the fully reversed cycle, but a reduction of nearly a factor of 2 is still experienced.

The effect of cyclic loading on strength is shown clearly by plotting the peak maximum and minimum stresses in strain controlled fatigue tests against the log cycles. Unlike the linear plots, these curves show no plateau, but instead a continuous, exponential decrease in strength with time. Cyclic strength appears to be strongly dependent on the frequency of the cycle but only weakly dependent on the wave shape of the strain history or the strain range. This suggests a simple first-order model of cyclic softening in which the current strength is represented as a function of the number of load cycles

and the load cycle frequency σ_y (N) = f_1(N) · f_2(f) where N = number of load cycles and f = frequency in cycles/unit time.

It is not very important whether yield or ultimate tensile strength is used to define current strength because these two quantities differ only slightly in softening materials.

To test the hypothesis, the uniaxial creep tests with interspersed load reversals have been plotted on the same graph as the softening curves in Fig. 3.7. These points fall close to the tensile stress softening line, and the specimen lives would be reasonably accurately predicted by simply assuming the strength to decrease with number of cycles until the tensile strength of the specimen is exceeded.

The same hypothesis holds for more complex stress situations. As also shown in Fig. 3.7, the lives of all notched specimens undergoing full load reversals are predicted quite well by the number of cycles required to reduce the cyclic strength to the effective stress at the notch net section at the specified cycle frequency.

The frequency dependence of cyclic strength can also be approximated relatively simply. The rate dependence of this material has been examined over a wide range of strain rates, and it is observed that the cycle-dependent softening curves for different frequencies vary in a way similar to the monotonic rate dependence. Fig. 3.18 includes such a curve for a 1-hour cycle time, constructed theoretically on the above hypothesis, which corresponds very well with the one Bridgman specimen tested at that frequency.

Further evidence for a simple cycle-dependent softening criterion can be deduced from the rapid cycling tests performed on notched bars (Fig. 3.9). All of these specimens displayed fatigue-like failures with cracks growing in from the notch root. A simplistic measure of the notch severity is the ratio of the strain required in a uniaxial specimen to produce the same fatigue life as the notched specimen, to the nominal elastic strain at the notch neck, referred to here as K_{ef}, $K_{ef} = \Delta\varepsilon(N_f)/\Delta\varepsilon_{nom}$ where $\Delta\varepsilon(N_f)$ = equivalent uniaxial strain to cause failure in N_f cycles (see Fig. 3.10) and $\Delta\varepsilon_{nom} = \sigma_{net}/E$.

In the case of purely elastic response, this ratio reduces to the classical fatigue strength reduction factor, K_f. The factor K_{ef} is given in Table 3.5 for the rapid cycle notch tests. In the case of both Bridgman and Vee-notch specimens, K_{ef} is consistent with typical values of K_f expected in these geometries. The most highly loaded specimens for each of the geometries display a significant increase in K_{ef}, suggesting that some other effect is present. When these failures are plotted on Fig. 3.9, the fatigue failure curves intersect the cyclic softening curve at just about the load levels chosen for these most highly loaded specimens. The apparent increase in K_{ef} is due to the transition of failure mode to plastic collapse as the cyclic strength drops below the maximum effective stress at the notch. Although the experimental evidence is sparse as yet, the fatigue/softening transition appears to be relatively sharp, suggesting that the interactive effect is not a strong one and that failure can be predicted by whichever is the dominant mechanism.

From the results of fully reversed load tests on notched bars, it is clear that cyclic softening can have a profound effect on component life, reducing the number of cycles to failure by fatigue and creep life in hours by factors of 10 to 20, and this despite the fact that the cyclic stress range is well below the initial yield range in some cases. For instance, in the testing of a Bridgman notch bar with a nominal net stress at the root of 171 MPa (see Table 3.2), the Mises effective stress is only 128 MPa, well below the initial yield stress of 310 MPa. The life, however, is only 4372 cycles. From the extrapolation of the rapid cycle data, the cyclic life at this load level is predicted as about 30,000 cycles, and a theoretical prediction based upon initiation at the notch root is nearly 70,000 cycles. Similarly, the creep life predicted from the steady load effective stress at the notch is approximately 3700 hours. In view of the fact that the load reversal is rapid, so that the cyclic stress distribution is approximately elastic, the stress range through most of the notch section is considerably less than the steady creep effective stress reaching only 124 MPa at the center. This demonstrates that cyclic softening can cause serious reduction of cyclic life at even modest strain levels.

On the basis of this evidence alone, it might be concluded that there is little point in heat treating a low alloy steel to improve its initial strength, if this is to be lost later as a result of cyclic softening. Before accepting this as a general conclusion, it should be observed that a notched bar is

a very severe test of stress concentration effects because the entire cross-section of the component is affected by any stress redistribution which may result from plastic deformation at the notch root. In an effort to simulate a more realistic situation, some of the notched bar tests were performed under an R-ratio of 0, thus ensuring that only a small volume of material near the notch root experienced stress reversals. These tests show little or no overall deterioration due to softening. As shown in Table 3.4, the Bridgman specimen showed no significant reduction in life compared with a similar steadily loaded specimen. The second Vee-notch specimen to be tested in this series did show some reduction in life compared with the equivalent steady creep test but examination of the fracture surface revealed clear evidence of fatigue crack growth. The cyclic life of 2250 cycles observed in this specimen is in good agreement with the 4959 cycles found in a similar test with no hold time, bearing in mind the reduction factor of about 2 caused by hold time effects in this study. No significant loss of creep life was experienced when the hold time was increased to 60 minutes to eliminate the fatigue effect, although the number of cycles, 447, was sufficient to allow full development of whatever softening effect there may have been (see Table 3.2).

It is concluded that the effect of cyclic softening on component behavior is extremely complex and far from being understood well enough to make full use of materials displaying this phenomenon. Clearly there are some situations in which the residual strength is little different from the same material in the annealed form, and in such cases there is no advantage in performing expensive heat treatment. A situation like this might arise, for instance, in a tube wall experiencing severe thermal gradients. On the other hand, there are many practical situations where cyclic stress reversals are confined very locally, to notches or thin surface layers in thick vessels, or where there are clearly no cyclically reversing stresses at all. It would be unjustifiably conservative, in these cases, not to utilize the improved strength gained by heat treatment. It is easy to identify the extremes of the spectrum. What remains to be done is to determine some reliable criterion for distinguishing between situations in which cyclic softening can be ignored from those in which it cannot.

There are two aspects to the problem just identified, the first relating to material behavior and the second to component response to cyclic load.

Cyclic softening seems to require at least reversal of stress. Uniaxial creep tests in which the load was simply removed and replaced have shown no reduction in life compared with steady load tests. On the other hand, the required degree of reversal to cause softening appears to be significantly less than the initial, or even the cyclically softened, yield range as shown by the strong effect displayed by the notched tests under full load reversal. There are too many variables involved to investigate the extent of softening by experiment alone, and there is a need for a robust constitutive relation to model the softening effect. Models such as Miller's MATMOD have possibilities here but these have yet to be examined fully.

The component design problem, which applies not only to cyclic softening but to a wide range of other design situations such as elastic follow-up and inelastic notch strains, is the need for a criterion to judge whether local strain concentrations are strain- or load-controlled. Local strain control amounts to saying that local cyclic softening will not interact with the component load carrying capacity. If conditions in highly strained regions can be determined as a property of the component and the load level only weakly dependent on material strength, then a detailed understanding of cyclic softening is not necessary to evaluate component performance. Some preliminary studies indicate that aspects of local strain behavior in components are, in fact, relatively independent of material constitutive behavior, and that it may be possible to define some classes of problems as insensitive to cyclic softening. So far this work is in its early stages and the precise nature of the criterion separating sensitive from insensitive components still must be identified.

3.7 REFERENCES

3.1. Klueh, R. L., "Creep and Creep-Rupture Behaviour of a Bainitic 2 1/4 Cr - 1 Mo Steel," Int. J. Pres. Ves. and Piping, Vol. 8, 1980, pp. 165-185.

3.2. Hayhurst, D. R., and J. T. Henderson, "Creep Stress Redistribution in Notched Bars," Int. J. Mech. Sci., Vol. 19, 1977, pp. 133-146.

3.3. Pejsa, P. N., "Elevated Temperature Low-Cycle Fatigue of Two Bainitic 2.25 Cr - 1 Mo Steels," M.S. Thesis, University of Illinois at Urbana-Champaign, Illinois, 1983.

3.4. Monkman, F. C., and N. J. Grant, "An Empirical Relationship between Rupture Life and Minimum Creep Rate," Deformation and Fracture at Elevated Temperatures, ed., Grant, N. J., and A. W. Mullendore, MIT Press, 1965.

3.5. Swindeman, R. W., "Response of Ferritic Steels to Nonsteady Loading at Elevated Temperatures," Research on Chrome-Moly Steels, ed., Swift, R. A., MPC-21, American Society of Mechanical Engineers, NY, 1984, pp. 31-42.

3.6. Kschinka, B. A., "Creep-Fatigue-Environment Interaction in Bainitic 2.25 Cr I Mo Steel," M.S. Thesis, University of Illinois at Urbana-Champaign, Illinois, 1986.

3.7. Juvinall, R. C., Fundamentals of Machine Component Design, John Wiley and Sons, NY, 1983.

Table 3.1 Softening rates in constant strain rate tests

Strain Rate %/Min	Hi MPa	Hf MPa
0.5	-690	-690
0.05	-758	-569
0.005	-1055	-483
Ave	-834	-581

Hi = Softening rate before "knee"
Hf = Softening rate after "knee"

Table 3.2 Low frequency creep-fatigue test results on smooth and notched bars (tests conducted on screw-driven creep-fatigue test machines)

Specimen Type	σ_{net} Stress MPa	σ_{eff} Stress MPa	Cycles to Failure N_f	Time to Failure Hours	Hold Time Min	Ramp Time Min	R Ratio
S	172	172	1976	197.6	5	1	-1
S	216	216	106	10.6	5	1	-1
S	243	243	29	2.9	5	1	-1
B	171	128	4372	437.2	5	1	-1
B	241	180	387	38.7	5	1	-1
B	289	216	153	15.2	5	1	-1
B	292	218	16	16.0	60	1	-1
V	172	123	2596	259.6	5	1	-1
V	244	174	374	37.4	5	1	-1
V	279	199	161	16.0	5	1	-1
V	233	166	4959	41.3	0	.5	0
V	233	166	447	447.0	60	.5	0

S = Smooth specimen, B = Bridgman specimen, V = Vee-notch specimen.

Table 3.3 High frequency (0.4 Hz) creep-fatigue test results on notched bars

Specimen Type	σnet Stress MPa	σeff Stress MPa	Cycles to Failure N_f	Time to Failure Hours
B	244	182	8480	5.84
B	292	218	3423	2.36
B	341	254	1444	0.99
V	244	174	4545	3.13
V	279	199	2829	1.95
V	314	224	1319	0.91

S = Smooth specimen, B = Bridgman specimen, V = Vee-notch specimen.
All tests were fully reversed and cycled at a rate of 0.4 Hz.

Table 3.4 Low frequency creep-fatigue test results on smooth and notched bars (tests conducted on Arcweld deadweight creep machines)

Specimen Type	σ_{net} Stress MPa	σ_{net} Stress MPa	Cycles to Failure N_f	Time to Failure Hours	Hold Time Min	R Ratio
S	152	152		1581		1
S	172	172		476		1
B	226	169		665		1
B	226	169	6130	613	5	0
V	232	166		594		1
V	232	166	2250	225	5	0

S = Smooth specimen, B = Bridgman specimen, V = Vee-notch specimen.

Table 3.5 Results of K_{ef} and K_f calculations for high frequency (0.4 Hz) creep-fatigue tests on notched bars

Specimen Type	σ_{net} Stress MPa	Cycles to Failure N_f	$\Delta\varepsilon_{nom}$ Strain Range	$\Delta\varepsilon$ for N_f	K_{ef}	K_f^*
B	244	8480	0.273	0.40	1.47	1.44
B	292	3423	0.326	0.47	1.44	1.44
B	341	1444	0.381	0.70	1.84	1.44
V	244	4545	0.273	0.44	1.61	2.50
V	279	2829	0.311	0.54	1.74	2.50
V	314	1319	0.350	0.74	2.11	2.50

S = Smooth specimen, B = Bridgman specimen, V = Vee-notch specimen.
All tests were fully reversed and cycled at a rate of 0.4 Hz.
All strains given in percent.
*Calculated according to Juvinall [7[.

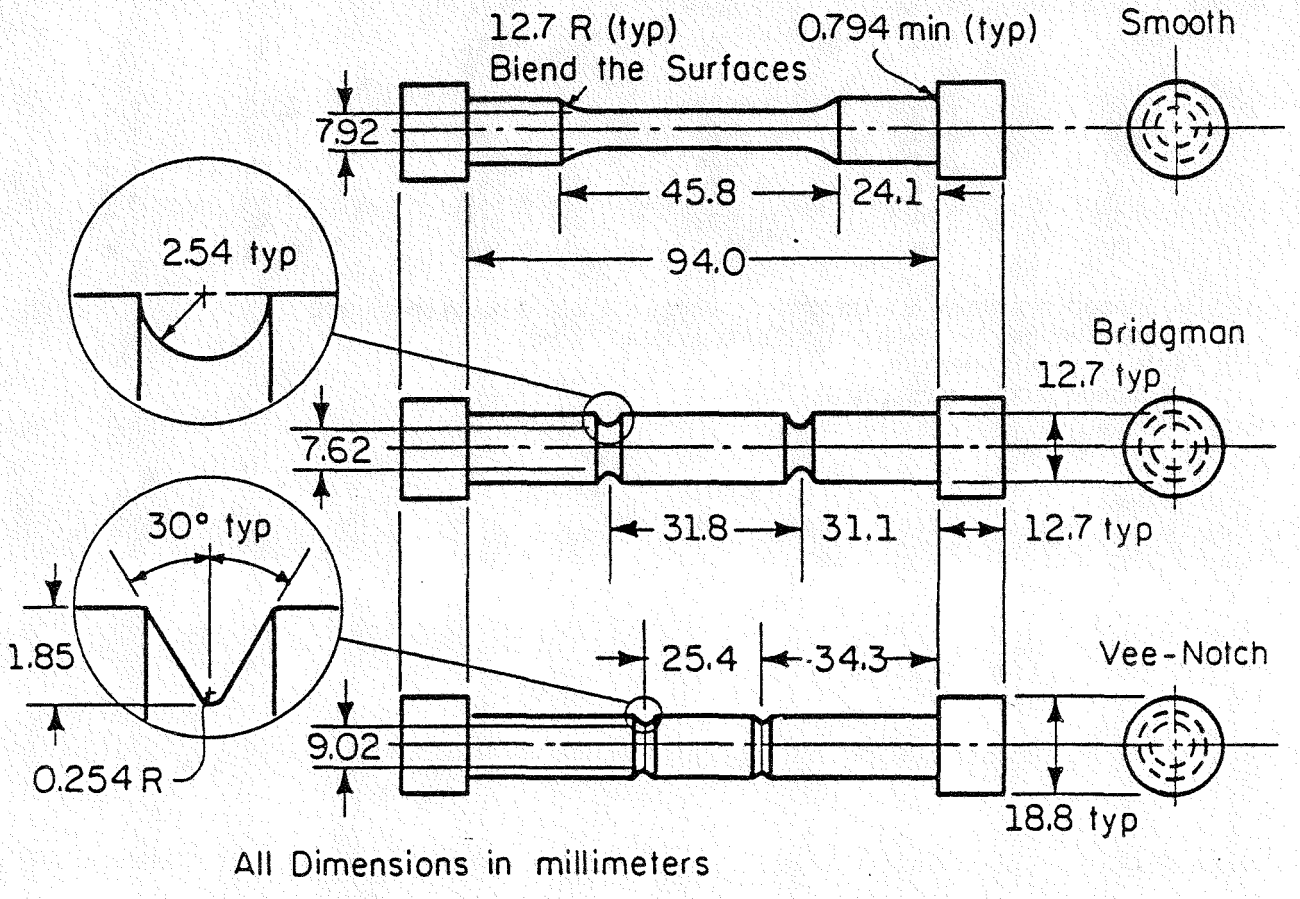

Fig. 3.1 Standard uniform section and notched bars used in test program

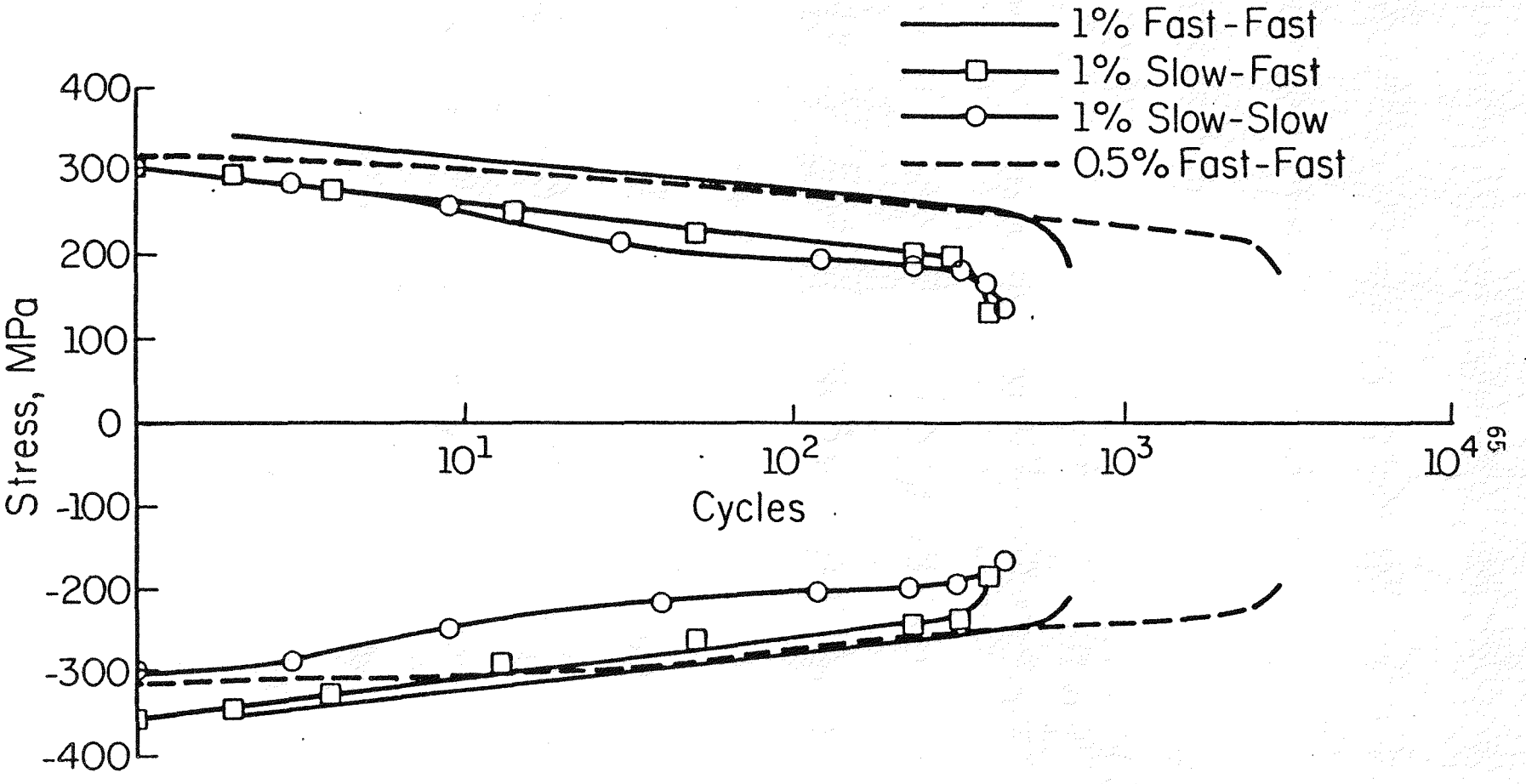

Fig. 3.2 Maximum and minimum stress versus number of cycles for a variety of cyclic conditions

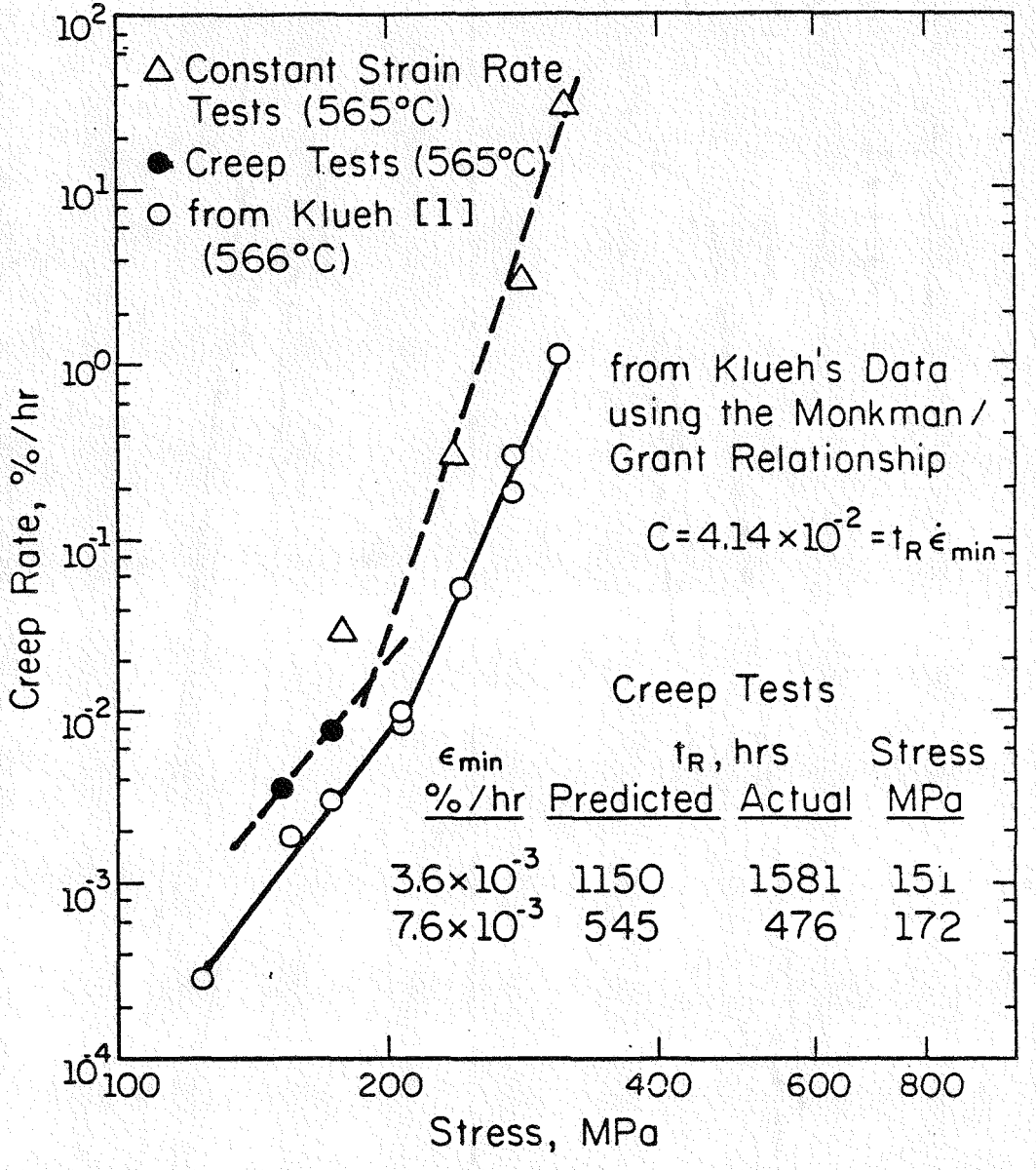

Fig. 3.3 Minimum creep rate versus stress

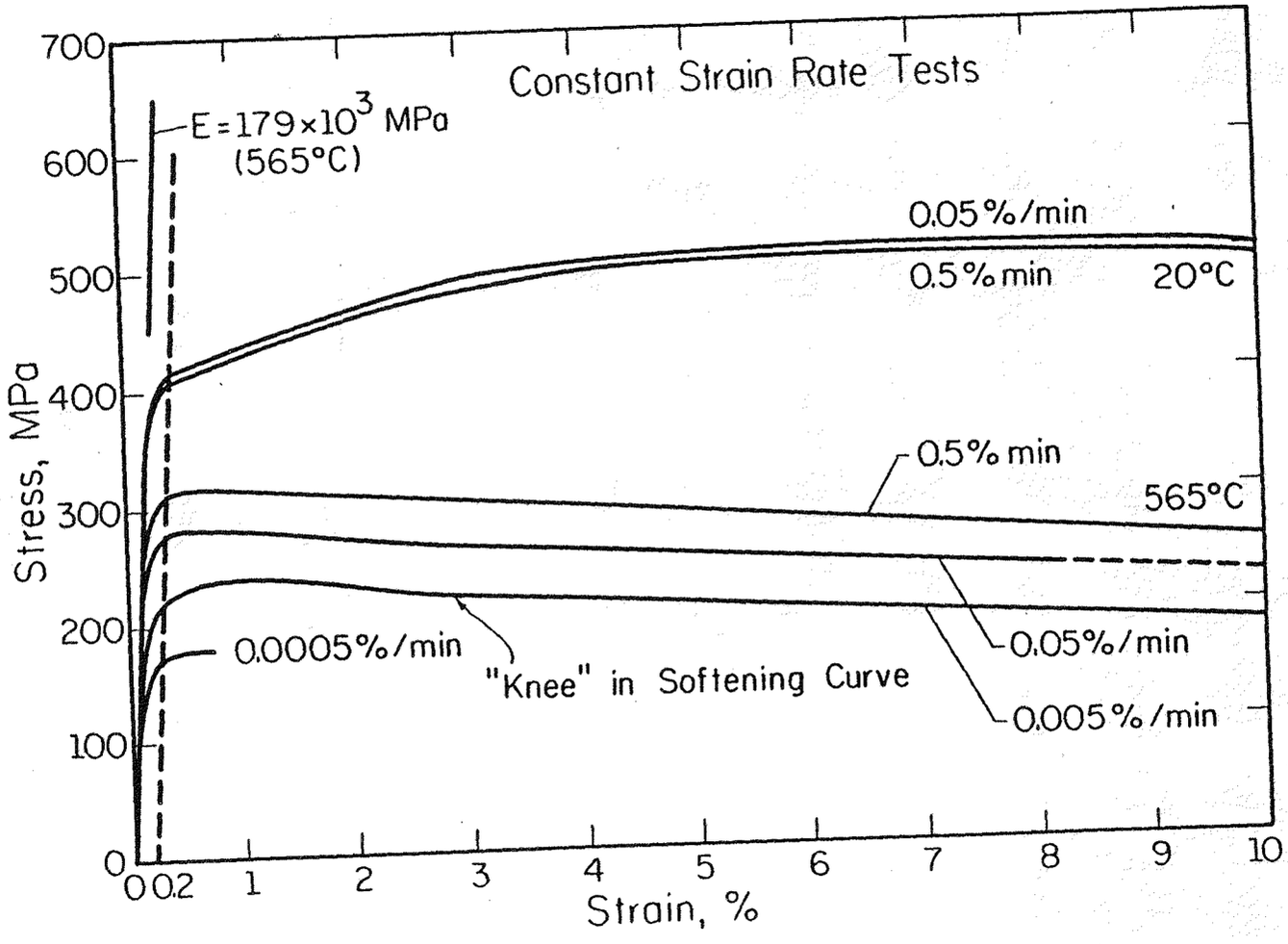

Fig. 3.4 Constant strain rate test results

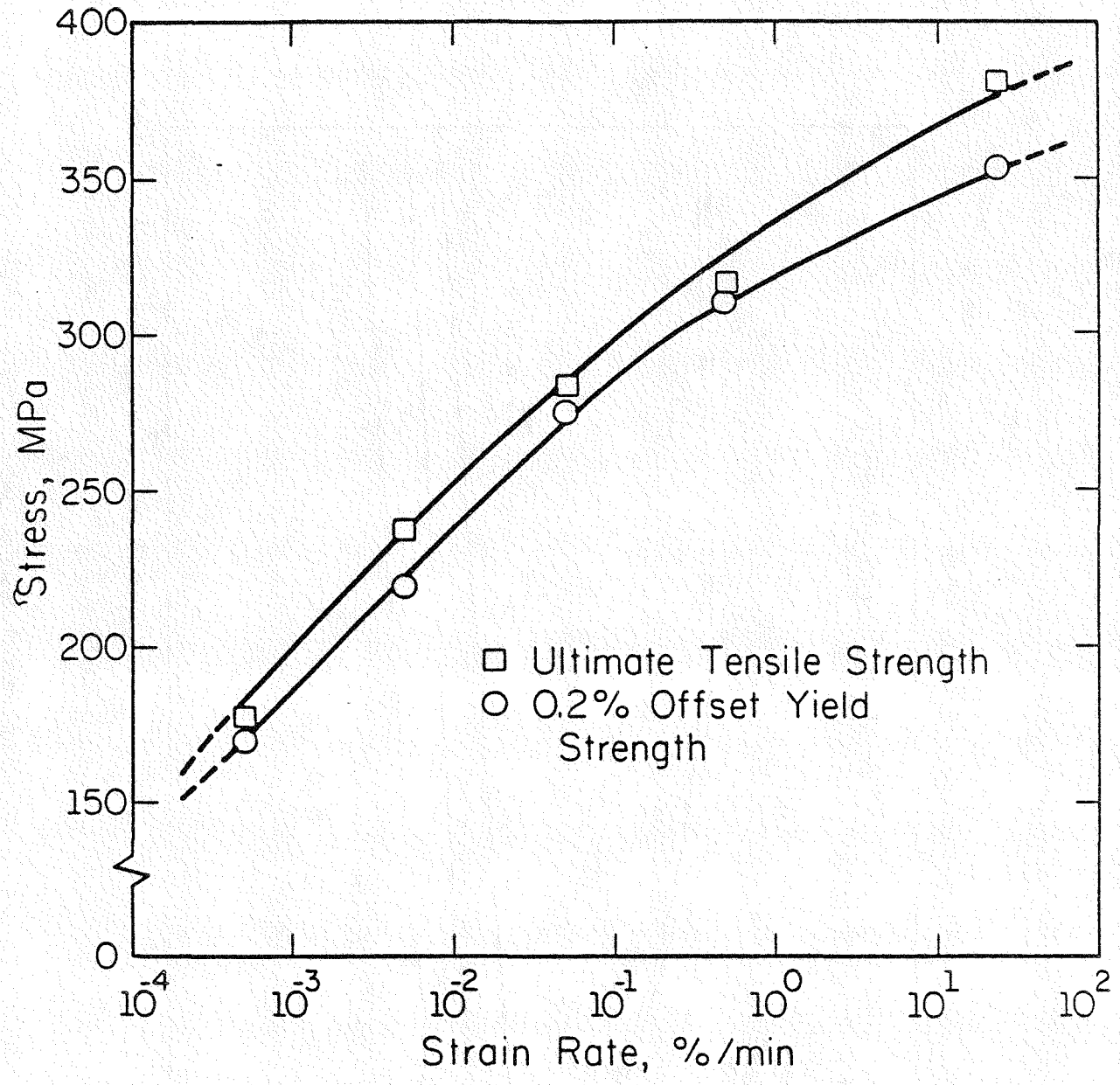

Fig. 3.5 Ultimate tensile strength and offset yield strength versus strain rate

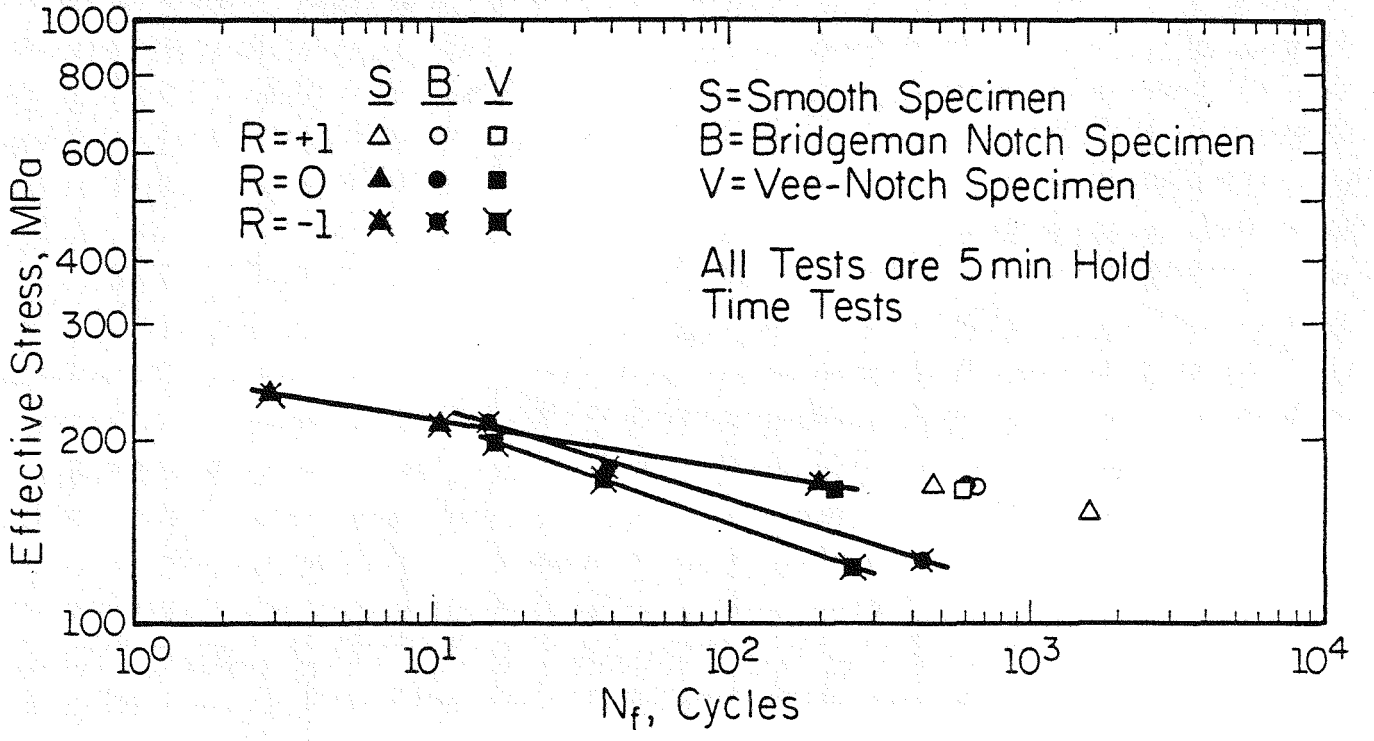

Fig. 3.6 R-ratio effects in smooth, Bridgman, and Vee-notched specimens

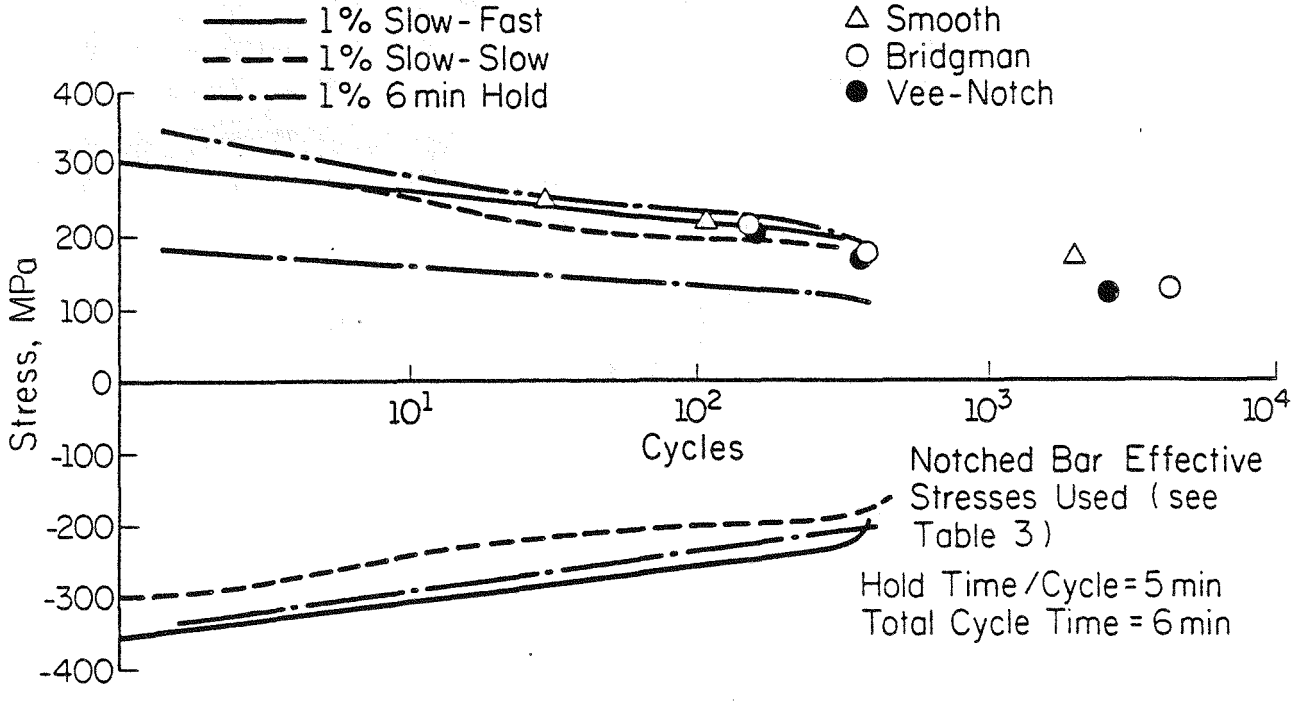

Fig. 3.7 Smooth and notched specimen creep tests with interspersed load reversals test data superimposed on cyclic softening curves

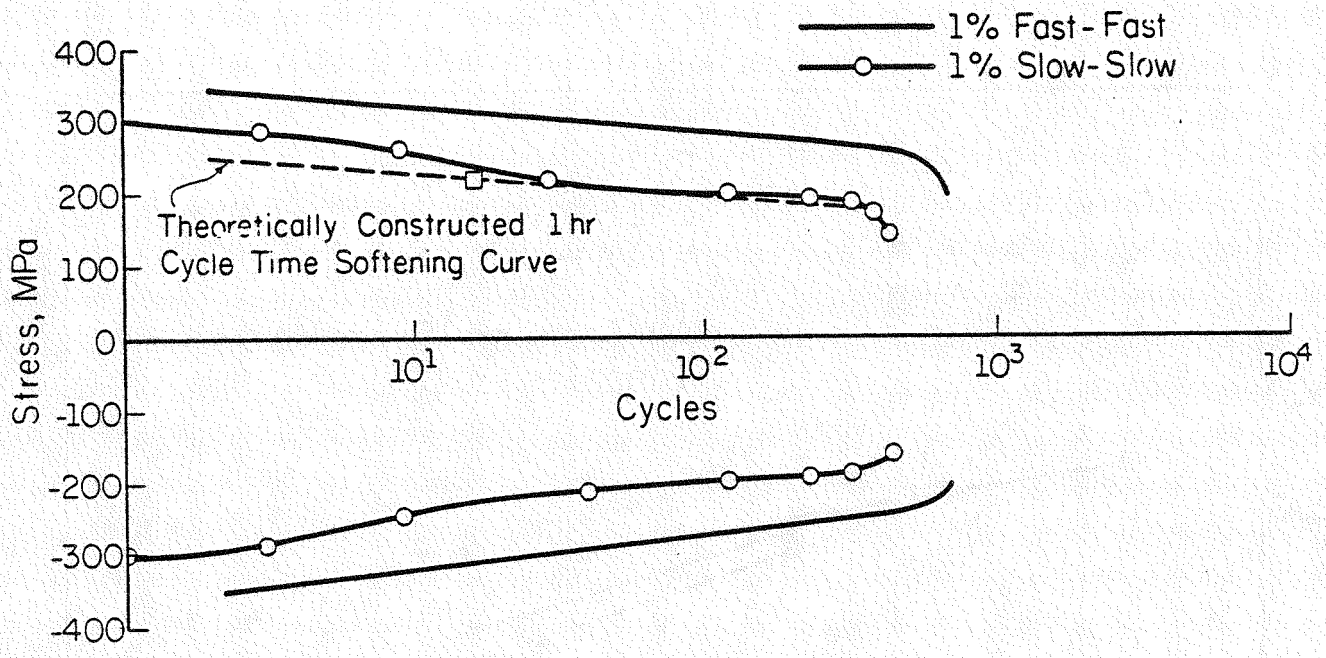

Fig. 3.8 Theoretical versus experimental frequency dependence of cyclic strength. Experimental data point ( ) consists of a Bridgman specimen creep test with superimposed load reversal every I hour. Result is plotted using effective stress (see Table 3)

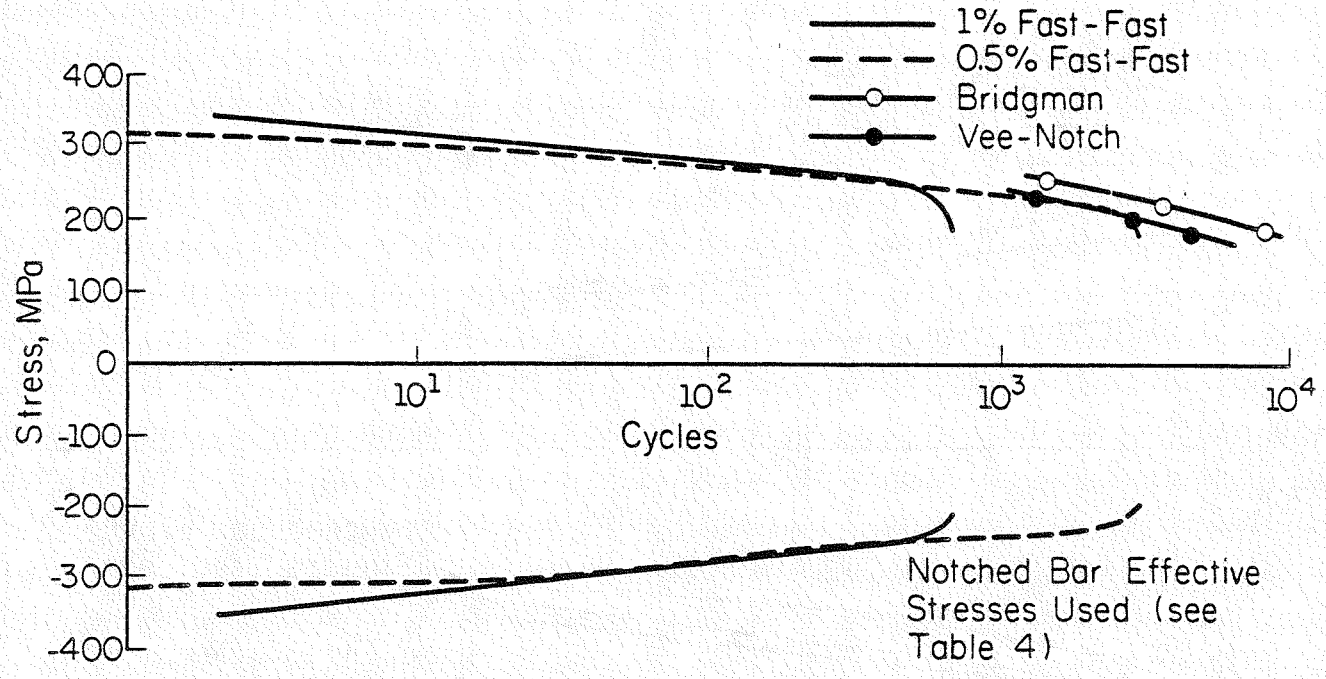

Fig. 3.9 Rapid cycle (0.4 Hz) notched bar fatigue test data superimposed on cyclic softening curves

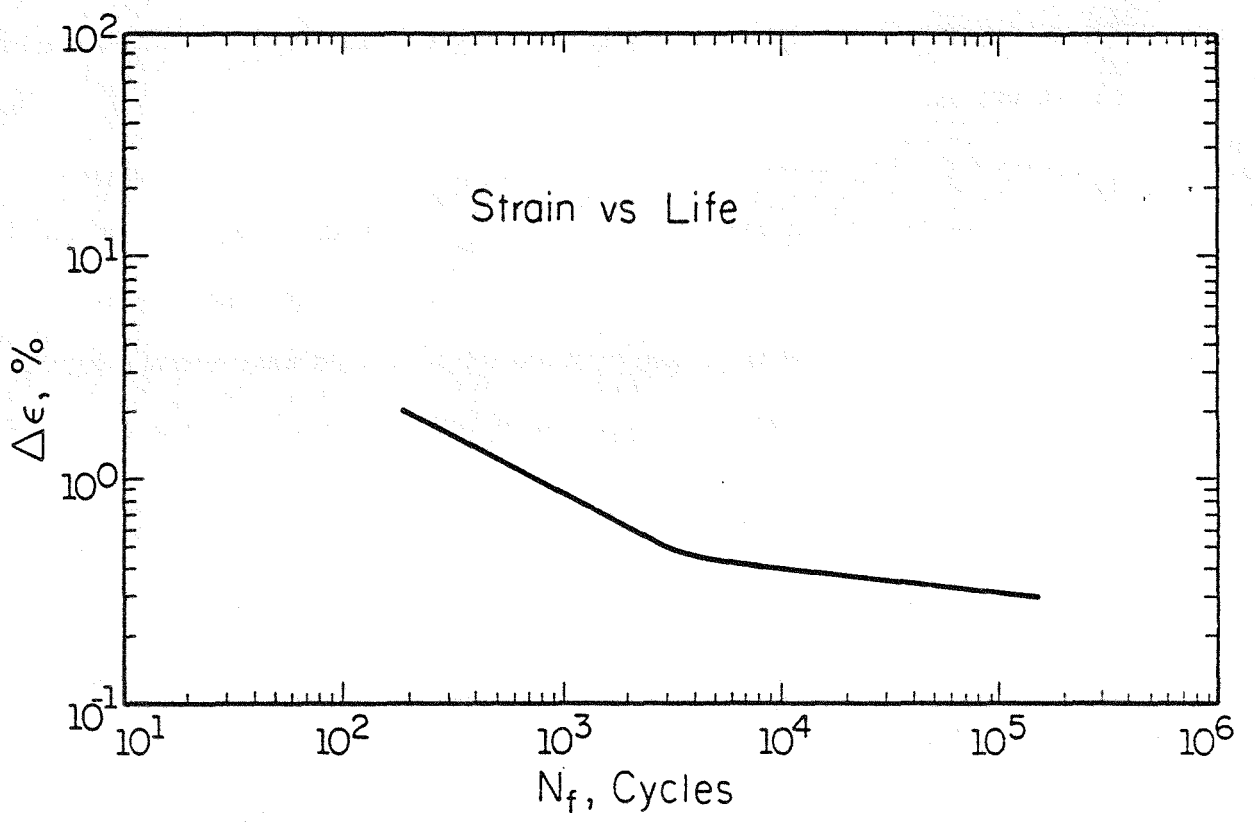

Fig.3.10 Smooth specimen high frequency = 0.004/sec) strain range versus life relationship

4. EFFECTS OF HOLD TIMES, PRE-NOTCHING, AND ENVIRONMENT ON THE ELEVATED TEMPERATURE FATIGUE LIFE OF BAINITIC 2.25 Cr-1 Mo STEEL

4.1 EXPERIMENTAL PROCEDURE

4.4.1 Material

The test material is a 2.25 Cr-1 Mo steel forging with low residuals manufactured by Kawasaki Steel (Heat 646363) and supplied by Oak Ridge National Laboratory. The composition is given in Table 2.1; note the low concentrations of P, S, As, Sn, and Sb impurities. The alloy was quenched and tempered in the form of 400 mm plate as follows: Austenitize at 1070°C (1960°F) for 18 hours--water quench. Temper at 650C (1200F) for 17 hours--air cool followed by a simulated post weld heat treatment at 695C for 19 hours. This processing produced a microstructure consisting of essentially 100% bainite, as confirmed by microscopic analysis. Room temperature strengths fell within ASME SA-336 Class F22 specifications. Complete tensile properties are given in Table 4.1.

4.1.2 Specimen Preparation

Uniform gage length fatigue specimens as depicted in Fig. 4.1 were prepared from the virgin material. The unique double shoulder geometry was designed for purposes of vacuum testing. The inner shoulders were provided to mount type 321 stainless steel flexible tubing which acted as a miniature retort encapsulating the gage section of the specimen in vacuum. The tubing was fastened to the specimen shoulders using an electron-beam brazing process. The entire brazing procedure was performed in a vacuum of about one microtorr. In this way the gage section of the specimen was encapsulated in a reasonable vacuum without resorting to a costly retort system. This technique also eliminate misalignment problems prevalent in complex retort arrangements.

The only drawback to this method was the necessity to place the extensometry on the same shoulders used to mount the flexible tubing. Hence correlations had to be made between strain in the gage section and strain between the shoulders. This was accomplished by using two extensometers simultaneously, one on the gage section and one on the shoulders. The shoulder

mounted extensometer was a one-inch extensometer specially adapted to accommodate the 2.42-inch distance between the shoulders. Strain was controlled ion the gage section and monitored between the shoulders. While the correlation is straightforward in the case of pure fatigue, it is somewhat more complex in hold time tests as stress relaxation effects accrue. However, in three separate correlation tests, the net displacement between the shoulders was nearly identical in every case and was constant throughout the majority of fatigue life., This displacement was then used as the controlling parameter in the vacuum tests.

The fatigue life of a component may be considered to be comprised of the nucleation of a crack and its subsequent propagation to a critical length. Dependent upon loading conditions, usually open mechanisms or the other consumes the majority of useful life. In an effort to separate the relative amounts of crack initiation and crack growth, tiny notches were manufactured in selected specimens by the process of electrodischarge-machining (EDM). Each notched specimen has four different notches as depicted in Fig. 4.2. notch dimensions were about 60 microns deep and 75 microns wide with a notch root radius of roughly 40 microns to yield an elastic stress concentration factor of approximately 2.5. Two sets of notches were provided so that one set was available for microscopic analysis after failure occurs at the other set.

4.1.3 Mechanical Testing

Uniaxial strain controlled fatigue tests were performed on a commercial closed-loop electrohydraulic test machine equipped with a resistance furnace. A standard high temperature axial extensometer was employed to maintain strain control. hysteresis loops were periodically recorded; the cyclic load imposed on the specimens was monitored on a stripchart recorder.

All tests were conducted at 565°C (1050°F) using a fully reversed strain range of 0.50 percent. This temperature, while above the anticipated service temperate of 482°C (900°F) was chosen to enhance creep without altering the original carbide structure. The strain range was selected for three reasons. Firstly, it is a reasonable estimate of anticipated service conditions. Secondly, there is currently fewer data at such strain levels than exist at 1percent and above. Finally, previous research

of annealed 2.25 Cr 1 Mo [4.4,4.5] found hold periods at low strain ranges to be ore damaging than at higher strains (>1%) relative to pure fatigue in each instance, suggesting a more severe creep-fatigue interaction effect.

Four basic strain histories were examined: Pure fatigue (no hold periods), fatigue with tensile hold periods, fatigue with compressive hold periods, and fatigue with both tensile and compressive hold periods. All hold periods were introduced at maximum absolute strain amplitude. Hold period duration was varied from 6 to 3 to 1.5 to 0.75 minutes.

All specimens were used in the as-machined condition with no grinding or polishing. Failure was defined as a 50 percent reduction in tensile stress amplitude from the initial (maximum) value.

4.2 RESULTS AND DISCUSSION

The material exhibited rapid and continuous cyclic softening, the majority occurring within the first 10 percent of life. This was true regardless of waveform but hold periods induced greater and more rapid softening. This is illustrated in the stress range versus cycles plot of Fig. 4.3. The same data are normalized with respect to failure life in Fig. 4.4.

The introduction of a hold period into the hysteresis loop caused a significant reduction in fatigue life as compared to the continuously cycled (no hold period) case, the exact amount depending on the type (tensile, compressive, or combined tensile and compressive) and duration of the hold. In general, tensile hold periods were somewhat more damaging than compressive holds but the combined tensile and compressive waveform was considerably more damaging than either of the previous cases. The deleterious influence of hold periods, regardless of their location in the hysteresis loop or their duration, suggests a strong creep damage component.

The effect of hold period duration was not marked. Except for the 6-minute tensile hold test, hold periods of shorter duration yielded higher lives; whoever, the effect was not strong and, in general, hold period duration had only minor influence on fatigue life for a given waveform. This is seen in Fig. 4.5 which compares the stress range versus cycles for various hold time durations for combined tensile and compressive hold waveforms. This behavior could indicates a saturation effect

which has been proposed elsewhere [4.6] or perhaps more plausibly may suggest that the hold periods were not long enough for any creep damage to occur. However, the strain hold waveform and temperature were such that considerable stress relaxation occurred during each hold period throughout the entire test. The subsequent creep strain is almost certainly deleterious to fatigue life The most reasonable explanation for the small effect of hold period duration is that the stress relaxes in an exponential-like fashion. Thus most stress relaxation occurs every rapidly and there is little difference in creep strain for the hold period durations studied here.

EDM notches reduced cyclic life compared to analogous tests of smooth specimens by an average of 22 percent. If the EDM notch is considered as a nucleated fatigue crack, these results verify that the majority of useful life is consumed by crack propagation. This is a reasonable conclusion in that the material is quite ductile and the testing is in the low-cycle regime. The largest reduction was observed in the pure fatigue case; there was little effect on the combined 3-minute tensile and compressive hold period test. These and other EDM results are summarized in Fig. 4.6.

The EDM notch data yield insight into the material response to the various waveshapes. Since tensile hold periods are more damaging than compressive holds and the major portion of fatigue life is spent in crack propagation, it follows that tensile holds promote crack propagation. This makes sense intuitively in that the crack tip is subjected to a greater stress intensity factor. Furthermore, the ingress of aggressive environment to the crack tip is facilitated while the crack is held open.

Compressive hold periods, although not as damaging as tensile holds, still significantly reduce life relative to continuously cycled tests. Since a compressive hold does not induce tensile stresses at the crack tip (except for possible oxide wedging action), it would not enhance propagation rates and yet clearly there is some mechanism present which reduces life from the pure fatigue case. Teranishi and McEvily [4.7] proposed that compressive hold period causes premature crack nucleation through an interaction between oxide formation and spallation and surface deformation. Using microscopic analysis, they observed that in compression after a tensile hold, the oxide spalls and reveals fresh surface, thus removing surface damage and inhibiting crack initiation. Conversely, in tension after a compressive hold, the oxide film cracks rather than spalls, creating localized stress and

strain concentrators which facilitate early crack nucleation. This behavior was later related to the tensile strain in the oxide [4.8]. The authors further suggested that a tensile hold might be more deleterious than a compressive hold in the absence of oxidation effects. Of course, an alternative damage explanation is simply the additional plastic strain due to stress relaxation.

It follows logically that the combined tensile and compressive waveform is the most damaging type. The compressive hold aids in the initiation of a fatigue crack through the oxide induced stress concentration and the tensile hold speeds its subsequent propagation. Conversely, one may again hypothesize that the additional creep strain (stress relaxation in both tension and compression) is the controlling damage mechanism.

Although hold periods reduce cyclic life, time to failure is increased by over an order of magnitude for even very short duration holds. The prolonged exposure to high temperature results in severe oxidation which can adversely affect fatigue life. In an attempt to determine the effect of oxidation on the creep-fatigue behavior of this material selected tests were conducted in vacuum. Preliminary results indicate that a vacuum increases fatigue life by a factor of 2 to 4 over identical tests in air. The results of the vacuum tests are compared to air results in Table 4.2. EDM notches appear to be more effective in reducing cyclic life in vacuum than in air, indicating that while crack growth rates are enhance by oxide formation, the environment may have even a larger effect on fatigue crack nucleation; that is, initiation comprises a greater portion of life in vacuum than in air. This lends credence to fatigue life models [4.8,4.9] where oxide fracture is a major factor in premature crack initiation. However, analogous pure fatigue tests of EDM notched specimens in both air and vacuum suggest that vacuum also retards crack propagation rates as well. It should be emphasized that it is difficult to draw any definite conclusions about the effect of environment at this time since testing is still in its preliminary states.

4.3 CONCLUSIONS

1. The initial strength advantage obtained by the bainitic microstructure gained by quenching is lost via cyclic softening.

2. The introduction of a hold period into the cyclic waveform, regardless of its type or duration, significantly reduces fatigue life.
3. Combined tensile and compressive hold periods are most damaging, compressive only holds are least damaging, and tensile only holds are intermediate.
4. Hold period duration has only marginal influence on life, probably since most creep strain occurs rapidly.
5. EDM notches reduce cyclic life by roughly 25 percent in air, indicating that the majority of useful life is consumed by crack propagation.
6. Compared to results obtained in air, vacuum enhances life at least two-fold. Both crack initiation and propagation are inhibited in the absence of oxidation.
7. Environmental interaction may well be more important than creep damage in the low-cycle fatigue regime.

4.4 REFERENCES

4.1 Kar, R. J., and Todd, J. A., "Alloy Modification of Thick Section 2.25 Cr-1 Mo Steel," Application of 2.25 Cr-1 Mo Steel for Thick-Wall Pressure Vessels," ASTM STP 755, 1982, pp. 228-252.

4.2 Brinkman, C. R., Oak Ridge National Laboratory, ORNL-5416, 1978.

4.3 Corum, J. M., and Dalcher, A. W., "Materials Data Requirements for the High Temperature Structural Design of 2.25 Cr-1 Mo Steel Components," Oak Ridge National Laboratory, CONF-770545-3, 1977.

4.4 Brinkman, C. R., et al., "Time-dependent Strain-controlled Fatigue Behavior of Annealed 2.25 Cr-1 Mo Steel for Use in Nuclear Steam Generator Design," J. Nucl. Mater., Vol. 62, pp, 181-204, 1976.

4.5 Ellis, J. R., et al., "Elevated Temperature Fatigue and Creep-fatigue Properties of Annealed 2.25 Cr-1 Mo Steel," Structural Materials for Service at Elevated Temperature in Nuclear Power Generation, ASME-MPC-1, 1975, pp. 213-246.

4.6 Carden, A. E., et al., "Time-dependent Fatigue of Structural Alloys--A General Assessment," Oak Ridge National Laboratory, ORNL-5073, 1975.

4.7 Teranishi, H., and McEvily, A. J., "the Effect of Oxidation on Hold Time Behavior of 2.25 Cr-1 Mo Steel," Metall. Trans., Vol. 10A, pp. 1806-1808, 1979.

4.8 "An Explanation for the Effects of Hold Periods on the Elevated Temperature Fatigue Behavior of 2.25 Cr-1 Mo Steel," J. Mater. Tech., Vol. 103, pp. 7-14, 1981.

4.9 Challenger, K. D., Miller, A. K., and Langdon, R. L., "Elevated Temperature Fatigue with Hold Times in a Low Alloy Steel: A Predictive Correlation," J. Mater. Energy Systems, Vol. 3, pp. 51-61, 1981.

Table 4.1 Tensile Properties of Kawasaki 2.25Cr-1Mo Steel

strain rate = 0.004 per second

	25°C	565°C
Elastic Modulus (GPA)	208	159
0.2% Yield Strength (MPa)	474	348
Ultimate Strength (MPa)	590	380
True Fracture Stress (MPa)	1280	838
corrected to (MPa)	1090	699
True Fracture Ductility	1.53	1.94
True Strain @ Ultimate Load	0.076	0.019
Strain Hardening Exponent	0.11	0.06
Strength Coefficient (MPa)	855	510

Table 4.2

Specimen	Test	Air	N_f	Vacuum
Smooth	Pure Fatigue	3783		-
Smooth	3 Min T Hold	1465		5447
EDM Notch	Pure Fatigue	2654		5276
EDM Notch	3 Min T Hold	(2000)[a]		3789

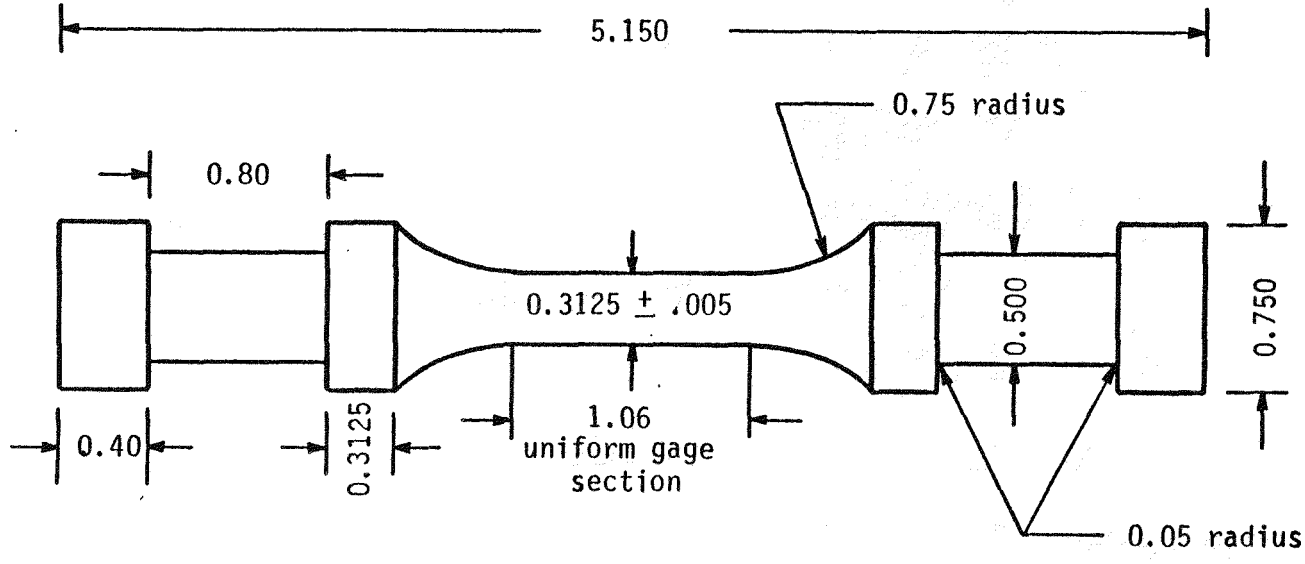

Fig.4.1 Double shoulder specimen geometry for encapsulated testing (add dimensions in mm.)

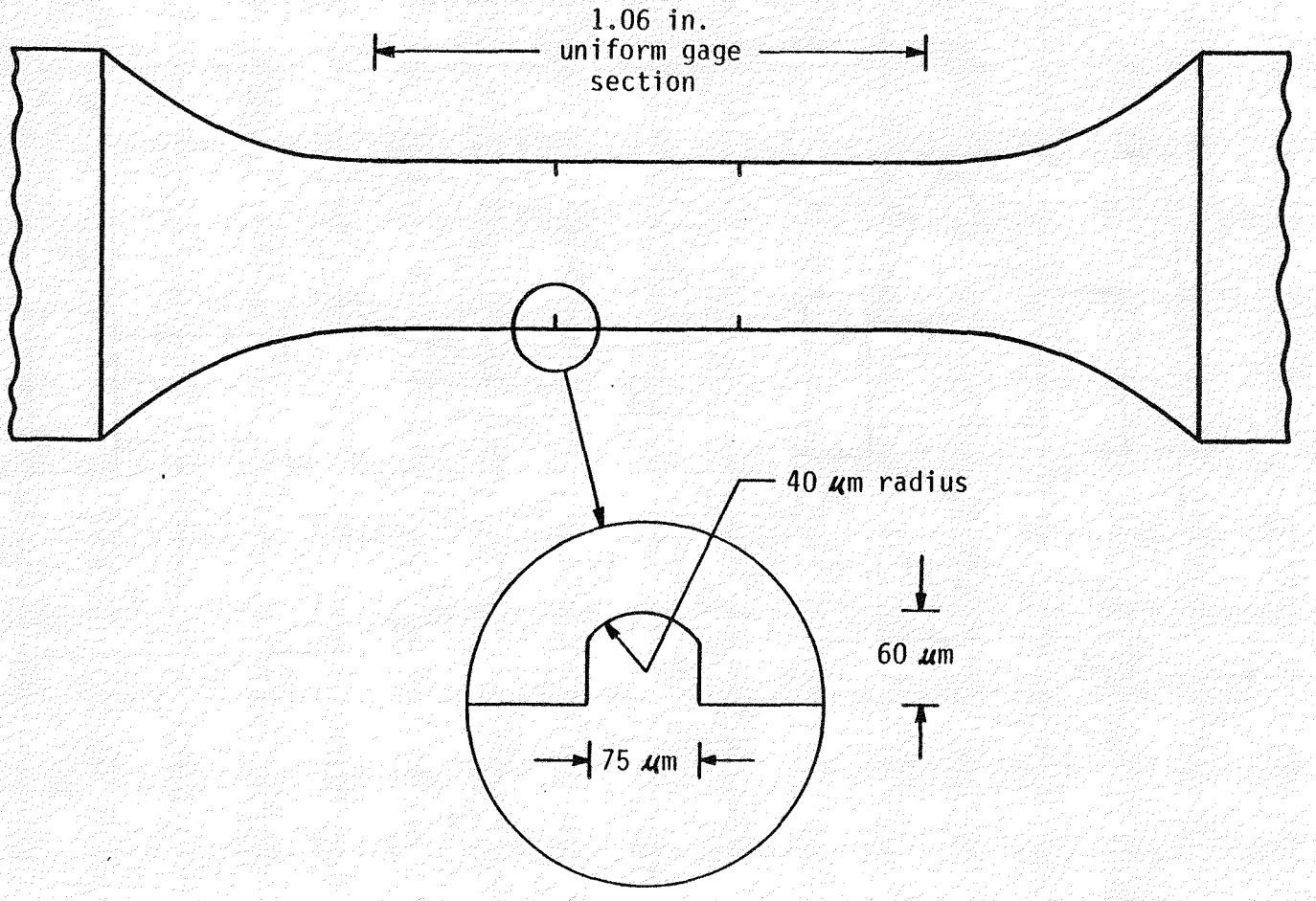

Fig.4.2 Schematic of electro-discharge machined (EDM) notch specimen

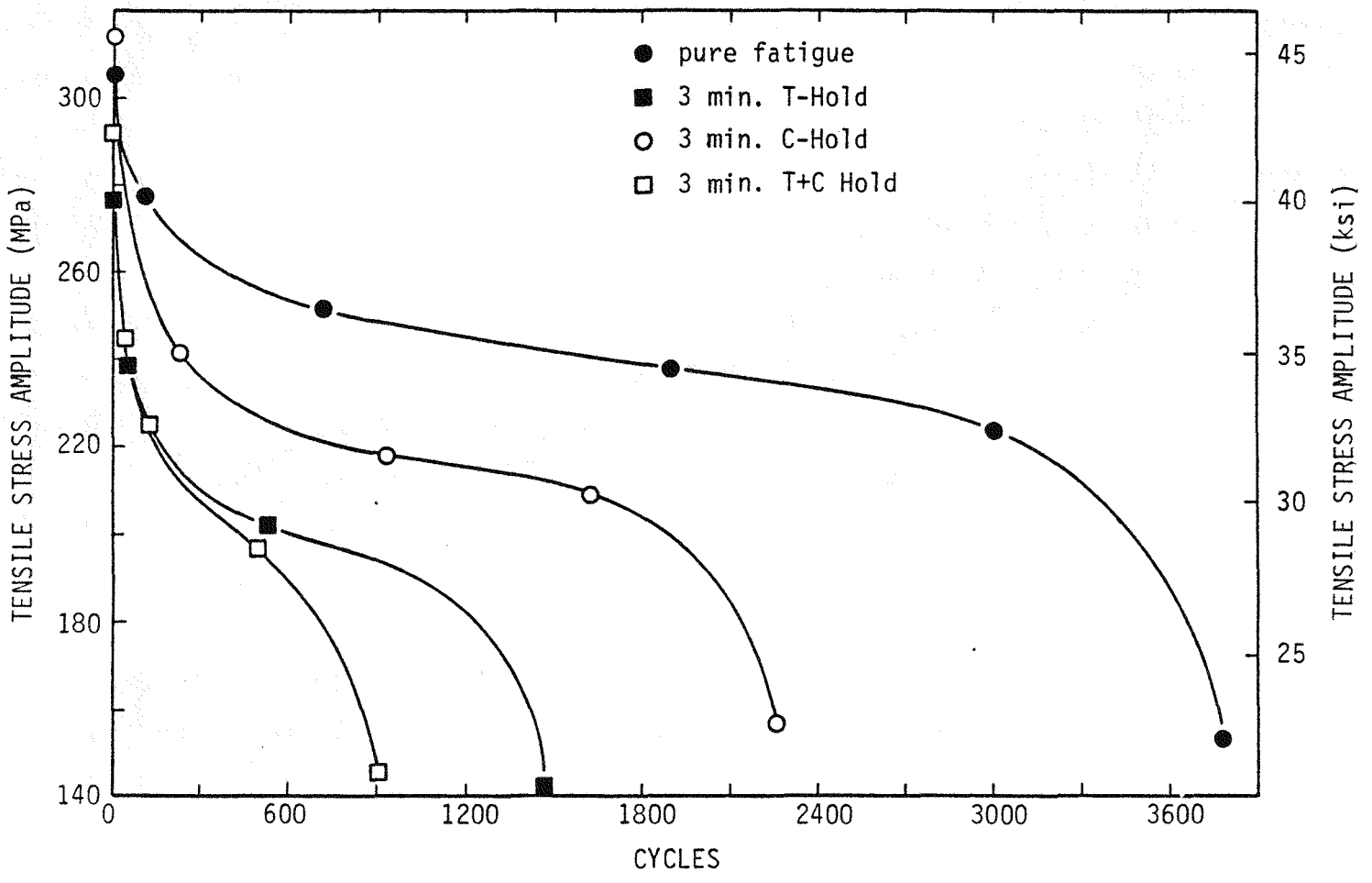

Fig. 4.3 Stress range versus fatigue cycles showing effects of different combinations of tension and/or compression holds. Lukens 2.25 Cr 1 Mo at 565°C

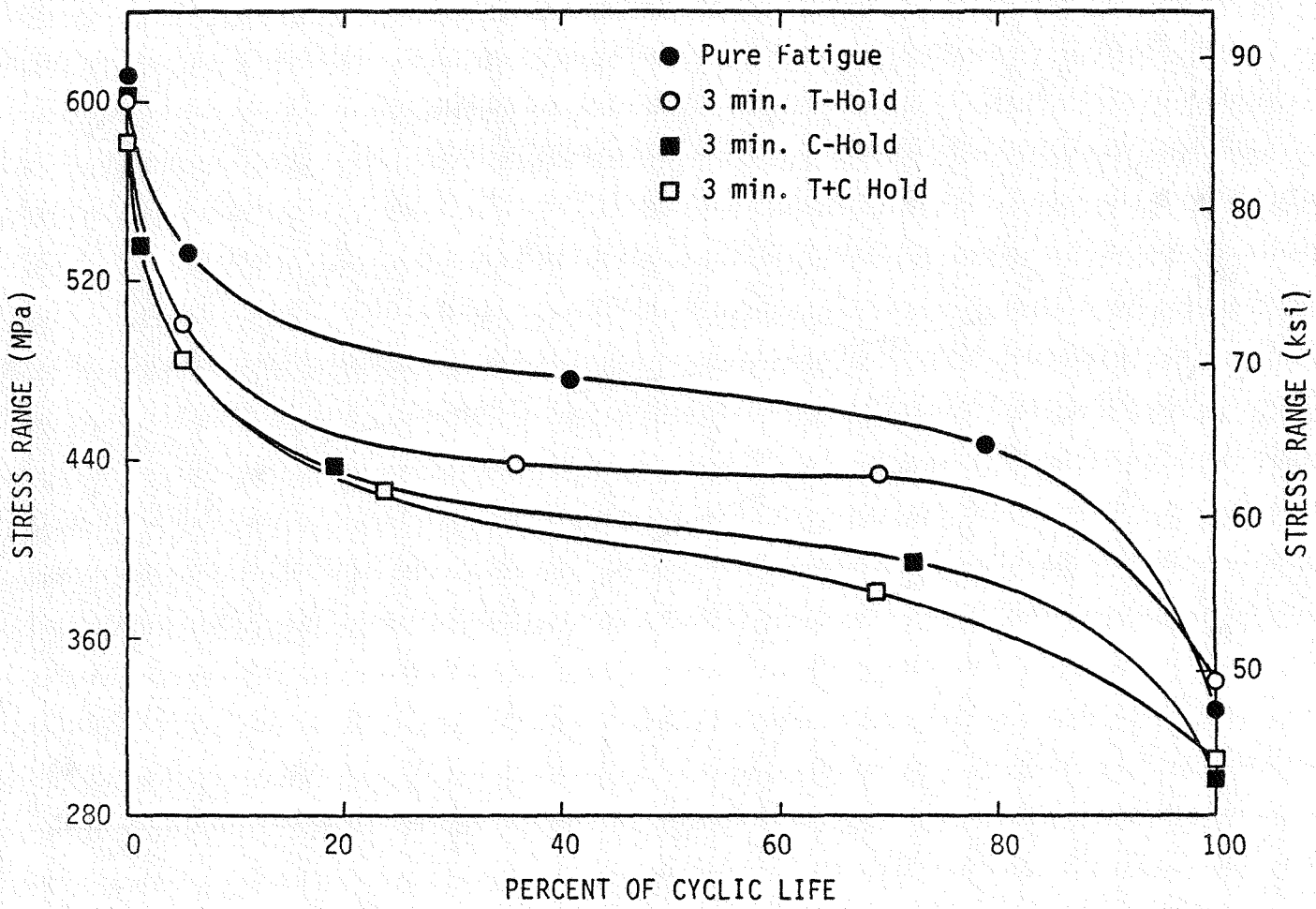

Fig.4.4 Data from Fig. 4.4 normalized with respect to fatigue life, showing effect of cyclic wave shape on relaxation

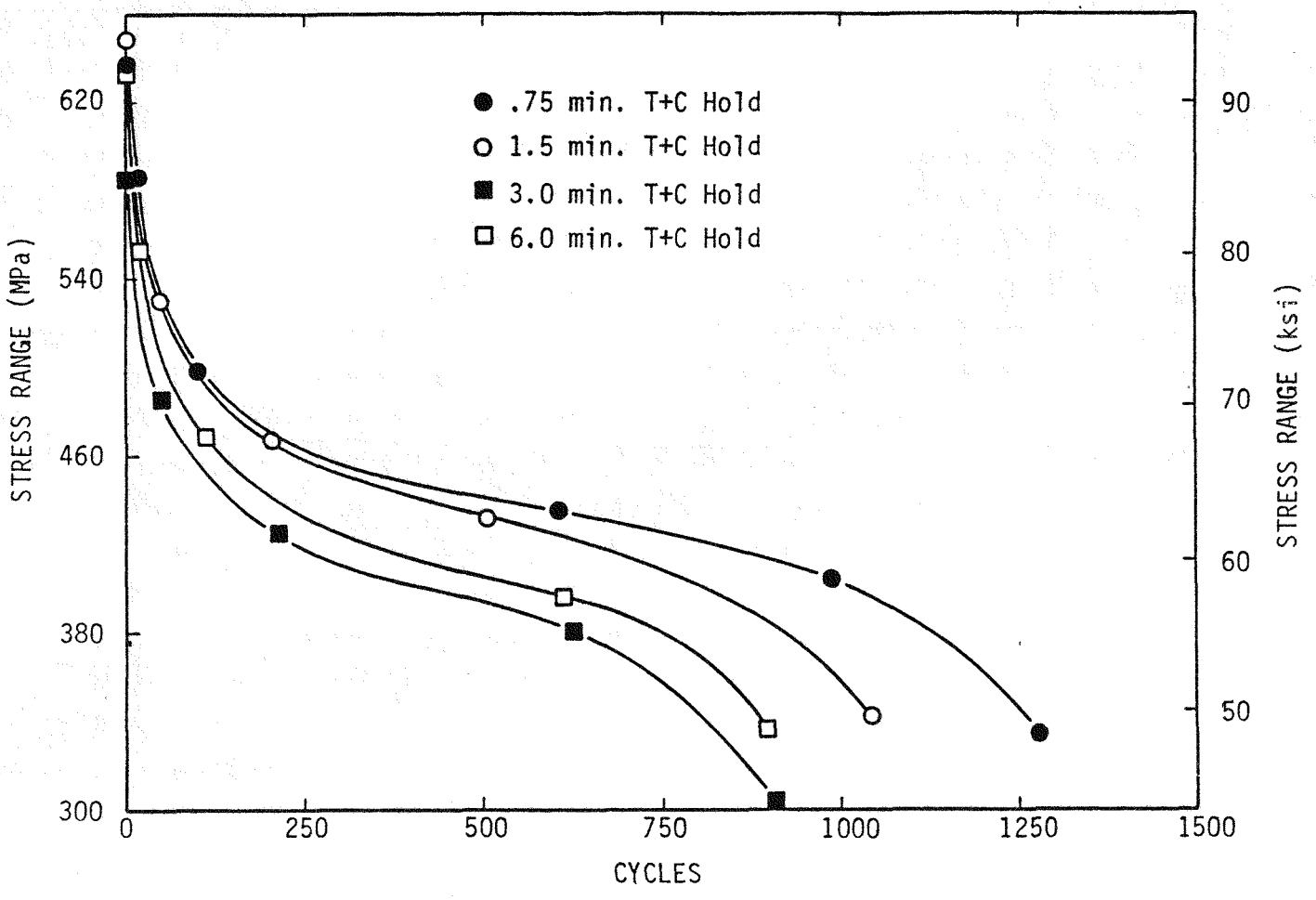

Fig. 4.5 Stress range versus fatigue cycles for combined tensile/compression waveforms illustrating only minor effects of hold time duration. Lukens 2.25 CXr 1 Mo at 565°C.

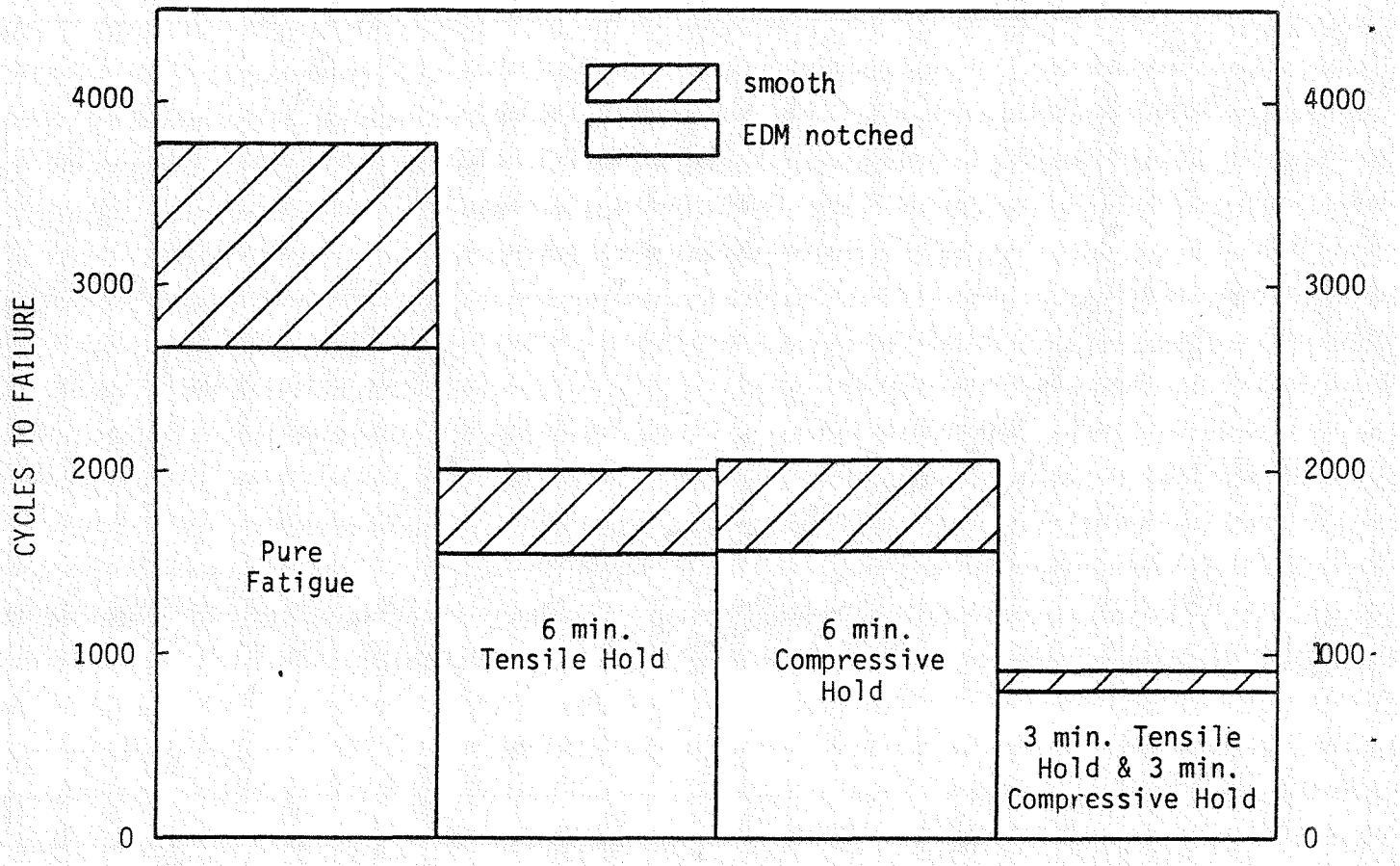

Fig. 4.6 Comparison of fatigue life data in air for smooth and EDM notched specimens

5. SUMMARY OF CONCLUSIONS

i) The most significant behavior of the bainitic materials examined is a persistent loss of strength with number of cyclic stress reversals which, within a small fraction of the fatigue life, causes the yield stress to reduce to a value approaching that of the same material in the ferritic/pearlitic state.

ii) The mechanism of softening can be correlated with lath broadening. Under cyclic conditions, the well defined lath structure transforms rapidly to a more blocky structure, approximately in step with the rate of cyclic strength decay. Under creep conditions, breakup of the lath structure is also observed, but the extent is much less than under cyclic loading. The softening mechanism is therefore believed to be a strain induced recovery of the oversaturated, highly tangled dislocation structure in the quenched and tempered state. The two materials examined were supplied in slightly different degrees of temper, with the Lukens material initially quite free of carbide particles, which precipitated rapidly in the first few cycles of a fatigue test. While this mechanism is considered to have some influence on strength changes during the specimen life, the recovery of the dislocation structure is believed to the primary softening mechanism.

iii) Fatigue life is reduced by holding periods of reduced load cycle frequency. However, no significant intergranular creep damage could be induced in this material, even under elevated hydrostatic conditions, of after prior plastic cold work, so that the fatigue/environment interaction is not a creep/fatigue damage interaction per se.

iv) Three causes of reduced fatigue life under extended times at elevated temperature were identified, i.e., direct effect of strain induced softening, oxidation and creep deformation.

v) The largest interaction effects observed in this study can be associated directly with strain softening leading to a limit-load type collapse mechanism as the cause of failure. Despite complex

constitutive behavior, which is not very well understood, component behavior can nevertheless be modeled rather simply by assuming that the component yield stress is decreasing monotonically, following the cyclic softening curve.

vi) Fears of bainitic materials losing load carrying capacity due to cyclic softening can be a deterrent to their use in some circumstances. From tests on notched components it is shown that the effects of localized softening need not preclude the full utilization of the quenched and tempered material. However, its suitability of otherwise is not something that can be judged in isolation from the application, because the extent of softening depends on the degree of strain control, and this is a factor which depends on the geometry of the component. Some investigation has been made of the boundary between applications in which softening can be safely ignored, and those in which the softened condition controls component strength, but this is a question which still needs a rational solution. An important unknown which still has to be considered is the influence of stress range and R-ratio on activation of strain softening, since this governs how much material in a component under complex stress conditions will experience loss of strength.

vii) Strain controlled fatigue, which does not appear to be affected by the softening phenomenon directly, still exhibits a frequency-dependent cyclic life. From tests in air and vacuum, it seems that propagation is the major component of fatigue life in the regime explored in this study. It is clear that environment is a significant, but not exclusive, cause of accelerated fatigue. It is concluded that an important contribution is the effect of creep deformation/stress-relaxation at the crack tip during slow loading or hold periods. A tentative model has been developed to explain this phenomenon, but it is only a hypothesis at this time, and is more appropriately discussed under future work.

viii) The effect of environment is major and complex. For instance, a fatigue test in air, with equal hold times in tension and compression, displayed much lower cyclic life than an equivalent test with the same cumulative hold time in tension only. In vacuum, the equal hold time test lasted longer than the

tension only hold test. There is a need for a robust crack propagation model which can include the effects of surface oxidation.

6. FUTURE RESEARCH DIRECTIONS

We have at present, only a qualitative correlation between lath broadening and strain softening. It would be helpful, both from the point of view of residual life assessment, and as a guide to the development of a practical constitutive relationship, to have a better definition of the effect of microstructural changes on strength. More TEM work is needed to see how lath and precipitate structure evolve with strain.

It is known that cyclic, reversed stresses induce the softening effect. On the other hand, cyclic stresses which do not reverse sign appear, on preliminary studies, to have no effect. It is uncertain what degree of reversibility is necessary to activate the softening phenomenon. For instance, softening has been observed in tests where the stress range is much less than the initial cyclic yield range. The number of parameter combinations required to explore all the possible conditions is too large to be carried out on a purely empirical basis. Therefore, once again, the need is foreseen for a reliable constitutive relation to guide the choice of definitive tests.

In the tests carried in this program, it seems that crack propagation is the dominant mechanism. However, it is difficult to trace the evolution of cracking except by interrupting tests and performing destructive examinations. There is a need for a means of monitoring in-situ fatigue damage, however crudely, and a candidate method with definite possibilities is AC potential drop measurements.

Also connected to crack growth, we need a model of deformation in small cracks, i.e. less than 1 to 10% of specimen thickness, in inelastic fields, including creep effects. An exact solution to this problem is a major task in itself, and is probably impossible until a reasonable constitutive model has been developed for this type of softening behavior. Some success is being had on a more approximate front however, using relaxation creep curves to represent material behavior at crack tips. This approach needs data in the form of isochronous stress-strain behavior for this type of material is relatively insensitive to load history, which will simplify the problem considerably. Only then is it believed that the frequency effects observed in this project can be explained adequately.

The component-dependent aspects of strain softening as a limit on allowable design stresses is a major problem. While it has been shown that local softening is not necessarily detrimental to the component as a whole, we do not as yet have a reliable criterion on which to judge this situation. Work has been started on evaluating inherent strain control properties of component geometries but a great deal more needs to be done in this field.

There is evidence that softening materials have inferior fatigue lives, for a given strain range, compared with cyclic hardening materials, even when the yield strength of the latter is lower. It is not possible to judge the situation as yet, but it is conceivable that cyclic softening can cause strain localization in crack tip zones, producing higher crack opening displacements for the same nominal remote strain range. This is a possibility that deserves to be investigated further.

APPENDIX A - APPROXIMATE ANALYSIS OF COMPONENTS COMPOSED OF STRAIN SOFTENING MATERIAL

A.1 INTRODUCTION

The behavior of components made of strain softening materials is not understood very well. From a theoretical point of view, it is easier to concentrate on strain hardening materials because they are easier to model. Strain hardening also conforms to a stability criterion, as stated for instance by Drucker [A.1], that allows unique solutions to be found, and general theorems, such as the Limit Theorems of Plasticity, to be formulated. In practical terms, strain hardening is a desirable property because it limits the degree of strain localization that might be experienced in regions of inelastic deformation such as notches or other forms of strain concentration, whereas softening may cause load material instability and severe strain intensification in some circumstances. In fact, it has been common practice to specify that the tensile strength and the yield strength of materials for use in pressure vessel construction should have a minimum ratio, typically about 1.3, for precisely the purpose of ensuring sufficient strain hardening capacity. It is not surprising, therefore, that strain softening materials, have attracted relatively little attention until recently.

In recent years the demands on material performance have grown in virtually all respects as a consequence of which many applications are being found where the prospect of some form of strain softening cannot be avoided. Examples are damage induced softening, as is experienced in the process zone of cracks during ductile fracture and inelastic deformation of concrete [A.2], and cyclically induced strain softening frequently observed in high strength materials [A.3]. It is probable therefore that standard design procedures will eventually have to be modified so that instead of avoiding strain softening, they will be able to include this behavior explicitly. Unfortunately, since the classical development of the mechanics of inelastic deformation has tended to ignore strain softening, with singular exceptions such as the work of Maier and Drucker [A.4], there are no generalized concepts available to guide designers in decisions regarding the probable performance of components constructed from materials which behave in this way.

The problem is receiving increased recognition, and efforts have been growing recently to formulate constitutive theories which adequately describe softening as, for instance, the MATMOD model developed by Lowe and Miller [A.5]. The current state-of-the-art in constitutive modeling is anything but complete however, and no widely accepted model of softening exists at present. Furthermore, the problem of designing in strain softening materials cannot be completely solved by the simple expedient of developing a detailed constitutive model, any more than this has been the case with other forms of material behavior.

The questions which have to be answered in design go much further than the single question of modeling a given component geometry and accurately simulating its performance under some closely specified loading history. While this may be part of the design process, it is one which is limited to the later stages of design verification when the purpose is verification and possibly some degree of fine tuning. Detailed constitutive models have limited value in the processes of initial selection of materials and basic component shape where many options may have to be considered in a relatively short time scale and where issues such as sensitivity of the design configuration to gross variations have to be investigated based on information of material properties limited to a few robust, generic characteristics such as yield strength and ductility. The case-specific material behavior required for detailed modeling is frequently only available very late in the development process, after material procurement and a lengthy period of materials testing. For early design purposes, it is also necessary to have more economical, robust models, which are not dependent for their application on data that are inherently impossible to obtain at the time they are needed.

In dealing with all aspects of design in stable, or strain hardening materials, a valuable store of experience has been developed, consisting of certain performance parameters such as yield strength. More importantly, characteristics of combined material/component behavior such as stiffness, limit load, and buckling load have been identified with which to scope out a satisfactory solution, in preparation for more detailed analysis at a later date. The mechanics of materials have contributed to this process in the form of models of the strain response to stress, temperature, and other environmental factors but also in the development of concepts such as the stress categories in

the ASME Pressure Vessel Code [A.6] which compactly describe the significance of different types of stress, depending on whether they are load-induced or self-equilibrating.

No such store of experience exists in the case of strain softening materials. There are indications that problems may arise sometimes in the form of local material instability leading to severe strain localization [A.7]. On the other hand, it has been common practice to ignore the influence of cyclic softening in the treatment of fatigue in high strength materials beyond the use of a cyclic stress-strain relationship based on the midlife strain range [A.3]. Clearly there is a need for criteria to judge whether a given case is one in which the peculiarities of strain softening have to be accounted for, (for instance by simply avoiding materials of this type altogether) or whether the phenomenon can be safely ignored. Detailed analyses, for example those performed by Tvergaard [A.7], show how strain localization can develop in simple geometries but this is not a practical tool in a design situation where neither the material type nor the geometry of the component has yet been fixed.

A.2 STRAIN SOFTENING IN COMPONENTS

Several questions needing answers are as follows:

(i) What is the effect of cyclic softening on the limit load and creep strength of a complex component?

Swindeman [A.8] has shown, for instance, that quenched-and-tempered low alloy steels for pressure vessel construction can suffer a serious loss of strength as a result of periodic load reversals in simple uniform section test specimens. On the other hand, mixed responses have been found in notched bars in which the cyclic plasticity is local and partially constrained [A.9]. A criterion is needed to discriminate between situations where the softening is general, and adversely affects the component strength, from those in which it is localized and, at most, leads to some strain amplification.

(ii) What effect has local cyclic softening on shakedown?

Shakedown is a generalized structural failure mode but, in the ASME Pressure Vessel and Piping Code, a conservative criterion is adopted, limiting the maximum local stress range effectively to within the elastic range. It is not certain when deriving design stress limits for cyclic softening materials whether it should be the initial or the softened yield stress range that should be adopted--or whether the choice depends in some way on the component geometry. Goodall, et al. [A.10], assert that the shakedown limit of stainless steel components is not improved by cyclic strain hardening. It remains to be seen if, as a corollary, cyclic softening has no detrimental effect. This is a fairly important problem because the difference between the initial and softened strengths of some of the new heat treated alloys can differ by as much as 30%, which could be a serious restriction on allowable cyclic stress ranges for design.

(iii) To what extent does softening lead to local strain intensification?

This is a particular instance of a general problem concerning the question of whether strain at any point in a component is subject to strain control or load control. Other important instances are the question of "elastic follow-up" and deciding on design stress categories for the stresses obtained from finite element analyses. Structures such as multiple parallel bar models can be devised in which the strain in a single element is under almost complete strain control whereas any statically determinate structure containing strain softening elements goes unstable as soon as the first element reaches its maximum load capacity. A strain softening material might be used safely in a strain controlled situation but greater caution would have to be exercised in a component which is close to statically determinate behavior.

The subject of this section is the last of these three problems. Probably the most frequent instance of inelastic behavior in practical components is localized strain concentration as found, for example, in notchlike details. It would, therefore, be a useful first step toward developing an appreciation of strain softening behavior in components if this problem were better understood.

Notchlike geometries are encountered so frequently that it would be costly to analyze every one exactly. Approximate methods such as Neuber's analysis [A.11] are indispensible design tools, if only to provide a filter to identify critical points for further evaluation. This paper explores the possibility of extending simplified notch analysis to include strain softening. The objective is to derive some generalized understanding of the combined material/component interaction. For this reason, no specific strain softening phenomenon is identified, although the conclusions can be applied directly, or indirectly, to monotonic deformation, cyclic softening, and the approximate representation of creep deformation including continuum damage.

A.3 DESCRIPTION OF EXAMPLE COMPONENTS

The investigation examined the elastic-plastic behavior of three simple component geometries under monotonic increasing load. These are shown in Figs. A.1 and A.2.

The constitutive relationship used was an elastic, linear strain hardening model with the degree of hardening or softening defined by a variable strain hardening coefficient, α, which could take negative values to represent softening behavior as illustrated in Fig. A.3.

The three-bar structure was used as a simple vehicle to make a preliminary examination of component response to strain softening. While not strictly a notchlike geometry, it was configured to produce a significant degree of strain concentration in the central bar. Its one disadvantage as a test case is that the plastic zone size (the central bar) is fixed. This is not typical of more continuous structures in which the plastic zone size grows with increasing applied deformation.

The remaining two geometries considered were all obtained by modifying the boundary conditions of an existing model of a Bridgman notch specimen to give

(a) a spherical hole in a cylindrical bar in tension and

(b) an axisymmetric C-notch in a cylindrical bar in tension.

These models, since they are continuous solids, allow for the progressive growth of the zone of plastic deformation which cannot be obtained in the three-bar model. Furthermore, they display

different degrees of local constraint at the strain concentration, constraint being greatest for the spherical hole and least for the C-notch.

The finite element models employed are relatively coarse and consisted of simple four-node, isoparametric elements using a limited bandwidth version of ANSYS. This was considered acceptable in this study because the object was not to develop accurate simulations of specific geometries but to investigate general characteristics for which the simplified models used can be considered valid test cases in their own right. Initially, more refined modeling was attempted but, combined with slow convergence in the case of negative "hardening", this led to extremely long computations which were not considered to be justified in an exploratory study of this nature.

A.4 DISCUSSION OF RESULTS OF ANALYSIS

The only result of relevance here is the relationship between the stress and the strain at the point of maximum strain concentration. As illustrated schematically in Fig. A.4, this relationship traces out a generalized hyperbolic locus, for a fixed load level, as the strain hardening/softening coefficient varies. In the case of a pure strain controlled situation, the locus is a vertical line at constant strain while, for load control (i.e. statically determinate), the locus is a horizontal line at constant stress. Neuber's hyperbolic rule is intermediate between these extremes and is adopted in this paper as an arbitrary dividing line between local behavior which is strain dominated and load dominated behavior. Stress/strain behavior lying on the strain controlled side of the Neuber curve will be referred to as "hypo-Neuber" and behavior on the load controlled side as "hyper-Neuber".

Results for all three structures considered are summarized in Figs. A.5, A.6 and A.7. In the case of the three-bar structure, the stresses and strains refer to the central, most highly strained bar which is assumed to deform uniformly, i.e. local instability in the length of the bar itself is not considered. For the remaining structures, the values refer to the mid-element Mises effective stresses and strains in the most highly strained element.

In all cases the locus of stress versus strain with changing strain hardening index shows a clear trend which extends continuously from positive to negative values of the hardening coefficient. Not

surprisingly, the Neuber rule is not correct for any of the geometries examined although it could present a first-order approximation for initial design scoping calculations. The main observation is, however, that the relaxation characteristics at a point of local inelastic deformation follows a trend which is not strongly dependent on the particular material constitutive relation and applies equally well whether the material hardens or softens as long as the inelastic strain is not too much greater than the elastic strain. To a first approximation, therefore, if a Neuber analysis is considered adequate for dealing with local inelastic deformation of a strain hardening nature, the same form of analysis should be acceptable if the material strain softens.

It can be inferred from the observations described in the previous paragraph that local deformations are largely a function of the component geometry. If so it should be possible to isolate this dependency as a parameter of the component without any reference to the detailed material behavior. So far no clear candidate for this purpose has been identified but experimentation with the three-bar structure indicates one possible direction to consider.

In the three-bar structure once the central bar has yielded, the overall stiffness is dominated by the remaining two (elastic) bars. It is expected, therefore, that a good approximation to the peak stress/strain locus could be obtained by varying the modulus of elasticity, E, in the central bar while maintaining constant load on the structure as a whole. As shown in Fig. A.8, this procedure does indeed give a very close approximation to the inelastic locus obtained incidentally at significantly less computational expense than the inelastic analyses required to obtain the exact solution.

Inelastic deformations of a simple component like the three-bar structure can, therefore, be reduced to a small number of elastic calculations to produce the peak stress/strain locus while the constitutive behavior can be considered as a virtually independent problem. Separation of essentially structural behavior from material behavior is a considerable simplification which should significantly reduce the amount of computation needed when complex constitutive relations are involved. More importantly, this separation allows predictions to be made for situations where the current knowledge of material constitutive behavior has not yet advanced to the state where it can be represented in the explicit form required for input to a full analysis--as is the case at present with strain softening.

The problem is somewhat more complicated in the case of continuous structures because, unlike the three-bar structure, the extent of the plastic zone is not a constant, but increases as the load increases and as the strain hardening coefficient decreases. It is possible to obtain the asymptotic behavior of the peak stress/strain locus for initial plastic deformation by perturbing the modulus of elasticity of the most highly strained element in the elastic state. The remainder of the locus can be approximated by a generalized hyperbola of the form

$$\varepsilon^N \sigma = \text{constant}$$

where N > 1 denotes hypo-Neuber behavior (strain dominated) and

N < 1 denotes hyper-Neuber behavior (load dominated).

Results of this approximate approach are included in Figs. A.6 and A.7 and show reasonable accuracy for modest increases of strain over the elastic limit. The procedure for constructing these approximate loci was slightly different from the truss example. A generalized hyperbola has fitted to points corresponding to elastic response and the maximum positive strain hardening coefficient and extrapolated to lower coefficients as well as negative or softening conditions.

Two elastic analyses could, therefore, provide sufficient information to give a reasonable estimate of local strain behavior under quite general inelastic conditions. This is only slightly more effort than is required to perform a Neuber analysis but has the advantage over the latter in that it includes an explicit measure of the degree of local constraint.

As is to be expected, the approximation only works well for small-scale yielding. As general yielding of the structure is approached, there is further strain amplification which cannot as yet be anticipated by simple methods. However, as it transpired, the examples considered in this study are severe tests because the window between first yield and the limit load is a narrow one in each case. In most cases of strain concentration, the plastic zone tends to be more localized and the maximum strain more severe compared with the nominal level and it is expected that a wider range of applicability would be available in more practical geometries.

A.5. FUTURE DEVELOPMENTS

The examples used in this study were somewhat ad hoc, being governed by which models were readily available. With hindsight, a clearer picture of local plastic deformation would be obtained with a structure with a more localized strain concentrating feature and a higher ratio of limit load to load at first yield, as might be expected, say, in a weldment or a pressure vessel nozzle.

It is apparent from this investigation that there is a need for two generalized measures of structural performance in order to cope with the problem of localized strain concentration in the presence of complex constitutive behavior. The first of these is needed to locate the structure on a scale ranging from kinematically determinate (total strain control) to statically determinate, total load control) in order to decide whether the use of strain softening material is acceptable or not. The examples given in this paper strongly suggest that such a characteristic does indeed exist and a heuristic approach shows that this characteristic can at least be obtained approximately by perturbing the elastic moduli of selected elements in a finite element model. However, it is believed that there is a more rigorous explanation for this behavior which still needs to be revealed.

The second characteristic relates to the proximity of generalized yielding and the strain amplification which accompanies it. If local inelastic deformation can be shown to be constrained, it appears that the strains themselves can be predicted reasonably well. We still do not have a reliable criterion to judge when it is valid to assume local conditions to be constrained, however. The work of Seeger [A.12] and Glinka [A.13] indicate that it is possible to cope with general yielding when dealing with strain hardening materials. It remains to be seen whether this work can be extended to include strain softening.

A.5 CONCLUSIONS

1. It has been shown that when local strains are constrained, the deformations obtained in strain softening materials are similar in character to those obtained in strain hardening material. This

means that simplified analytical techniques such as the Neuber analysis may still be applicable, even when the material softens.

2. An approximate method for estimating local strain has been proposed which, unlike the Neuber approach, includes the specific geometry of the component and its effect on the degree of local constraint.

3. The approximate method of strain prediction presented in this paper is heuristic, based largely on observation of a few numerical examples. Nevertheless, there is a consistency in this observed behavior which suggests some fundamental structural characteristic which still needs to be identified.

A.6 REFERENCES

A.1 Drucker, D. C., "Reflections on the Development of Plasticity Theory and its Successful Application," The Author Newell Talbot Lecture, Nov. 8, 1984, University of Illinois at Urbana-Champaign, Department of Theoretical and Applied Mechanics Report T&AM 471, Feb. 1985.

A.2 Symposium on Constitutive Equations: Macro and Computational Aspects, ed. K. J. William, ASME Winter Annual Meeting, New Orleans, Dec. 9-14, 1984, jointly sponsored by Applied Mechanics, Pressure Vessels and Piping, and Materials Divisions.

A.3 Socie, D. F., M. R. Mitchell, and E. M. Caulfield, "Fundamentals of Modern Fatigue Analysis," University of Illinois FCP Report 26, January 1978.

A.4 Maier, G., and D. C. Drucker, "Elasto-plastic Continue containing Unstable Elements Obeying Normality and Convexity Relations," Schwiezerischen Bauzeitung, Vol. 23, No. 9, June 1966, pp. 1-4.

A.5 Lowe, T. C., and A. K. Miller, "Improved Constitutive Equations for Modeling Strain Softening-Part I: Conceptual Development," ASME J. Eng. Matls. and Tech., 1984, ASME Paper No. 84-Wa/Mats-15.

A.6 ASME Boiler and Pressure Vessel, ASME 1985.

A.7 Tvergaard, V., "Analysis of Material Failure by the Nucleation, Growth and Coalescence of Voids," Symposium on Constitutive Equations, ASME Winter Annual Meeting, New Orleans, Dec. 9-14, 1984, pp. 179-192.

A.8 Swindeman, R. W., "Response of Ferritic Steels to Nonsteady Loading at Elevated Temperatures," Research on Chrome-Moly Steels, ed. R. A. Swift, MPC-21, ASME, 1984, pp. 31-42.

A.9 Handrock, J. L., and D. L. Marriott, "Cyclic Softening Effects on Creep Resistance of Bainitic Low Alloy Steel, Plain and Notched Bars," paper submitted for 1986 PVP Conference, Chicago, July 1986.

A.10 Goodall, I. W. R. Hales, and D. J. Walters, "On Constitutive Relations and Failure Criteria of an Austenitic Steel under Cyclic loading at Elevated Temperature," Central Electricity Generating Board, Berkeley Nuclear Laboratories Research Division Report RD/B/N4916, Oct. 1980.

A.11 Neuber, H., "Theory of Stress Concentration for Shear-Strained Prismatical Bars with Arbitrary Non-Linear Stress-Strain Law," J. Appl. Mech., Trans. ASME, Vol. 28, Dec. 1961, pp. 544-550.

A.12 Seeger, T., and P. Heuler, "Generalized Application of Neuber's Rule," J. Test. Eval., Vol. 8, 1980, pp. 199-204.

A.13 Glinka, G., "Energy Density Approach to Calculation of Inelastic Strain-Stress near Notches and Cracks," Eng. Fract. Mech., Vol. 22, No. 3, 1985, pp. 485-508.

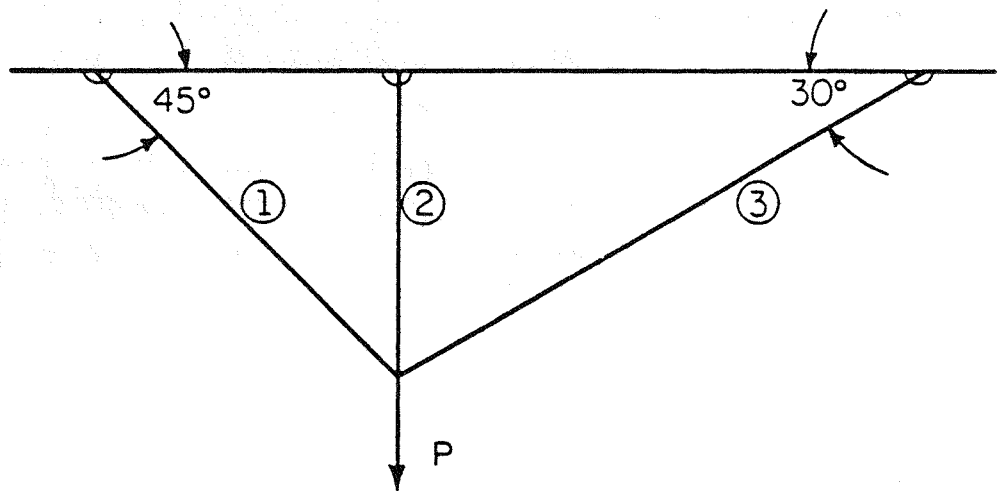

Fig. A.1 Three-Bar Structure (all members have equal, uniform sections; Bar 2 is the highest strained member)

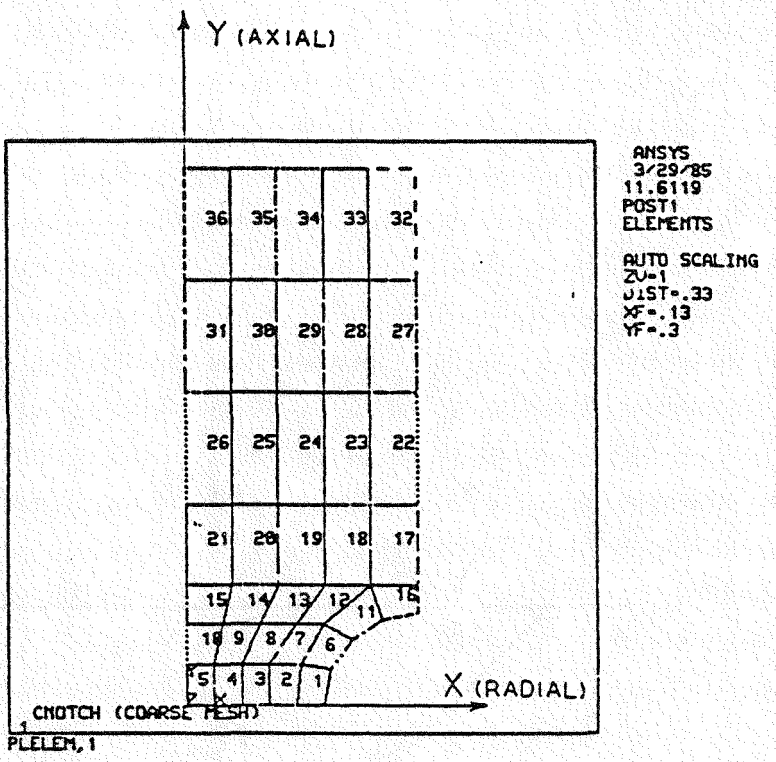

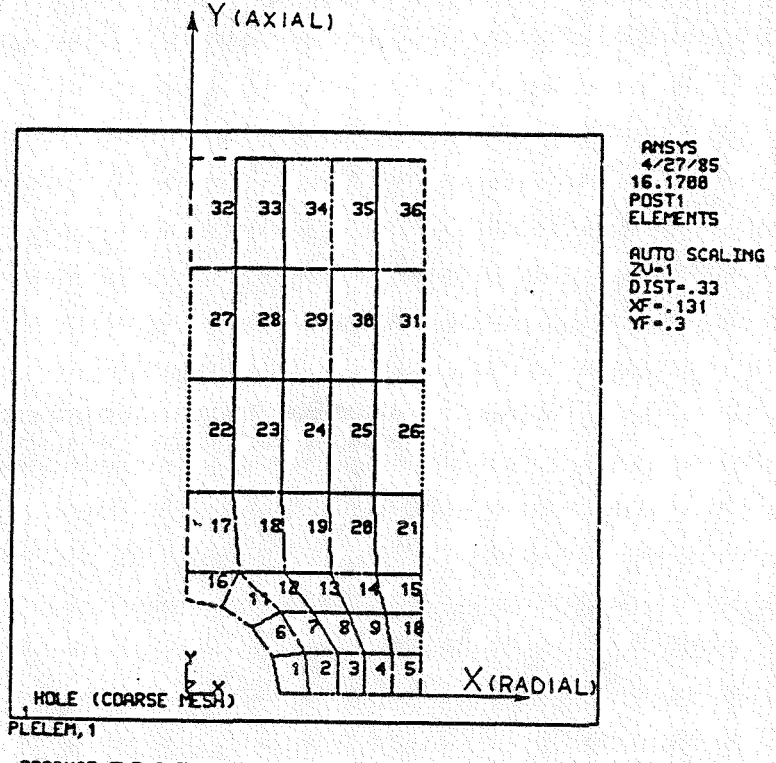

Fig. A.2 Geometries of Notched Bar and Bar with Spherical Cavity

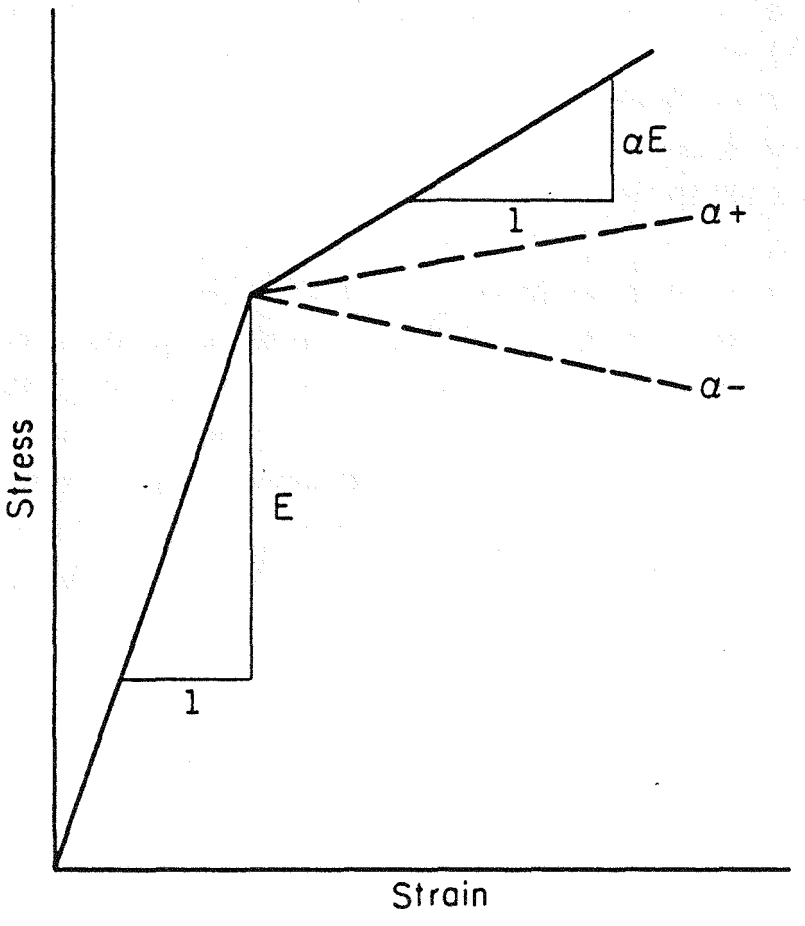

Fig. A.3 Schematic Representation of the Constitutive Relation is the strain hardening coefficient nondimensionalized with respect to Young's modulus, E)

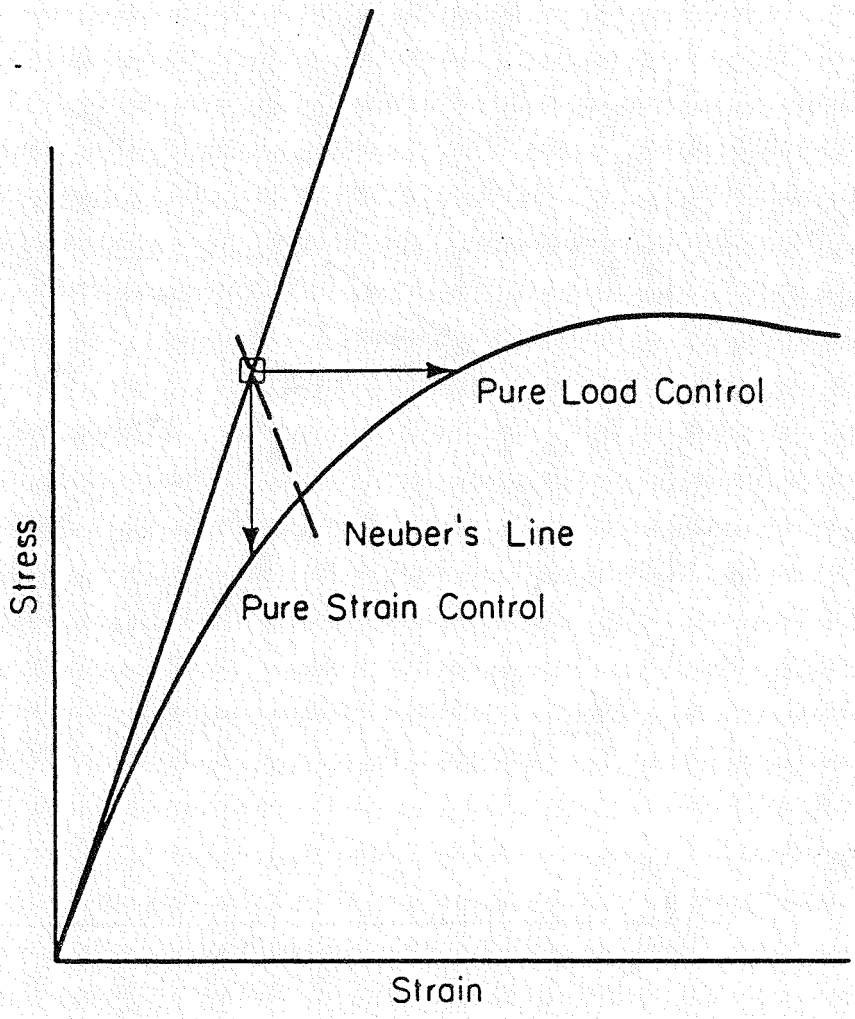

Fig. A.4 Schematic Representation of Redistribution Behavior at Point of Peak Stress

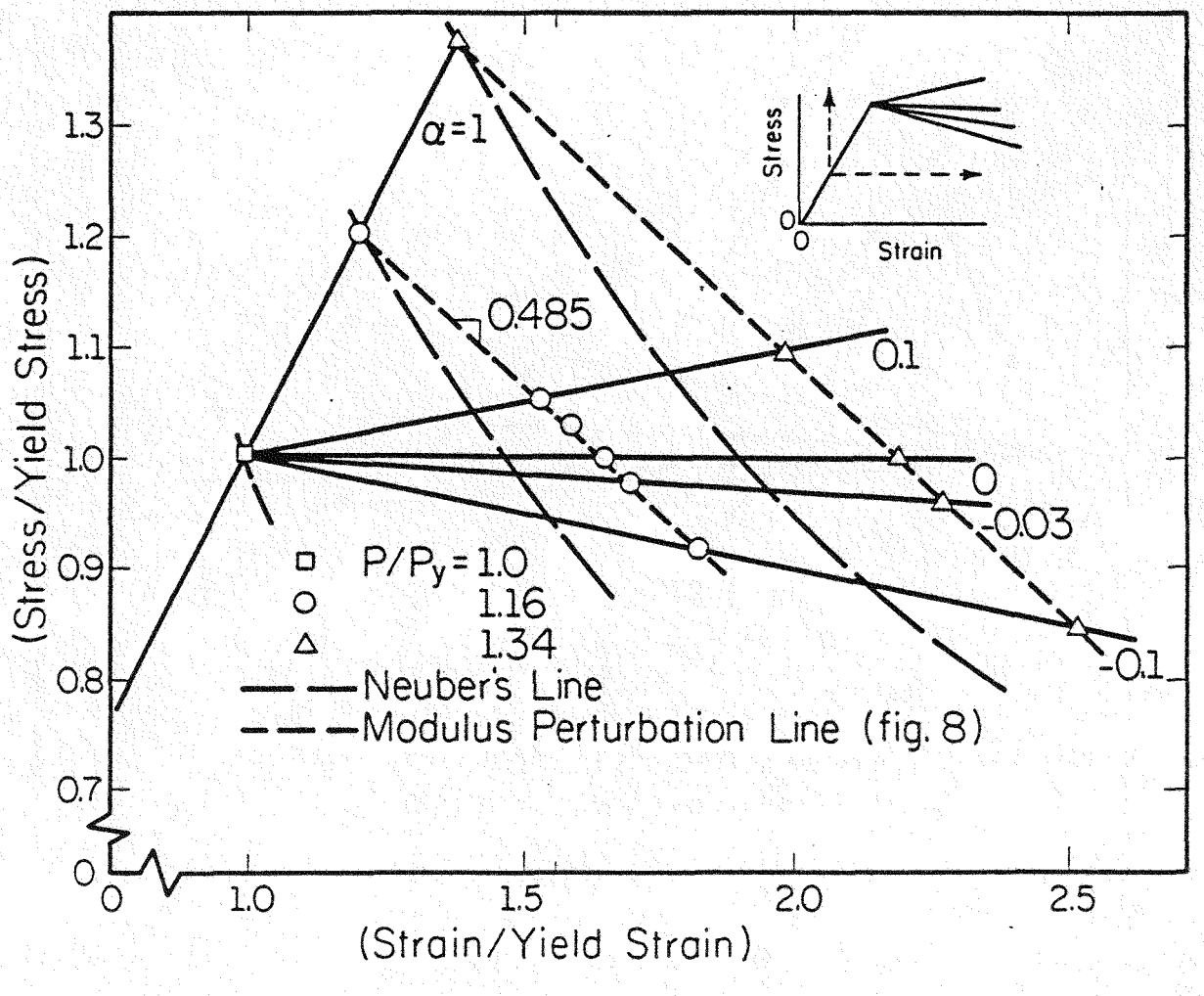

Fig. A.5 Peak Stress versus Peak Strain Relationship for Bar 2 of the Three-Bar Structure

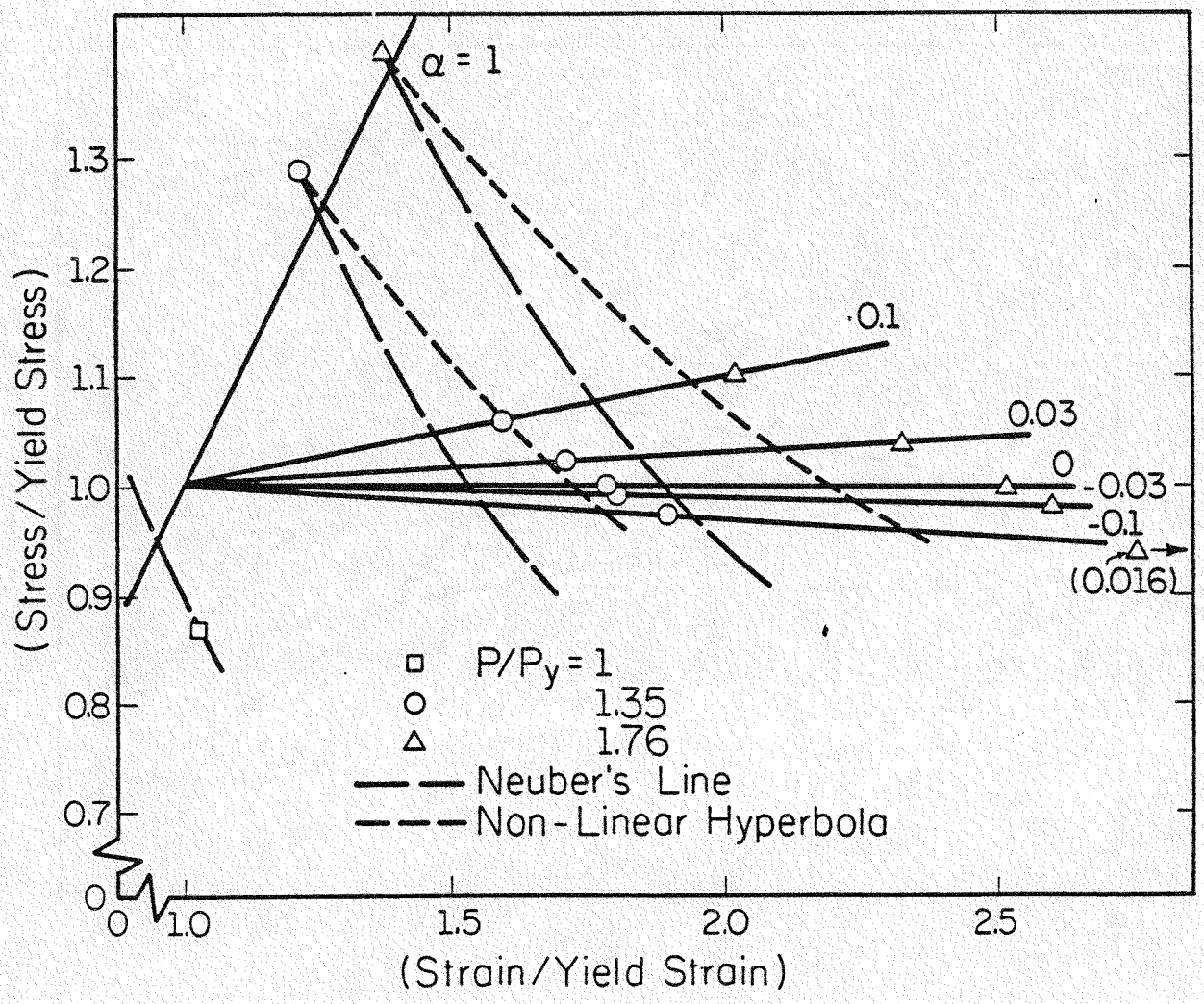

Fig. A.6 C-Notch: Peak Stress versus Peak Strain Relationship for Most Highly Strained Element

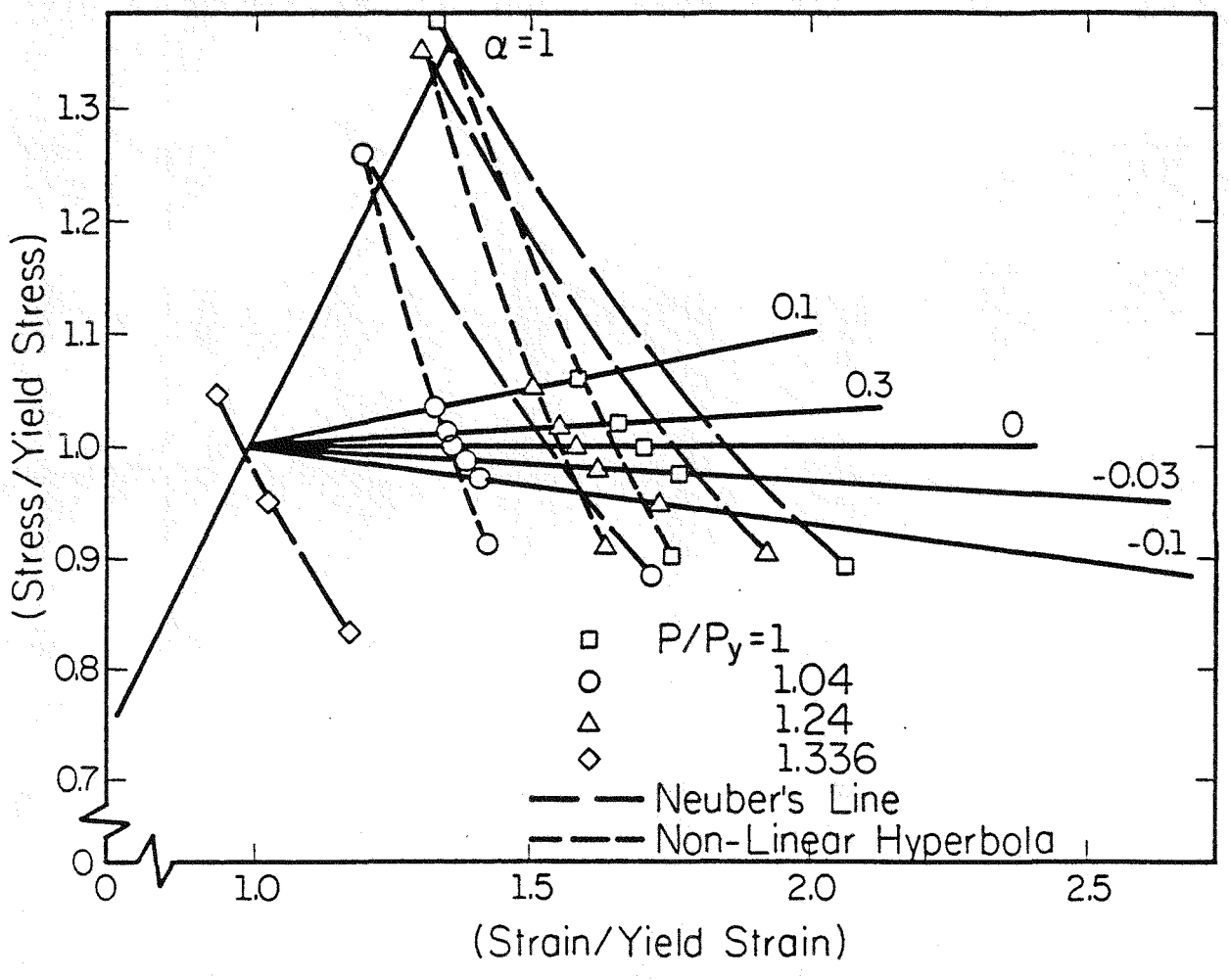

Fig. A.7 Cavity in Cylindrical Bar: Peak Stress versus Peak Strain for Most Highly Strained Element

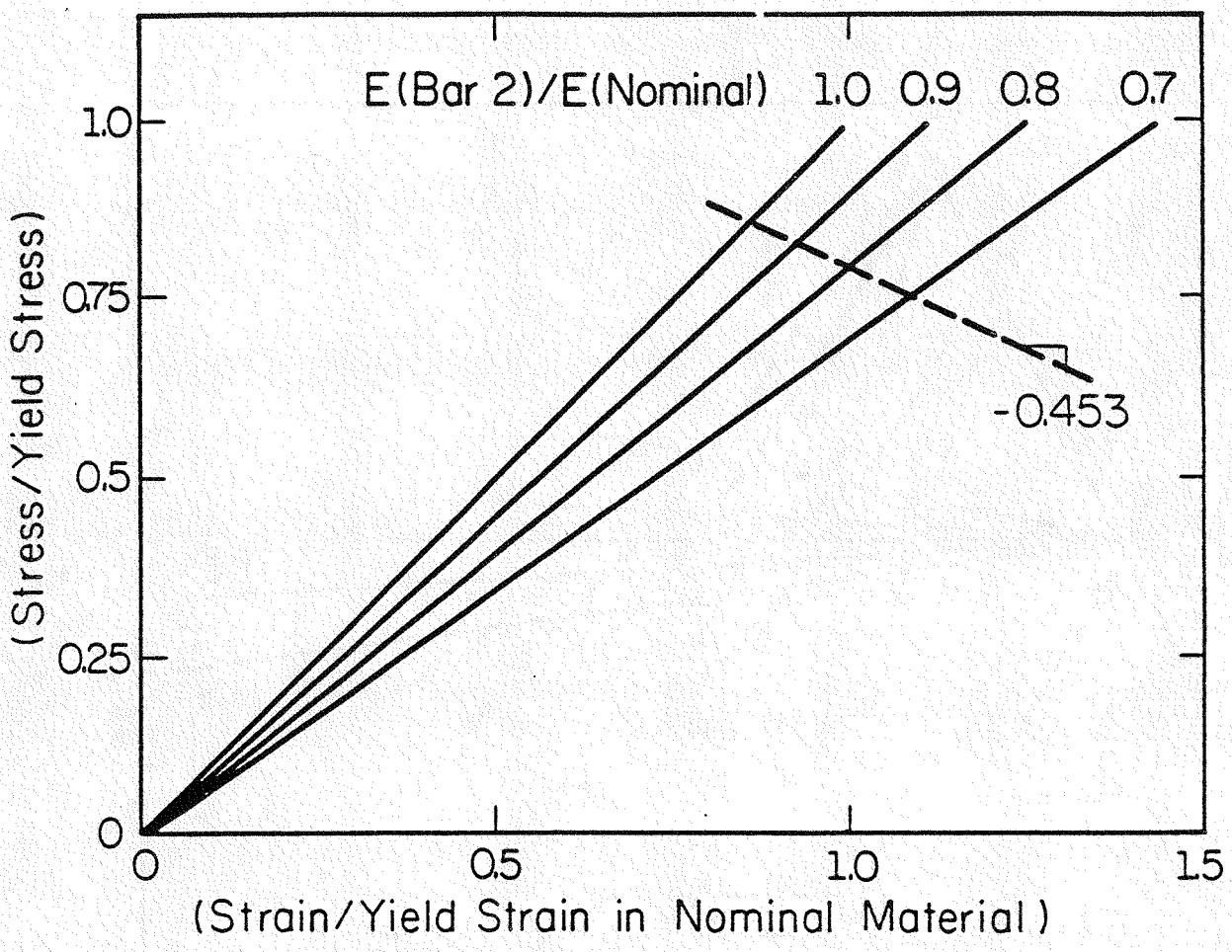

Fig. A.8 Three-Bar Structure: Locus of Peak Stress and Strain at Constant Load in Bar 2 as Young's Modulus of Bar 2 only is Varied

Attachment

1. ALLISON GAS TURBINE OPERATIONS, Mail Stop W-5, P.O. Box 420, Indianapolis, Indiana 46206

   P. Khandelwal

2. ARGONNE NATIONAL LABORATORY, 9700 S. Cass Avenue, Argonne, Illinois 60439

   W. A. Ellingson

3. AMERICAN WELDING SOCIETY, 550 LeJeune Road, Miami, Florida 33126

   H. G. Ziegenfuss

4. BABCOCK AND WILCOX, Fossil Power Generation Division, 20 South Van Buren Avenue, Barberton, Ohio 44203

   M. Gold

5. BATTELLE COLUMBUS LABORATORIES, 505 King Avenue, Columbus, Ohio 43201

   I. G. Wright

6. BETHLEHEM STEEL CORPORATION, Bethlehem, Pennsylvania 18016

   B. L. Bramfitt

7. CBI INDUSTRIES, 800 Jorie Blvd., Oak Brook, Illinois 60521

   W. R. Mikesell

8. CANADA CENTER FOR MINERAL AND ENERGY TECHNOLOGY, 555 Booth Street, Ottawa, Ontario, Canada K1A 0G1

   Mahee Sahoo

9. CHEVRON CORPORATION, P. O. Box 4012, Richmond, California 94804

   A. G. Imgram

10. CLIMAX MOLYBDENUM COMPANY OF MICHIGAN, P.O. Box 1568, Ann Arbor, Michigan 48106

    T. B. Cox

11. COLORADO SCHOOL OF MINES, Department of Metallurgical Engineering, Golden, Colorado 80401

    G. R. Edwards

12. CORNELL UNIVERSITY, Materials Sciences and Engineering Department, Bard Hall, Ithaca, New York 14853

Che-Yu Li

13. DOW CORNING CORPORATION, 3901 S. Saginaw Road, Midland, Michigan 48640

T. W. Foglesong

14. EG&G IDAHO, INC., Idaho National Engineering Laboratory, P.O. Box 1625, Idaho Falls, Idaho 83415

A. D. Donaldson

15–16. ELECTRIC POWER RESEARCH INSTITUTE, 3412 Hillview Avenue, P.O. Box 10412, Palo Alto, California 94303

W. T. Bakker
J. T. Stringer

17. FOSTER WHEELER DEVELOPMENT CORPORATION, Materials Technology Department, John Blizard Research Center, 12 Peach Tree Hill Road, Livingston, New Jersey 07039

J. L. Blough

18. GAS RESEARCH INSTITUTE, 8600 West Bryn Mawr Avenue, Chicago, Illinois 60631

H. S. Meyer

19. GIBBS & HILL ENGINEERING-DRAVO, 11 Penn Plaza, New York, New York 10001

T. A. Flynn

20. KENTUCKY CENTER FOR ENERGY RESEARCH, Iron Works Pike, P.O. Box 13015, Lexington, Kentucky 40512

V. K. Sethi

21. KENNAMETAL, INC., Philip McKenna Laboratory, 1011 Old Salem Road, P. O. Box 639, Greensburg, Pennsylvania 15601

B. North

22. LUKENS STEEL COMPANY, R&D Center, Coatesville, Pennsylvania 19320

J. A. Gulya

23. THE MATERIALS PROPERTIES COUNCIL, INC., United Engineering Center, 345 E. Forty-Seventh Street, New York, New York 10017

M. Prager

24. MOBIL RESEARCH AND DEVELOPMENT CORPORATION, P. O. Box 1026, Princeton, New Jersey 08540

R. C. Searles

25. NASA-LEWIS RESEARCH CENTER, Lewis Library, MS 60-3, 21000 Brookpark Road, Cleveland, Ohio 44135

K. Grasse

26. NATIONAL BUREAU OF STANDARDS, Materials Building, Gaithersburg, Maryland 20899

S. J. Dapkunas

27. NATIONAL MATERIALS ADVISORY BOARD, National Research Council, 2101 Constitution Avenue, Washington, DC 20418

K. M. Zwilsky

28–39. OAK RIDGE NATIONAL LABORATORY, P.O. Box X, Oak Ridge, Tennessee 37831

R. A. Bradley
P. T. Carlson
W. N. Drewery, Jr. (8)
R. R. Judkins
R. W. Swindeman

40. OFFICE OF NAVAL RESEARCH, Code 431, 800 N. Quincy Street, Arlington, Virginia 22217

S. G. Fishman

41. SHELL DEVELOPMENT COMPANY, P.O. Box 1380, Houston, Texas 77001

L. W. R. Dicks

42. THE TORRINGTON COMPANY, Research Department, 59 Field Street, Corrington, Connecticut 06790

W. J. Chmura

43. UNITED TECHNOLOGIES RESEARCH CENTER, East Hartford, Connecticut 06108

K. M. Prewo

44. UNIVERSITY OF CALIFORNIA AT BERKELEY, Department of Materials Science and Mineral Engineering, Berkeley, California 94720

E. R. Parker

45. UNIVERSITY OF ILLINOIS, Department of Mechanical and Industrial Engineering, 1206 West Green Street, Urbana, Illinois 61801

D. L. Marriott

46. UNIVERSITY OF SOUTHERN CALIFORNIA, Department of Materials Science, Los Angeles, California 90089

J. A. Todd

47. UNIVERSITY OF TENNESSEE, Department of Chemical and Metallurgical Engineering, Knoxville, Tennessee 37916

C. D. Lundin

48. UNIVERSITY OF WASHINGTON, Department of Materials Science and Engineering, Roberts Hall, FB-10, Seattle, Washington 98195

J. Mueller

49. DEPARTMENT OF THE ARMY, Army Materials and Mechanics Research Center, Watertown, Massachusetts 02172

D. R. Messier

50-52. DOE, MORGANTOWN ENERGY TECHNOLOGY CENTER, P.O. Box 880, Morgantown, West Virginia 26505

D. Dubis
M. Ghate
J. S. Wilson

53. DOE, OFFICE OF FOSSIL ENERGY, Washington, DC 20545

J. P. Carr
K. N. Frye
F. M. Glaser

54. DOE, OFFICE OF BASIC ENERGY SCIENCES, Materials Sciences Division, Washington, DC 20545

F. V. Nolfi, Jr.

55. DOE, ENERGY CONVERSION & UTILIZATION TECHNOLOGIES DIVISION, Route Symbol CE-142, Forrestal Building, Washington, DC 20585

J. J. Eberhardt

56. DOE, OFFICE OF VEHICLE AND ENGINE R&D, Route Symbol CE-131, Forrestal Building, Washington, DC 20585

R. B. Schulz

57. DOE, OAK RIDGE OPERATIONS OFFICE, P.O. Box E, Oak Ridge, Tennessee 37831

E. E. Hoffman

58. DOE, PITTSBURGH ENERGY TECHNOLOGY CENTER, P.O. Box 10940, Pittsburgh, Pennsylvania 15236

S. W. Chun